# MODELLING DIFFUSION THROUGH ENVIRONMENTS THAT CONTAIN IMMOBILE OBSTACLES: THE SHORT-TIME TRANSIENT REGIME, ANOMALOUS DIFFUSION AND CROWDING

Neo NGUIYA PASSI

Thesis submitted in partial fulfillment of the requirements
for the M.Sc. degree in Physics

Ottawa-Carleton Institute of Physics
Department of Physics
Faculty of Science
University of Ottawa
Ottawa, Canada

# SUMMARY

Diffusion plays a major role in many domains of our daily life. Many studies of this phenomenon have been done since the discovery of the Brownian motion by Robert Brown in 1827.

The work presented in this thesis was motivated in part by Adam Ellery's Ph.D thesis [1] from the Queensland University of Technology (QUT), Brisbane in Australia. In his thesis, he studied the 2D dynamics of an agent and a population of agents moving in an environment crowded randomly with obstacles of different sizes and shapes. The purpose of these studies was to propose an approach to characterize the short time dynamics of particles in different media. The method used to define the limits of the transient regime was arbitrary since considering a fixed interval of the transient regime of the mean square displacement (MSD), and that interval was the same for all obstacle concentrations in the medium.

In the current thesis, in order to improve the standard algorithm and better model the continuum, we propose a novel Monte Carlo algorithm allowing the particle to stay put to obtain a better distribution of displacements.

We have described a more objective method to determine the characteristic exponent $\alpha$ of the particle's anomalous diffusion in the transient regime. This exponent comes from the fact that many theories propose that the MSD of the particle in the transient can be described by the power law $\langle r^2 \rangle \sim t^\alpha$. We have defined and estimated the distance $r^*$ and the time $t^*$ necessary to the particle to reach the steady state. We have discovered that the excess diffusion $\beta$, which is due to the fact that diffusion is faster in the transient regime and thus measures the importance of the latter, contains potentially useful information. We have shown that the variables $\beta$ and $r^*$ are related to each other by a function of $\alpha$. All these studies are done for media that contain respectively obstacles distributed periodically and randomly.

# SOMMAIRE

Le processus de diffusion joue un rôle majeur dans plusieurs domaines de notre quotidien. De nombreuses études sur ce phénomène ont été faites depuis la découverte du mouvement Brownien par Robert Brown en 1827.

Le travail accompli dans cette thèse a été motivé en partie par la thèse de doctorat de Adam Ellery [1] à la Queensland University of Technology (QUT), Brisbane, Australie. Dans sa thèse, Ellery a étudié le mouvement à 2D d'un agent et d'une population d'agents se déplaçant dans un environement peuplé aléatoirement par des obstacles de différentes tailles et formes. Le but de ses études était de proposer une approche pour caractériser la dynamique à court temps des particules dans différents milieux. La méthode utilisée pour définir les limites temporelles de la phase transitoire était arbitraire puisque considérant un intervalle donné du régime transitoire de la moyenne des carrés du déplacement de la particule (MSD) et cet intervalle était le même quelque soit la concentration d'obstacles dans le milieu.

Dans cette thèse, dans le but de reproduire au maximum ce qui se passe dans le continuum, nous proposons un nouvel algorithme Monte Carlo en permettant à la particule de rester sur place pour obtenir une meilleure distribution des déplacements.

Par la suite, nous décrivons une méthode plus objective pour déterminer l'exposant caractéristique $\alpha$ du mouvement de la particule dans le régime transitoire. Cet exposant vient du fait que plusieurs théories proposent que la MSD de la particule dans le régime transitoire peut être décrite par la loi de puissance $\langle r^2 \rangle \sim t^\alpha$. Ensuite, nous définissons et estimons la distance $r^*$ et le temps $t^*$ au bout desquels la particule commence à avoir une vision de l'ensemble du système. Nous avons découvert que l'excédant de diffusion $\beta$, qui est dû au fait que la diffusion est rapide dans le regime transitoire, et qui mesure donc l'importance de ce dernier, contient de l'information potentiellement utile. Nous avons montré que les variables $\beta$ et $r^*$ sont reliées l'une à l'autre par une fonction de $\alpha$. Toutes ces études sont faites pour des milieux contenant respectivement des obstacles distribués périodiquement et aléatoirement.

# STATEMENT OF ORIGINALITY

I attest that the work presented in this thesis is my personnal effort, produced under the supervision of Gary W. Slater.

The paper in this thesis (Chapter 2) has been written first by me and my supervisor Gary W. Slater revised it after. The data was obtained using simulation programs that I wrote and I did all of the data analysis.

# ACKNOWLEDGEMENTS


- Thanks to the almighty God.
- Thanks to all who supported me during this difficult step of my life that I went through.
- Thanks to my supervisor Dr. Gary Slater.
- Thanks to the Queen Elisabeth Scholarship (QES II) for funding.

# LIST OF ACRONYMS

- LMC: Lattice Monte Carlo.
- MSD: Mean Square Displacement.
- PBCs: Periodic Boundary Conditions.
- STP: Single Particle Tracking.
- FRAP: Fluorescence Recovery After Photo-bleaching.
- FCS: Fluorescence Correlation Spectroscopy.

# TABLE OF CONTENTS

# List of Figures

# 1

# Introduction

Diffusion is a phenomenon that controls several aspects of our daily life. Examples of that phenomenon are in action every day. We have for example the smell of a perfume that propagates in a room or the odor of the food that spreads when you are cooking in your kitchen. This phenomenon is not limited only to gas but it is also present in liquids: we have for example coffee that mixes with milk without any agitation. We have a similar process after dissolving a solid in a liquid, for example sugar in coffee. Diffusion is essential to the functioning of our organism in the sense that a great part of the transport of molecules in our organism is possible because of diffusion processes [2].

Several studies have been done to study the problem of diffusion in biological environments. For example, Mathis Weiss et al [3] and Eli Barkai et al[4] showed (using Single Particle Tracking (SPT)) that by inserting a tracer particle in the cytoplasm of a living cell the particle undergoes anomalous diffusion. Michael J. Skaug et al [5] have similarly characterized the anomalous movement of a lipid in a biological membrane. Several other experimental methods can also be used to study diffusion, for example Fluorescence Recovery After Photo-bleaching (FRAP) and Fluorescence Correlation Spectroscopy (FCS) [6].

In addition to all these experiments, theoretical and numerical methods have been

developed. For example in 50 to 60's, the simulation technique called Cellular automata [7] appeared, and began to be applied in the mid-80's. This method allows the modelling of dynamic systems through discretization in time, space and state variables. Other simulation methods such as Monte Carlo also started to be used to model the movement of particles in environments containing obstacles [8]. Other computational and theoretical methods like the Method of Volume Averaging [9] have also been developed to characterize the phenomenon of diffusion in porous media. We must remember that all these methods were intended to produce a clear interpretation of the diffusion process in environments containing obstacles.

What increases our desire to study this phenomenon is the need to understand the behaviour of a diffusing particle in its medium. When the particle diffuses in a medium crowded with obstacles, its movement describes two regimes: the short time transient regime and the long time stationary regime.

Many studies have been done on the motion of particles in environments crowded with immobile obstacles. The effect of obstacles concentration on the diffusion coefficient of the particle have been studied for different cases [10, 11, 12, 13, 14]. Saxton [8] and Ellery et al [15, 16, 17] have studied the motion of random walkers moving in environments crowded with obstacles of different sizes and shapes. The goal of their studies was to design an approach to characterize the dynamics of particles in such media.

Researchers usually consider that in the transient regime, the movement of the particle is described by the equation (here for two dimensions)

$$\left\langle r^2(t)\right\rangle = 4D_\alpha t^\alpha, \tag{1}$$

where $D_\alpha$ is the generalized diffusivity in the transient regime and $\alpha$ is the characteristic exponent. For $\alpha = 1$ the movement of the particle corresponds to Fickian diffusion, for $\alpha < 1$ the movement corresponds to an anomalous subdiffusion, and for $\alpha > 1$ the movement corresponds to an anomalous superdiffusion.

In fact, some points are not clear about the limits of eq. (1) such as its applicability, and how the transition between the different regimes takes place. A central question is how to characterize the different regimes of the motion of an agent in a given medium, and how the parameters that characterize this motion depend on the obstacle size and shape, the concentration of obstacles and the distribution of obstacles. This is why it still remains important to understand the behaviour of the particle in the transient regime through for example the best estimate of the characteristic exponent of the particle

motion.

In order to characterize the movement of the particle, Ellery and his colleagues have proposed a way to find the characteristic exponent $\alpha$ of the mean square displacement (MSD) of the particle in the transient regime. Their method was to consider a given interval of the transient regime and fit the MSD in that interval in order to get the exponent $\alpha$. In fact that interval was the same for all obstacle concentrations in the medium. Because of that one can say that their method was arbitrary.

Among all these limitations, there is also the fact that these authors used the traditional Lattice Monte Carlo (LMC) algorithm which considers only jumps in four directions [18, 19]. In the next chapter, we present the limitations of the traditional LMC algorithm by comparing it with a new algorithm that we have developed. However, it is important to note that our new LMC algorithm is only an improvement of the traditional one since even for this algorithm, the fourth moment is not perfectly correct. In free space, it was shown that the fourth moment is totally correct only when one considers diagonal jumps and the fact that the particle can remain on the same site [20], noting that longtime ago, the necessity of the use of diagonal jumps when working in more than one dimension has been shown by Gauthier and Slater [21]. Due to the difficulty to manage diagonal collisions of the particle with the obstacles, it remains a challenge to implement the LMC considering the diagonal jumps. However, it should be noted that our new LMC algorithm considers the fact that the particle can stay put and it gives a fourth moment whose correction factor decreases three times faster than the one obtained with the traditional algorithm. This shows that our new LMC algorithm is the intermediate between the standard LMC algorithm and the one proposed by Chubynsky and Slater [20].

## 1.1 General considerations about Diffusion

### 1.1.1 Brownian motion

In 1827, the English botanist Robert Brown did an observation of a movement that will soon be known as Brownian motion. It is true that Brown was not the first to observe it but he was the first to seriously study it. Observing pollen grains in water, Brown noticed that their motion was irregular and incessant. He was the first to show that this movement did not have an organic origin. To prove that, he hermetically sealed pollen grains and water for many days, and the movement did not stop. If that movement were

caused by a living mechanism, the grains wouldn't have had enough food to stay alive and the movement would have stopped. Brown repeated the same experiments with inorganic particles and he observed the same movement. A few decades later, to be more precise in 1865, G. Cantoni [22] confirmed the fact that Brownian motion has no organic origin by showing that the movement of particles did not stop even after spending a full year in a liquid hermetically sealed between two glass plates. In 1877, Delseaux formulated the generally accepted idea that Brownian motion was generated by the successive collisions between liquid molecules and solid particles. That idea was developed later by Einstein [23]. After many decades of speculation and experimentation, it became accepted that Brownian motion becomes more important as the temperature of the system increases.

### 1.1.2 Unbiased Brownian Motion

Brownian motion is frequently modelled using the 1D random walk of a walker which executes random jumps of length $l$ to the right or the left with a time step $\tau$. Two consequences can be derived: the average displacement of the walker is equal to zero and the mean square displacement is proportional to time.

If one considers a one dimensional random walk with $N$ steps, the final position of the walker will be given by:

$$X(N) = \sum_{i=1}^{N} l_i, \tag{2}$$

where $l_i$ can be positive or negative according to the direction of the jump (i.e., $l_i$ is randomly equal to $\pm l$). Since the average of $l_i$ is zero ($\langle l_i \rangle = 0$), the total average will be equal to zero as well ($\langle X \rangle = 0$). We study a random walk where the jumps are independent from each other, which is written mathematically as $\langle l_i \cdot l_j \rangle = \delta_{ij} l^2$, with $\delta_{ij}$ the Kronecker delta function defined to be 0 for $i \neq j$ and 1 for $i = j$. To have more information on the properties of the random walk, one needs to evaluate the MSD of the particle since it is the smallest even order moment; all odd order moments are equal to zero by symmetry. After $N$ steps the mean square displacement is given by:

$$\begin{aligned}
\left\langle (X(N))^2 \right\rangle &= \left\langle (X(N-1) + l_N)^2 \right\rangle \\
&= \left\langle (X(N-1))^2 + 2X(N-1) \cdot l_N + (l_N)^2 \right\rangle \\
&= \left\langle (X(N-1))^2 \right\rangle + 2 \left\langle X(N-1) \cdot l_N \right\rangle + \left\langle (l_N)^2 \right\rangle ;
\end{aligned}$$

with

$$\langle X(N-1)\cdot l_N\rangle = \left\langle \sum_{j=1}^{N-1} l_j \cdot l_N \right\rangle = \sum_{j=1}^{N-1} \langle l_j \cdot l_N\rangle = \sum_{j=1}^{N-1} \delta_{jN} = 0, \tag{3}$$

one obtains

$$\left\langle (X(N))^2 \right\rangle = \left\langle (X(N-1))^2 \right\rangle + l^2. \tag{4}$$

Applying the recursive method, we get:

$$\begin{aligned} \left\langle (X(N))^2 \right\rangle &= \left\langle (X(N-2))^2 \right\rangle + 2l^2 \\ &= \cdots \\ &= \left\langle (X(0))^2 \right\rangle + Nl^2 \end{aligned}$$

Since the walker starts its walk at $X(0) = 0$, we have $\langle (X(0))^2\rangle = 0$, and consequently:

$$\left\langle (X(N))^2 \right\rangle = Nl^2. \tag{5}$$

We define the diffusivity $D$ by:

$$D = \frac{l^2}{2\tau}. \tag{6}$$

Knowing that the total time is $t = N\tau$, we can use it with eq. (6) in eq. (5). We then obtain the one dimension diffusion law given by:

$$\left\langle X^2 \right\rangle = 2Dt. \tag{7}$$

This equation can be extended to two and three dimensions, but we need to keep in mind that the expression in each direction remains the same. So we have: $\langle X^2\rangle = \langle Y^2\rangle = \langle Z^2\rangle = 2Dt$. Considering that the random walk is isotropic, the movement of the walker is described by the position vector $\vec{r}$, which has two components $X$, $Y$ in two dimensions and $X$, $Y$ and $Z$ in three dimensions. Thus in two dimensions, we have:

$$\begin{aligned} \left\langle r_{2d}^2 \right\rangle &= \left\langle X^2 \right\rangle + \left\langle Y^2 \right\rangle \\ &= 2Dt + 2Dt = 4Dt \end{aligned} \tag{8}$$

and then, in three dimensions, we have:

$$\begin{aligned} \left\langle r_{3d}^2 \right\rangle &= \left\langle X^2 \right\rangle + \left\langle Y^2 \right\rangle + \left\langle Z^2 \right\rangle \\ &= 2Dt + 2Dt + 2Dt = 6Dt \end{aligned} \tag{9}$$

All these diffusion laws are applicable in almost every free media (without any obstacle) and for all particles sizes.

### 1.1.3 Brownian Motion and the Einstein-Smoluchowski relation

Let's consider a free Brownian particle moving in a fluid [24]. The molecules of the fluid are much smaller than the particle size. The equation of the particle's motion is given by

$$m\frac{dv(t)}{dt} = -\zeta v(t) + \xi(t), \tag{10}$$

where $m$ is the mass of the particle and $\zeta$ is the friction coefficient. The first term on the right side of this equation represents the viscous friction force that acts on the particle; the second term is the force due to the incessant collisions between the particle and the molecules of the fluid, the average of that force is equal to zero ($\langle \xi(t) \rangle = 0$). Equation (10) is called Langevin equation and can be rewritten as:

$$\frac{dv(t)}{dt} = -\frac{1}{\tau}v(t) + \frac{1}{m}\xi(t). \tag{11}$$

In this equation, $\tau = m/\zeta$ is the relaxation time. Multiplying eq. (11) by $x(t)$, the position of the particle, that equation becomes

$$x(t)\frac{dv(t)}{dt} = -\frac{1}{\tau}x(t)v(t) + \frac{1}{m}x(t)\xi(t). \tag{12}$$

Taking the average of this equation knowing that $x(t)\cdot v(t) = \frac{1}{2}(dx^2(t)/dt)$, $x(t)(dv(t)/dt) = \frac{1}{2}(d^2x^2(t)/dt^2) - v^2(t)$ and that $\langle x(t) \cdot \xi(t) \rangle = 0$ (because for homogeneous media, there is no expectation of a statistical correlation between the particle's position $x(t)$ and the force $\xi(t)$ exerted on it by the molecules of the fluid), one obtains:

$$\frac{d^2 \left\langle x^2(t) \right\rangle}{dt^2} + \frac{1}{\tau}\frac{d \left\langle x^2(t) \right\rangle}{dt} = 2 \left\langle v^2 \right\rangle. \tag{13}$$

Considering that the particle has reached the equilibrium temperature of the fluid, we have $\langle v^2 \rangle = k_B T/m$, with $k_B$ the Boltzmann constant and $T$ the temperature. The solution of eq. 13 is given by:

$$\left\langle x^2(t) \right\rangle = \frac{2k_B T}{m}\tau^2 \left[ \frac{t}{\tau} - \left( 1 - \exp\left( -\frac{t}{\tau} \right) \right) \right]. \tag{14}$$

For $t \ll \tau$ we have

$$\left\langle x^2(t) \right\rangle = \frac{k_B T}{m} t^2 = \left\langle v^2 \right\rangle t^2. \tag{15}$$

For $t \gg \tau$ we have

$$\left\langle x^2(t) \right\rangle = \frac{2k_B T \tau}{m} t = \frac{2k_B T}{\zeta} t. \tag{16}$$

Comparing eq. (16) with eq. (7), we obtain the Einstein-Smoluchowski equation:

$$D = \frac{k_B T}{\zeta}. \tag{17}$$

For a spherical particle, the friction coefficient is related to particle size by the following formula also know as Stokes formula:

$$\zeta = 6\pi\eta R, \tag{18}$$

where $R$ is the particle radius in meter $(m)$, $\eta$ the fluid viscosity. Then, the diffusivity becomes:

$$D = \frac{k_B T}{6\pi\eta R}. \tag{19}$$

The diffusivity of a particle depends not only on its size, but also on the viscosity and the temperature of the medium.

## 1.2 Fick's law: Macroscopic aspects of Diffusion

Most discussions about the diffusion process start with Fick's equations. In fact Fick's equations are just differential equations that describe the spatial and temporal variations of a distribution of particles in a medium.

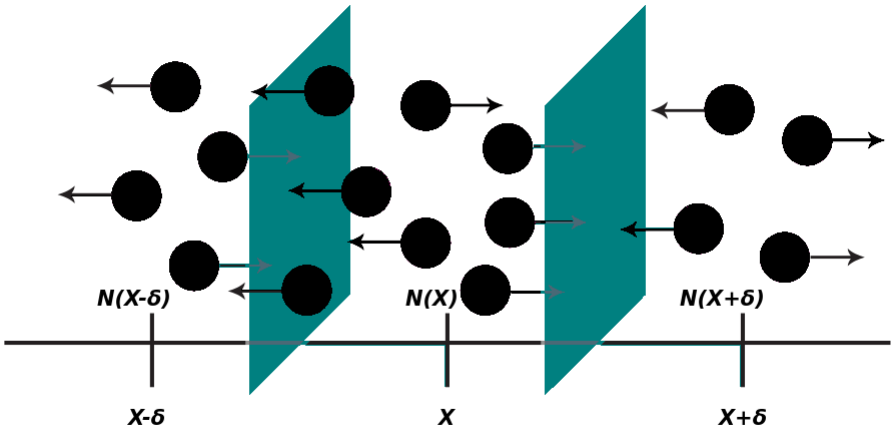


Figure 1: A model to illustrate Fick's first law. The net number of particles moving out of the zone centered at $x$ during a time step $\tau$ is 8 (4 particles moving to the right and 4 moving to the left). No particle stays in that zone.

Let us consider Fig. (1) where particles move along the $x$ axis at time $t$. The number of particles in the volume $V$ centered at $x$ is $N(x)$ and the concentration is $C(x)$. The axis is discretized such that we have successive spaces of volume $V = A\delta$. These spaces are separated by imaginary membranes of surface area $A$ located at $x \pm \frac{n\delta}{2}$, where $n$ is an odd integer. The number of particles $N(x)$ between each pair of membranes is expressed with respect to the central position $x$.

During a period of time $\tau$, $\Delta N$ particles move through the membrane; the flux is then defined as

$$J = \frac{\Delta N}{A\tau}. \tag{20}$$

Every time step, each particle moves randomly in the $\pm x$ direction. Therefore, on average, at time $\tau$, half of the particles located at $x$ at time zero will be located at $x + \delta$ and the other half at $x - \delta$. The number of particles that cross the membrane located at $x + \frac{\delta}{2}$ at every time step is thus given by:

$$\Delta N_{x+\frac{\delta}{2}} = -\frac{1}{2}\left[N(x+\delta) - N(x)\right]. \tag{21}$$

Substituting eq. (21) into eq. (20) the flux through the membrane located at $x + \frac{\delta}{2}$ is given by:

$$J_{x+\frac{\delta}{2}} = -\frac{1}{2}\left[\frac{N(x+\delta) - N(x)}{A\tau}\right]. \tag{22}$$

Multiplying this equation by $\delta^2/\delta^2$, considering that $C(x) = \frac{N(x)}{A\delta}$, $C(x+\delta) = \frac{N(x+\delta)}{A\delta}$ and that $\delta^2/2\tau$ is the definition of the diffusion coefficient $D$, eq. (22) becomes:

$$J_{x+\frac{\delta}{2}} = -\frac{D}{\delta}\left[C(x+\delta) - C(x)\right]. \tag{23}$$

Using the definition of the derivative for small $\delta = dx$ this equation becomes:

$$J_x = -D\frac{dC(x)}{dx}. \tag{24}$$

This equation is Fick's first law. It states that the flux is proportional to the concentration gradient and the coefficient of proportionality is the diffusion coefficient $D$.

If we consider a box centered at position $x$, Fick's second law deals with the variation of the local concentration as a function of time. The flux through the membranes located at $x - \frac{\delta}{2}$ and $x + \frac{\delta}{2}$ determine the number of particles that pass through the box located at $x$. During a time step $\tau$, if the flux has a positive sign, $J_{x-\frac{\delta}{2}}\tau A$ particles will enter in the box centred at $x$ and $J_{x+\frac{\delta}{2}}\tau A$ will move out. The change in the number of particles at $x$ in a time step $\tau$ is thus given by:

$$\Delta N(x) = A\tau\left(J_{x-\frac{\delta}{2}} - J_{x+\frac{\delta}{2}}\right). \tag{25}$$

Fick's second law follows from the first and insures that the total number of particles is conserved. In other words, particles are neither created nor destroyed. Dividing both sides of eq. (25) by the volume, one can see that the variation of the concentration with respect to the time step $\tau$ is equal to the variation of the flux in the step length $\delta$. This allows us to write:

$$\frac{1}{\tau}\left[C(x,t+\tau) - C(x,t)\right] = -\frac{1}{\delta}\left[J_{x+\frac{\delta}{2}} - J_{x-\frac{\delta}{2}}\right]. \tag{26}$$

In the limit $\tau \to 0$ and $\delta \to 0$ we obtain:

$$\frac{dC}{dt} = -\frac{dJ_x}{dx}. \tag{27}$$

Equation (27) is Fick's second equation and it can be written substituting $J_x$ by its value in eq. (24):

$$\frac{dC}{dt} = D\frac{d^2C}{dx^2}. \tag{28}$$

This equation is known as the diffusion equation. It shows that the temporal and spatial variations of the concentration are related via the diffusion coefficient $D$.

The diffusion equation can be solved in order to obtain the concentration profile. For example, if we consider the particles initially at $x = 0$, i.e. $C(x, 0) = \delta(x)$, where $\delta(x)$ is the Dirac function, the concentration profile in one dimension is given by:

$$C(x,t) = \frac{N}{(4\pi Dt)^{1/2}} exp\left(-\frac{x^2}{4Dt}\right). \tag{29}$$

Dividing eq. (29) by $N$, we obtain the probability density given by:

$$p(x,t) = \frac{1}{(4\pi Dt)^{1/2}} exp\left(-\frac{x^2}{4Dt}\right); \tag{30}$$

its representation as a function of position $x$ is shown in Fig. 2. The variance $\langle x^2 \rangle$ of this

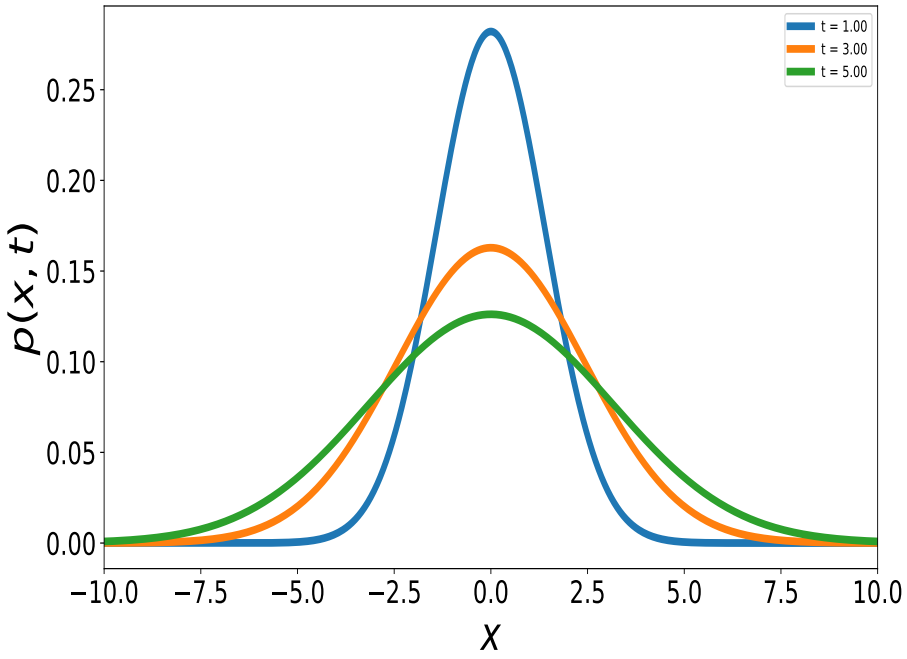


Figure 2: Plot of the probability density of particles as a function of position x. The evolution of the concentration profile is given by eq. (30). Particles have been released at time $t = 0$ at position $x = 0$. The scaled diffusion coefficient has been chosen to be 1. The probability density follows a Gaussian distribution that spreads over the time. The width of the peak is proportional to $\sqrt{2Dt}$.

distribution is given by:

$$\left\langle x^2 \right\rangle = \int_{-\infty}^{+\infty} x^2 p(x,t) dx = \int_{-\infty}^{+\infty} \frac{x^2}{(4\pi Dt)^{1/2}} exp\left(-\frac{x^2}{4Dt}\right) dx = 2Dt. \tag{31}$$

The fourth moment is then given by:

$$\left\langle x^4(t) \right\rangle = \int_{-\infty}^{+\infty} x^4 p(x,t) dx = 3(2Dt)^2 = 3\left\langle x^2(t) \right\rangle^2. \tag{32}$$

It is important to mention that because of symmetry, all the odd order moments are equal to zero: $\langle x^{2i+1}(t) \rangle = 0$ with $i \in \mathbb{N}$.

## 1.3 Monte Carlo Algorithm for Diffusion

In this section, we show how one can use the Monte Carlo method to find the scaled diffusivity of a particle moving in a given medium. The Monte Carlo methods, with or without lattice, consist in choosing the directions of the jumps of the particle using random numbers. When there is no transient regime, the value of the diffusion coefficient in 1D is given by:

$$D = \frac{\langle x^2(t) \rangle}{2t} \tag{33}$$

for all times, where $\langle x^2(t) \rangle$ is the variance of the displacement and $t$ the time.

To find the diffusion coefficient of a particle using the Monte Carlo algorithm, we should note its initial position, let it diffuse during a time interval $t$ and record its final position. Repeating that procedure many times, one can evaluate the variance of the displacement. Then diffusivity is obtained dividing the final variance by $2t$.

Experimentally, a Brownian particle executes a continuous movement. To design the Monte Carlo method, we perform a double discretization, one in time and the other in space.

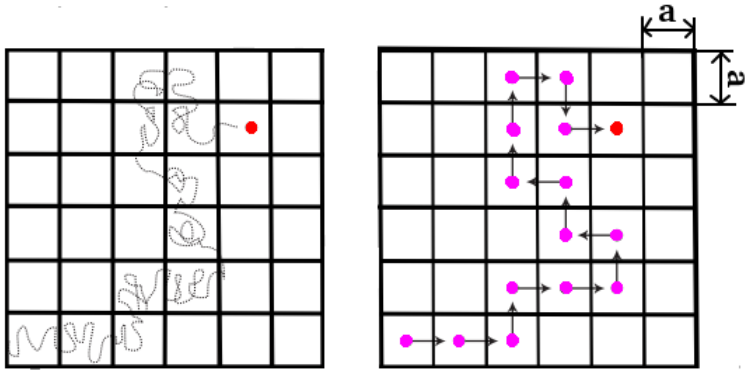


Figure 3: Random walk of a particle in two dimensions. The left is the continuous motion of the particle (red spot) and the right is the discretization. The particle executes jumps of length a, since the size of the square regions has been chosen to be a.

Figure 3 shows the random walk of a particle over a two dimensional lattice. The system is built so that a jump is completed once the particle touches one of the lines. So the particle executes jumps of length a (the step size of the lattice) in one of the 4 directions allowed by the lattice with a probability given by:

$$P = \frac{1}{4}. \tag{34}$$

This method is sometimes used to study the diffusion of a particle in a given structure such as a hydrogel for example. Figure 4(a) shows a representation of a gel.

To build a gel for a Monte Carlo simulation, a common method consists in placing obstacles on the lattice in order to model the cross-section of the gel fibers. If a particle executes a jump to a site which is occupied by an obstacle, that jump is rejected and the particle stays at the same place but the clock advances. The effect of obstacles on the diffusion of particles is generally characterized by the scaled diffusion ratio $D/D_0$, where $D$ is the diffusion coefficient in the presence of obstacles and $D_0$ is the diffusion coefficient in a free medium.

## 1.4 The Exact Solution for the Lattice Monte Carlo Algorithm

To solve the problem of the unbiased random walk of a particle on a lattice, Mercier et al [18, 19] used the Nernst-Einstein relation between the diffusion coefficient of the particle in the absence of an external bias and its velocity in the presence of a very weak force $F$:

$$D = \frac{k_B T}{F} v, \tag{35}$$

where $k_B$ is the Boltzmann constant and $T$ is the absolute temperature. Under a very weak force, we can thus write

$$\frac{D}{D_0} = \lim_{F \to 0} \frac{v(F)}{v_0(F)};$$

the index zero simply refers to the value of the variable in free solution. In the limit where $F \to 0$ one obtains the scaled (normalized) diffusion coefficient $D^* = \frac{D}{D_0}$ in the direction of the force $F$ by evaluating $\frac{v}{v_0}$. The method proposed by Mercier et al [18, 19] starts with the calculation of the probability of presence of the particle on each free site of the lattice when a weak force is applied.

Once the probabilities are obtained, multiplying them by the corresponding local velocities, one can obtain the mean velocity of the particle on the lattice. In the previous section, we have shown that in a free solution, the probability for the particle to jump to the adjacent sites in the absence of an external field is equal to 1/4 for each of the possible four directions. However, when there is an external field applied, the probability

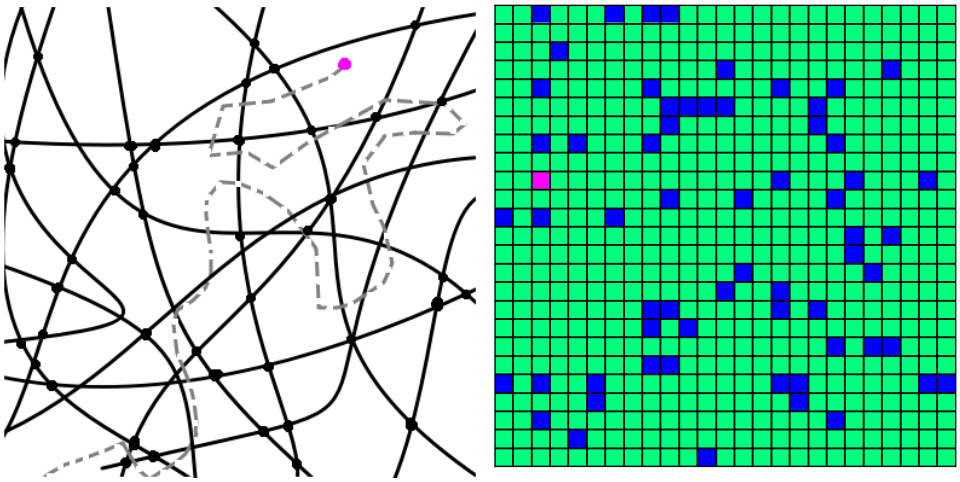

(a) (b)

Figure 4: (a) A schematic representation of a small part of a 3D hydrogel. Black lines represent the cross-linked polymers. The particle (pink) moves randomly between the gel fibers and the dark spots represent the crosslinks between the polymers. (b) A 2D lattice representation of a cross-section of a 3D hydrogel. The green sites represent the free sites which can be considered as the volume occupied by the liquid phase. The blue sites are the cross-sections of the gel fibers that we consider as obstacles.

of jumping in the field direction depends on the magnitude of the field. Slater et al [25, 26] have evaluated the exact probability by solving a first passage problem. For a 2D lattice they have shown that the probability for each direction of the jump (for $\epsilon$ very weak) is given by:

$$P_{\pm x} = \frac{1 \pm \epsilon}{4}, \tag{36}$$

where $P_{+x}$ and $P_{-x}$ respectively represent the probabilities for the particle to jump in the direction and in the opposite direction of the dimensionless force $\epsilon$:

$$\epsilon = \frac{Fa}{2k_B T}. \tag{37}$$

The unit of length is $a$ and the unit of time is $a^2/D_0$, with $D_0$ the diffusion coefficient in a free solution.

It has been shown in [25] that the (scaled) mean time duration of a jump is not changed and its dimensionless expression is

$$\tau \approx 1 + O(\epsilon^2). \tag{38}$$

The mean free (scaled) velocity of the particle in the absence of obstacles is given by

$$v = \frac{(P_{+x} - P_{-x})\, a}{\tau}. \tag{39}$$

The lattice in Fig. 5 presents nine sites among which seven are accessible to the particle and the two remaining ones are occupied by obstacles. Periodic boundary conditions are applied at every side of the lattice. At each time step, the particle attempts a jump. If the chosen site is occupied by an obstacle, the jump is rejected and the particle remains at the same place but the clock advances. The probability for the particle to be on site $i$ at time $t+1$ depends on the probability for the particle to be on one of the four neighbouring sites at time $t$.

If one considers site number 5, the probability of being on that site at time $t+1$ is given by

$$n(5, t+1) = P_{-x} n(3, t) + P_{+x} n(4, t) + P_{-y} n(2, t) + P_{+y} n(7, t), \tag{40}$$

with $n(i, t)$ the probability of finding the particle on site $i$ at time $t$. Site number 3 is adjacent to an obstacle. Therefore, $n(3, t+1)$ is given by:

$$n(3, t+1) = P_{-x} n(4, t) + P_{+x} n(5, t) + P_{-y} n(1, t) + P_{+y} n(3, t). \tag{41}$$

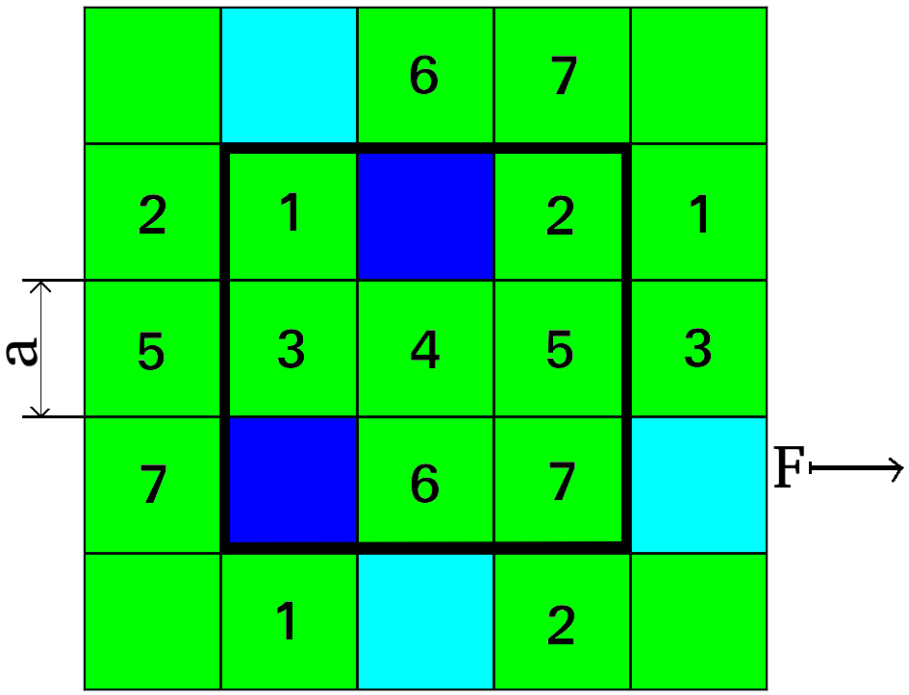


Figure 5: The $3 \times 3$ lattice used to illustrate the exact solution for the LMC. We have 7 free sites (green) that are accessible to the particle and 2 sites (blue) occupied by obstacles. The sites in sky blue indicate that periodic boundary conditions are used. An external force is applied in the x direction.

This set of linear equations can be written as $T\,|n\rangle = |n(t+1)\rangle$, where $T$ is the transition matrix and $|\cdot\rangle$ stands for a column vector. The stationary state being defined by $|n(t+1)\rangle = |n(t)\rangle \equiv |n\rangle$, we need to solve the system $T\,|n\rangle = |n\rangle$ in order to obtain the different probabilities. For the system shown in Fig. 5, the transition matrix is given by:

$$T \equiv \frac{1}{4}\begin{pmatrix} 2+\epsilon & 1+\epsilon & 1 & 0 & 0 & 0 & 0 \\ 1-\epsilon & 1-\epsilon & 0 & 0 & 1 & 0 & 1 \\ 1 & 0 & 1 & 1-\epsilon & 1+\epsilon & 0 & 0 \\ 0 & 0 & 1+\epsilon & 1 & 1-\epsilon & 1 & 0 \\ 0 & 1 & 1-\epsilon & 1+\epsilon & 0 & 0 & 1 \\ 0 & 0 & 0 & 1 & 0 & 2-\epsilon & 1-\epsilon \\ 0 & 1 & 0 & 0 & 1 & 1+\epsilon & 1+\epsilon \end{pmatrix} \tag{42}$$

To solve the system $T\,|n\rangle = |n\rangle$, we rewrite it as:

$$(T-I)\,|n\rangle = |0\rangle\,, \tag{43}$$

where $|0\rangle$ is a zero vector. We can then include the normalization condition $\sum_{i=1}^{7} n_i = 1$ directly into eq. (43). To do that, we just replace all the elements of the last line of the matrix $T-I$ by 1 and the last element of the vector $|0\rangle$ by 1. The final equation becomes

$$M\,|n\rangle = |b\rangle \tag{44}$$

with

$$|b\rangle = |0, 0, \cdots, 1\rangle\,, \tag{45}$$

and $M$ given by:

$$M \equiv \frac{1}{4}\begin{pmatrix} -2+\epsilon & 1+\epsilon & 1 & 0 & 0 & 0 & 0 \\ 1-\epsilon & -3-\epsilon & 0 & 0 & 1 & 0 & 1 \\ 1 & 0 & -3 & 1-\epsilon & 1+\epsilon & 0 & 0 \\ 0 & 0 & 1+\epsilon & -3 & 1-\epsilon & 1 & 0 \\ 0 & 1 & 1-\epsilon & 1+\epsilon & -4 & 0 & 1 \\ 0 & 0 & 0 & 1 & 0 & -2-\epsilon & 1-\epsilon \\ 4 & 4 & 4 & 4 & 4 & 4 & 4 \end{pmatrix} \tag{46}$$

This can be simplified by cancelling the use of $\epsilon$. To do that, we separate the different terms in eq. (44) into a constant term (with subscript $c$) and a $\epsilon$ dependent term (with subscript $\epsilon$) [18, 19].

$$M = M_c + \epsilon M_\epsilon, \tag{47}$$

$$|n\rangle = |n_c\rangle + \epsilon\,|n_\epsilon\rangle\,, \tag{48}$$

$$|b\rangle = |b_c\rangle\,. \tag{49}$$

Making use of eq. (47), eq. (48) and eq. (49) into eq. (44), we obtain:

$$M_c\,|n_c\rangle + \epsilon\,(M_c\,|n_\epsilon\rangle + M_\epsilon\,|n_c\rangle) + \epsilon^2 M_\epsilon\,|n_\epsilon\rangle = |b_c\rangle\,. \tag{50}$$

Considering the terms of order in $\epsilon$ less or equal to one, this relation is verified only if

$$M_c\,|n_c\rangle = |b_c\rangle \qquad \text{and} \qquad M_c\,|n_\epsilon\rangle = -M_\epsilon\,|n_c\rangle\,. \tag{51}$$

The first relation is related to the case where no force is applied and leads to the solution $n(i) = 1/J$ (with J the number of free sites). The second relation contains the non trivial effects of fixed obstacles on the diffusion coefficient. In the second relation, the unknown is $|n_\epsilon\rangle$ and that value can be found numerically using an algorithm to invert a matrix. In fact, for small lattice sizes as the one used for our example, software package like Maxima, Maple or Mathematica can easily find the solution. For large lattice sizes, it is more efficient to use numerical methods already established [18]. For our example, the probability of presence of the particle on each site is given by the vector

$$|n(t)\rangle = \begin{pmatrix} n(1,t) \\ n(2,t) \\ n(3,t) \\ n(4,t) \\ n(5,t) \\ n(6,t) \\ n(7,t) \end{pmatrix} = \frac{1}{7}\begin{pmatrix} 1 \\ 1 \\ 1 \\ 1 \\ 1 \\ 1 \\ 1 \end{pmatrix} + \frac{\epsilon}{28}\begin{pmatrix} 4 \\ -1 \\ 1 \\ -1 \\ 0 \\ -4 \\ 1 \end{pmatrix}. \tag{52}$$

Since the probabilities have been found, we need to determine the velocity of the particle on each site. That velocity in the direction of the bias is expressed as:

$$v_i = P_{+x} L_{+i} - P_{-x} L_{-i}. \tag{53}$$

In this expression, $L_\pm = 1$ if there is no obstacle in the given direction and zero otherwise. Thus, we can express the velocity as $|v\rangle = |v_c\rangle + \epsilon\,|v_\epsilon\rangle$:

$$|v\rangle = \begin{pmatrix} v(1) \\ v(2) \\ v(3) \\ v(4) \\ v(5) \\ v(6) \\ v(7) \end{pmatrix} = \frac{1}{4}\begin{pmatrix} -1 \\ 1 \\ 0 \\ 0 \\ 0 \\ 1 \\ -1 \end{pmatrix} + \frac{\epsilon}{4}\begin{pmatrix} 1 \\ 1 \\ 2 \\ 2 \\ 2 \\ 1 \\ 1 \end{pmatrix}. \tag{54}$$

The mean velocity of the particle on the lattice is found computing the following scalar product $\langle v|n\rangle$:

$$\begin{aligned} v = \langle v|n\rangle &= (\langle v_c| + \epsilon\,\langle v_\epsilon|) \cdot (|n_c\rangle + \epsilon\,|n_\epsilon\rangle) \\ &= \langle v_c|n_c\rangle + \epsilon\,(\langle v_c|n_\epsilon\rangle + \langle v_\epsilon|n_c\rangle) + \epsilon^2\,\langle v_\epsilon|n_\epsilon\rangle\,. \end{aligned}$$

The term $\langle v_c|n_c\rangle$ is equal to zero since it gives the global velocity when $\epsilon = 0$ and the term $\epsilon^2\,\langle v_\epsilon|n_\epsilon\rangle$ vanishes in the limit $\epsilon \to 0$. For the lattice that we study, we find that the velocity of the particle on the lattice is $v = \frac{15}{56}\epsilon$. In order to relate the velocity and the diffusivity, we should evaluate the normalized velocity with respect to $v_0$. Note that we have $v_0 = P_{+x} - P_{-x} = \epsilon/2$. Then, the normalized diffusivity in the $+x$ direction for the lattice that we took as an example is given by:

$$\frac{D}{D_0} = \lim_{\epsilon\to 0}\frac{v}{v_0} = \frac{15\epsilon/56}{\epsilon/2} = \frac{15}{28} \approx 0.535714. \tag{55}$$

We can see that we don't need to know the value of $\epsilon$ for this method to find the diffusivity since $\epsilon$ cancels out at the last step of the calculation. This closes the demonstration of the exact solution for the LMC Algorithm. The method allows us to obtain the exact diffusion coefficient for any given obstacle configuration. The method works only for finite size lattices and it is thus necessary to impose periodic boundary conditions. In order to obtain the diffusivity close to the thermodynamic limit, it is also necessary to use very large systems.

## 1.5 Markov Chains

A Markov process is a stochastic process characterized by the fact that to predict the next state of a system, one only needs information about the present state [27]. That means there is no memory effect in the process. The process can be described by the following relation:

$$p(t+1) = Tp(t) = T^t p(t=0). \tag{56}$$

In this relation, $p(t)$ represents the state of the system at step $t \in N$, and $T$ is the transition matrix. Indeed, for the diffusion problem over the lattice, $p(t)$ is the probability vector that contains the probability of presence of the particle on each site at time $t$, the transition matrix $T$ contains all the jumping probabilities of the particle over the lattice corresponding to the LMC algorithm. The initial state (location) of the particle is defined by $p(0)$.

Let's consider the lattice of size $3\times3$ defined in Fig. 5 in Section 1.4. For this example, we apply repulsive boundary conditions at the edges of the lattice. When there is no external field, the transition matrix is given by

$$T \equiv \frac{1}{4}\begin{pmatrix} 3 & 0 & 1 & 0 & 0 & 0 & 0 \\ 0 & 3 & 0 & 0 & 1 & 0 & 0 \\ 1 & 0 & 2 & 1 & 0 & 0 & 0 \\ 0 & 0 & 1 & 1 & 1 & 1 & 0 \\ 0 & 1 & 0 & 1 & 1 & 0 & 1 \\ 0 & 0 & 0 & 1 & 0 & 2 & 1 \\ 0 & 0 & 0 & 0 & 1 & 1 & 2 \end{pmatrix}. \tag{57}$$

If the particle starts its motion on site number 4, the initial probability vector is

$$p(0) = (0,0,0,1,0,0,0)^T. \tag{58}$$

The symbol $(T)$ stands for transpose. Applying the Markov process, at the first time step, we have

$$p(t=1) = Tp(0) = (0,0,1/4,1/4,1/4,1/4,0)^T. \tag{59}$$

After the second time step, the probability is given by

$$p(t=2) = Tp(1) = (1/16, 1/16, 3/16, 1/4, 1/8, 3/16, 1/8)^T . \tag{60}$$

The steady state is obtained after an infinite number of iterations and is given by

$$p(\infty) = T^{\infty}p(0) = (1/7, 1/7, 1/7, 1/7, 1/7, 1/7, 1/7)^T . \tag{61}$$

This shows how one apply the Markov process to study the diffusion process over a 2D lattice.

## 1.6 Random systems

A random system is a system that contains a population of randomly distributed obstacles. There are many ways to randomly populate a given medium with obstacles. For example, one can place the obstacles and let them diffuse; one can also simply place the obstacles by randomly selecting a site and if the selected site is already occupied we try again until we find a free site. The latter method is the one that we have used.

To obtain the diffusion coefficient for a particle moving in a system randomly populated with obstacles, at a given concentration of obstacles, we have to find the diffusion coefficient for each configuration of obstacles in the system. The diffusivity of the particle in the system is then obtained by averaging all the diffusion coefficients over the set of configurations of obstacles.

## 1.7 Correlation length

The correlation length $\xi$ of a medium is defined as the mean distance between two sites on the same aggregate and represents the characteristic length scale in percolation. For any random system, the correlation length is known to increase as the concentration of obstacles increases. When periodic boundary conditions (PBCs) are applied to a system, if the size $L$ of the system is much larger than the correlation length ($L \gg \xi$), the system looks infinite and consequently, all particles moving over such systems will be able to reach the true steady state. This is the thermodynamic limit.

As the concentration of obstacles $\phi$ gets close to the percolation threshold $\phi^*$, the correlation length of the obstacles increases as: [28]

$$\xi \propto |\phi - \phi^*|^{-\sigma} . \tag{62}$$

The percolation threshold $\phi^*$ is the concentration limit beyond which the particles can not continue to diffuse over long distances in the medium. For a 2D square lattice, $\sigma = 4/3$ and when the lattice is crowded with random obstacles of size $1 \times 1$, we have $\phi^* = 40.7254\%$ [19]. Thus, for $\phi > \phi^*$ the diffusivity of the particle in the medium is simply equal to zero in the thermodynamic limit. When we have $L \gg \xi$ the system looks infinite but, for $L < \xi$, the particle motion is affected by finite size effects and thus, the particle never reaches the true steady state regime. As we approach $\phi = \phi^*$ the correlation length $\xi$ diverges and it becomes impossible to properly simulate those systems in the thermodynamic limit.

It is important to consider the size of the system when studying random systems because the concentration of obstacles will have a great impact on the correlation length.

## 1.8 Presentation of the thesis

In the second Chapter of this thesis, which is a manuscript to be submitted for publication, we first present our modified LMC algorithm for a particle moving over a lattice, including the fact that during a given time step it can stay at the same position, and we show that with this algorithm, the correction factor of the fourth order moment of the distribution of displacements decreases three time faster than the one of the standard algorithm. We describe the methodologies on which our thesis is based, namely the long time exact solution for the LMC algorithm, as well as the Markov process which allows us to study the short time propagation of the particle. Using these methodologies, we give a meaningful description of the particle's motion in a medium crowded with obstacles of different sizes. Thereby, after estimating the anomalous exponent $\alpha$, the excess short time diffusion $\beta$ that appears because anomalous diffusion is faster than normal diffusion is evaluated. The crossover length $r^*$ and the crossover time $t^*$ of the point characterizing the limit between the transient regime and the steady state are presented. We end this Chapter by showing that $\beta$ and $r^*$ are related to each other by a function of $\alpha$. The study done here presents the analysis of the particle's motion in media crowded firstly with periodic obstacle distributions and secondly with random obstacle distributions. In Chapter 3, we present supplementary results that we couldn't present in Chapter 2. We end this thesis with a Conclusion in Chapter 4 and the data are given in a series of Tables in Chapter 5.

# 2

# Random walk on a lattice in the presence of obstacles: The short-time transient regime, anomalous diffusion and crowding.

Nguiya P. Neo, Gary W. Slater.

# Random walk on a lattice in the presence of obstacles: The short-time transient regime, anomalous diffusion and crowding.

Nguiya P. Neo and Gary W. Slater
*Department of Physics, University of Ottawa,*
*Ottawa, Ontario K1N 6N5, Canada*

(Dated: April 29, 2019)

The diffusion of a particle in a crowded environment typically proceeds through three regimes: for very short times the particle diffuses freely until it collides with an obstacle for the first time, while for very long times diffusion the motion is Fickian with a diffusion coefficient $D$ that depends on the concentration and type of obstacles present in the system. For intermediate times, the mean-square displacement of the particle often increases approximately as $t^\alpha$, with $\alpha < 1$, typical of what is generally called anomalous diffusion. However, it is not clear how one can identify or choose a time or displacement interval that would give a reliable estimate of $\alpha$. In this paper, we use two exact numerical approaches to obtain diffusion data for a simple Lattice Monte Carlo model in both time limits. This allows us to propose an objective definition of the transient regime and a unique value for $\alpha$. Furthermore, our methodology directly gives us the length scale over which the transient regime switches to the steady-state regime. We test our proposed approach using several types of obstacle systems, and we introduce the novel concept of excess diffusion lengths. Finally, we show that the values of the parameters describing the anomalous transient regime depend on the Monte Carlo moves used to describe the dynamics of the particle, and we propose a new algorithm that correctly models the short time diffusion of a particle on a lattice.

## I. INTRODUCTION

Diffusive transport taking place in media crowded by immobile and passive obstacles continues to be a source of intense discussions. Diffusion of a particle in such systems should show three regimes. In the first regime the particle simply undergoes free diffusion until it starts colliding with obstacles [1] (this regime is essentially absent in very crowded systems). For long times and large distances, on the other hand, one would expect normal diffusion where the mean square displacement (MSD) increases linearly with time $t$: $\langle r^2(t)\rangle = 2dDt$, with $D$ the diffusion coefficient and $d$ the dimensionality of space. Many researchers characterize the intermediate or transient regime by fitting the data using the expression that defines the concept of anomalous diffusion

$$\langle r^2(t)\rangle = 2dD_\alpha t^\alpha, \tag{1}$$

where $\alpha$ is the anomalous exponent and $D_\alpha$ is often called the anomalous diffusion coefficient although it does not have the proper units unless $\alpha = 1$. We have Fickian diffusion when $\alpha = 1$, anomalous subdiffusion when $\alpha < 1$, and superdiffusion when $\alpha > 1$ [2].

In practice, using eq. (1) to characterize the transient regime of simulation or laboratory data is not trivial. Indeed, it is generally unclear whether there is a range of times for which a unique value of $\alpha$ exists; the presence of error bars can hide the fact that $\alpha$ may be time-dependent (which would make it a much less useful parameter). Identifying the time interval, or equivalently the displacement interval, that one should use to estimate $\alpha$ is often somewhat subjective and non-reproducible. A good example is provided by the work of Ellery et al [2] in which the anomalous exponent has been estimated by considering a given interval of the transient regime, and then fitting the MSD in that interval in order to get the exponent $\alpha$. In fact that interval was the same for all obstacle concentrations in the medium.

In principle, the transition to the $\alpha = 1$ steady-state occurs when the particle has diffused over distances comparable to the correlation length of the obstacles, $\lambda$, assuming that the system size $L_o > \lambda$. Identifying the limits of the transient regime should thus provide us with an estimate of $\lambda$. The central question is thus how one can objectively define the limits of the transient regime and find a reliable estimate of $\alpha$ and $D_\alpha$.

In this article, we present a detailed analysis of the transition to the steady-state for diffusion on crowded two-dimensional lattices, both for periodically and randomly distributed immobile obstacles. As such lattice models are used to study diffusion in real environments, we also examine the type of Monte Carlo moves that better represent diffusion in the continuum limit. We use two numerical methods that provide us with exact data for short and long times, thus avoiding the pitfalls of fitting data with error bars. We propose an objective way to estimate the value of $\alpha$ and the time at which the transition to normal diffusion takes place. We also propose a way to understand the values of $D_\alpha$ in spite of the fact that the units of $D_\alpha$ depend on $\alpha$. Finally, we introduce a new length scale, the excess diffusion length $\beta$, and we show how it is related to the parameters of

the transient and steady- state regimes.

This article is structured as follows. In Section II, we describe the Lattice Monte Carlo (LMC) model that we use and the various algorithms employed to obtain exact numerical results. In Section III we present the methodology and Data analysis that allows us to obtain our results. Section IV present the different results obtained taking into account the obstacles distributions that we used. We end this paper with a discussion in Section V.

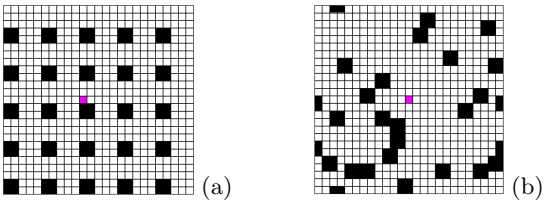

FIG. 1. The lattice random-walk model studied here. The lattice is of size $25 \times 25$ in this example while the obstacles are of size $2 \times 2$ (in black) and the diffusing particle (in red) is of unit size. Periodic boundary conditions are used. (a) Periodically distributed obstacles with a surface concentration of $\phi = \frac{4}{25}$. (b) Randomly distributed non-overlapping obstacles with the same concentration.

## II. METHODS: LMC ALGORITHMS

### A. The Random Walk model

We study the diffusion of a particle in the presence of immobile obstacles by using a Monte Carlo model for the random walk of a particle on a two dimensional square lattice with fixed obstacles (see Fig. 1 for two examples). We do not study the role of the particle size, and thus the latter is simply the lattice mesh size.

In the spirit of Lattice Monte Carlo (LMC) models, at each time step the particle can move to a neighbouring site along the $\hat{x}$ or the $\hat{y}$ axis, or stay put. If the selected move makes the particle overlap with an obstacle, the move is rejected but the jump time is added to the clock.

We will be using two versions of this LMC model. In the first one, the probability of staying put is zero and the probability of jumping to each of the four neighbouring sites is thus $\frac{1}{4}$. In the second version, the probability of staying put will be chosen in such a way that we can better represent the short time dynamics of the particle. Both versions are described in Section II B below.

The long-time diffusion coefficient of the particle in a system with periodic boundary conditions (PBC) is calculated using the numerical method described in Section II C. For short times, the MSD is obtained using the Markov chain method described in Section II D.

### B. Derivation of the LMC parameters for a free particle (no obstacles)

The theoretical arguments presented here are based on previous work by our group [3]. However, we will not allow diagonal moves because it is unclear how one would then treat collisions with the obstacles. We thus consider a 2D square lattice (Fig. 1) and the jumping probabilities shown in Fig. 2. Since the system is isotropic, we can set $p_{\pm x} = p_{\pm y} \equiv p_1 = \frac{1}{4}(1 - p_o)$, where $p_o$ is the probability of staying put during a LMC iteration. The master equation for the probability $n_{j,l}(t)$ for the particle to be on site $(j, l)$ at time $t$ is

$$n_{j,l}(t+\tau) = p_o n_{j,l}(t) + p_1 \left[ n_{j-1,l}(t) + n_{j+1,l}(t) + n_{j,l+1}(t) + n_{j,l-1}(t) \right], \quad (2)$$

where $\tau$ is the LMC time step.

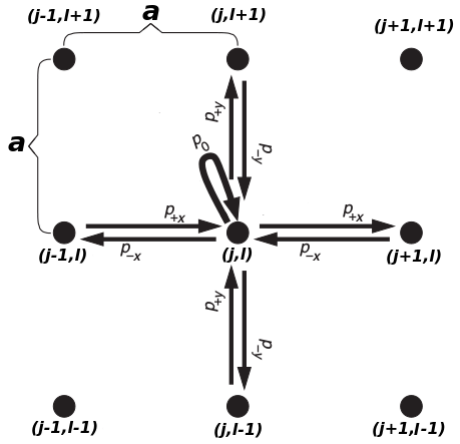


FIG. 2. A schematic of the general $2d$ LMC algorithm considered in this paper. Only moves to and from site $(j, l)$ are shown. In addition to the traditional axial moves (arrows of medium thickness), there is a probability to stay put (the thickest arrow). **a** is the length of a site.

The general solution of this system of equations is

$$n_{j,l}(t) = \int_{-\pi/a}^{\pi/a} \int_{-\pi/a}^{\pi/a} C(k_x, k_y) dk_x dk_y \times \exp\left[ i k_x a j + i k_y a l - \omega_d(k_x, k_y) t \right], \quad (3)$$

where $C(k_x, k_y)$ is an arbitrary complex function, $k_x$ and $k_y$ represent the wave number in each of the two directions respectively, and $\omega_d$ is the frequency (the subscript $d$ means that we are in a discrete medium). Substituting eq. (3) into eq. (2) we obtain the dispersion relation

$$\omega_d(k_x, k_y) = -\frac{\ln\left[ p_o + 2p_1(\cos(k_x a) + \cos(k_y a)) \right]}{\tau}. \quad (4)$$

Considering the solution of the diffusion equation for the longest length scales i.e. for small k, we expand eq. (4) to the fourth order, and using the fact that $p_0 = 1 - 4p_1$, we obtain

$$\omega_d(k_x,k_y) = \frac{p_1 a^2}{\tau}\left[(k_x^2+k_y^2) + p_1 a^2 k_x^2 k_y^2 + a^2\left(\tfrac{1}{2}p_1 - \tfrac{1}{12}\right)\times\left(k_x^4+k_y^4\right) + O(k^6)\right]. \quad (5)$$

Such lattice models are designed to reproduce the properties of the diffusion equation

$$\frac{\partial n(x,y,t)}{\partial t} = D_o\left(\frac{\partial^2 n(x,y,t)}{\partial x^2} + \frac{\partial^2 n(x,y,t)}{\partial y^2}\right), \quad (6)$$

where $D_o$ is the diffusion coefficient for a free particle. The general solution of this equation is

$$n_{x,y}(t) = \int_{-\infty}^{\infty}\int_{-\infty}^{\infty} C(k_x,k_y)dk_x dk_y \times \exp[ik_x x + ik_y y - \omega_c(k_x,k_y)t], \quad (7)$$

where the subscript $c$ stands for continuum. From eqs. (6) and (7) we obtain the dispersion relation

$$\omega_c = D_o\left(k_x^2+k_y^2\right). \quad (8)$$

### 1. The solution of the diffusion equation and its moments

In two dimensions the solution of the diffusion equation for the initial condition $n(r,0) = \delta(r)$ is the Gaussian distribution

$$n(r,t) = \frac{1}{4\pi D_o t}\exp\left(-\frac{r^2}{4D_o t}\right), \quad (9)$$

The second and fourth moments of this distribution are

$$\left\langle r^2(t)\right\rangle_{\rm G} = 4D_o t, \quad (10)$$

$$\left\langle r^4(t)\right\rangle_{\rm G} = 2\left\langle r^2(t)\right\rangle_{\rm G}^2 = 32 D_o^2 t^2, \quad (11)$$

where the G subscript refers to the Gaussian distribution. These two results will now be used to design and test the accuracy of LMC algorithms.

### 2. The standard LMC algorithm

The simplest LMC algorithm is found when we only match the second order terms in eqs. (5) and (8); this leads to the condition

$$p_1 a^2/\tau = D_o. \quad (12)$$

Given eq. (10), this relation immediately gives

$$p_1 = \tfrac{1}{4}, \quad (13)$$

and hence a probability $p_o = 0$ of staying put. In other words, the particle must attempt a move at each time step, and the duration of the latter is

$$\tau = a^2/4D_o. \quad (14)$$

This is the standard LMC model described in almost all textbooks and frequently used in research.

In order to better understand the performance of this algorithm, we first evaluate the mean-square displacement of a free particle after $N$ time steps, $\left\langle r^2(N)\right\rangle = \left\langle x^2(N)\right\rangle + \left\langle y^2(N)\right\rangle$. In the $\hat{x}$-direction we have

$$\begin{aligned}\left\langle x^2(N)\right\rangle &= \Big\langle \tfrac{1}{4}\left(x(N-1)+a\right)^2 + \tfrac{1}{4}\left(x(N-1)-a\right)^2 \\ &\quad + \tfrac{2}{4}x^2(N-1)\Big\rangle \\ &= \left\langle x^2(N-1)\right\rangle + \tfrac{1}{2}a^2. \end{aligned} \quad (15)$$

Applying this relation recursively we obtain

$$\left\langle x^2(N)\right\rangle = \tfrac{1}{2}Na^2. \quad (16)$$

Since $\left\langle y^2(N)\right\rangle = \left\langle x^2(N)\right\rangle$, the second moment is simply

$$\left\langle r^2(N)\right\rangle = Na^2. \quad (17)$$

The time duration of $N$ steps being $t = N\tau$, eqs. (14) and (17) give $\left\langle r^2(N)\right\rangle = 4D_o t$, which is eq. (10). The standard algorithm thus gives the correct second moment of the distribution of displacements, as expected.

Let us now compute the fourth moment

$$\begin{aligned}\left\langle r^4(N)\right\rangle &= \left\langle \left(x^2(N)+y^2(N)\right)^2\right\rangle \\ &= \left\langle x^4(N)\right\rangle + \left\langle y^4(N)\right\rangle \\ &\quad + 2\left\langle x^2(N)y^2(N)\right\rangle. \end{aligned} \quad (18)$$

We start by calculating

$$\begin{aligned}\left\langle x^4(N)\right\rangle &= \Big\langle \tfrac{2}{4}x^4(N-1) + \tfrac{1}{4}\left(x(N-1)+a\right)^4 \\ &\quad + \tfrac{1}{4}\left(x(N-1)-a\right)^4\Big\rangle \\ &= \tfrac{1}{2}a^4 + \left\langle x^4(N-1)\right\rangle \\ &\quad + 3a^2\left\langle x^2(N-1)\right\rangle. \end{aligned} \quad (19)$$

Applying this expression recursively, we obtain

$$\left\langle x^4(N)\right\rangle = \tfrac{1}{4}N(3N-1)a^4, \quad (20)$$

and similarly for $\left\langle y^4(N)\right\rangle$. The term $\left\langle x^2(N)y^2(N)\right\rangle$ is more subtle. Here, $N$ means that a total of $N$ steps were made with, on average, half of them in each of the

two Cartesian directions. However, if the particle makes $n$ steps in the $x$ direction, it has to make $N-n$ steps in the $y$ direction, hence the constraint that we must take into account while estimating these cross terms. We thus have to average over both the value of $n$ and an ensemble of walks all with the same value of $n$ (subscript $ens$):

$$\begin{aligned}\left\langle x^2(N)y^2(N)\right\rangle &= \left\langle \left\langle x^2(n)y^2(N-n)\right\rangle_{ens}\right\rangle_n \\ &= \left\langle na^2(N-n)a^2\right\rangle_n \\ &= \left\langle n\right\rangle_n Na^4 - \left\langle n^2\right\rangle_n a^4. \end{aligned} \tag{21}$$

The probability $q_N(n)$ for the particle to make $n$ of its $N$ jumps in the $\hat{x}$ direction is the binomial distribution

$$q_N(n) = \frac{N\,!}{n\,!N-n\,!}\left(\frac{1}{2}\right)^N. \tag{22}$$

The moments can then be calculated using

$$\left\langle n^j\right\rangle_n = \sum_{n=0}^{N} q_N(n)n^j; \tag{23}$$

we obtain $\left\langle n\right\rangle_n = \frac{1}{2}N$ and $\left\langle n^2\right\rangle_n = \frac{1}{4}N(N+1)$. Therefore, the correlation term gives

$$\left\langle x^2(N)y^2(N)\right\rangle = \tfrac{1}{4}N(N-1)a^4, \tag{24}$$

and the fourth moment becomes

$$\left\langle r^4(N)\right\rangle = N(2N-1)a^4. \tag{25}$$

Substituting $N = t/\tau$ and $D_o = a^2/(4\tau)$, we obtain

$$\left\langle r^4(t)\right\rangle = 32D_o^2t^2 - 4a^2D_ot. \tag{26}$$

Comparing this result to eq. (11) we obtain

$$\frac{\left\langle r^4(t)\right\rangle}{\left\langle r^4(t)\right\rangle_{\rm G}} = 1 - \frac{a^2}{8D_ot}. \tag{27}$$

The standard LMC algorithm thus underestimates the $4^{th}$ moment by a term $\sim 1/t$; as a consequence, the distribution of displacements is narrower than a Gaussian. This impacts short time dynamics since the first collisions with obstacles are delayed. The standard LMC algorithm is frequently used to investigate anomalous diffusion (see, *e.g.*, Ellery et al [2, 4, 5]); while it does produce the right second moment, and hence the right diffusion coefficient at long times, it is not reliable for short times where first-passage issues (such as colliding with the nearest obstacle) are key. We will now derive an improved LMC algorithm that gives a smaller $\sim 1/t$ term.

### *3. An improved LMC algorithm*

In order to improve upon the standard LMC algorithm, we can try to match both the $k^2$ and $k^4$ terms in eqs. (8) and (5). Since eq. (5) does not include terms of order $k^4$, we need to find how to cancel these terms in eq. (8). However, the cross-product $p_1^2a^4k_x^2k_y^2$ cannot be eliminated unless $p_1 = 0$, the trivial solution where the particle does not move. We thus restrict ourselves to the other two terms, leading to eq. (12) and

$$\tfrac{1}{2}p_1 - \tfrac{1}{12} = 0 \quad \Rightarrow \quad p_1 = \tfrac{1}{6}\ ;\ p_o = \tfrac{1}{3}. \tag{28}$$

According to eq. (12) the required time step is then

$$\tau = a^2/6D_o. \tag{29}$$

The LMC time step is shorter than for the standard LMC algorithm, eq. (14), because the particle stays put with a probability $p_o = \frac{1}{3}$. The particle thus requires

$$m = 1/(1-p_o) = \tfrac{3}{2} \tag{30}$$

time steps, on average, before attempting a jump. Accordingly, the duration of the LMC steps in this modified algorithm must be shortened by a factor of $1/m = 2/3$ in order to keep $D_o$ constant.

We now compute the second moment:

$$\begin{aligned}\left\langle x^2(N)\right\rangle &= \Big\langle \tfrac{4}{6}x^2(N-1) + \tfrac{1}{6}\left(x(N-1)+a\right)^2 \\ &\qquad + \tfrac{1}{6}\left(x(N-1)-a\right)^2\Big\rangle \\ &= \left\langle x^2(N-1)\right\rangle + \tfrac{1}{3}a^2. \end{aligned} \tag{31}$$

Applying this expression recursively we obtain

$$\left\langle x^2(N)\right\rangle = \tfrac{1}{3}Na^2, \tag{32}$$

and similarly for $\left\langle y^2(N)\right\rangle$. We thus have

$$\left\langle r^2(N)\right\rangle = \tfrac{2}{3}Na^2. \tag{33}$$

Since $N = t/\tau = 6Dt/a^2$, we recover $\left\langle r^2(t)\right\rangle = 4Dt$. The fourth order moment in $x$ is given by

$$\begin{aligned}\left\langle x^4(N)\right\rangle &= \Big\langle \tfrac{4}{6}x^4(N-1) + \tfrac{1}{6}\left(x(N-1)+a\right)^4 \\ &\qquad + \tfrac{1}{6}\left(x(N-1)-a\right)^4\Big\rangle \\ &= \left\langle x^4(N-1)\right\rangle + 2a^2\left\langle x^2(N-1)\right\rangle \\ &\quad + \tfrac{1}{3}a^4. \end{aligned} \tag{34}$$

Applying this expression recursively we obtain

$$\left\langle x^4(N)\right\rangle = \tfrac{1}{3}N^2a^4, \tag{35}$$

and similarly for $\langle y^4(N)\rangle$. Once again, the only remaining part to be calculated in eq. (18) is the cross-correlation $\langle x^2(N)y^2(N)\rangle$. Here, if the particle makes $n$ steps in the $x$ direction, it must make $N-n-n_0$ steps in the $y$ direction, where $n_0$ is the number of times the particle stayed put. We can thus write

$$\begin{aligned}\langle x^2(N)y^2(N)\rangle &= \left\langle \langle x^2(n)y^2(N-n-n_0)\rangle_{ens}\right\rangle_{\{n,n_0\}} \\ &= \left\langle na^2(N-n-n_0)a^2\right\rangle_{\{n,n_0\}} \\ &= \left(N\langle n\rangle_n - \langle nn_0\rangle_{\{n,n_0\}} - \langle n^2\rangle_n\right)a^4. \end{aligned} \tag{36}$$

We can use eq. (23) to compute two of the terms, but the probability $q_N(n)$ is now given by:

$$q_N(n) = \frac{N\,!}{n\,!N-n\,!}\left(\frac{1}{3}\right)^n\left(\frac{2}{3}\right)^{N-n}. \tag{37}$$

This gives

$$\langle n\rangle_n = \tfrac{1}{3}N; \qquad \langle n^2\rangle_n = \tfrac{1}{9}N(N+2). \tag{38}$$

Calculating $\langle nn_0\rangle_{\{n,n_0\}}$ requires the joint probability $q_N(n,n_0)$ of having a walk with $n$ jumps in the $\hat{x}$ direction and $n_0$ iterations without a jump:

$$\langle nn_0\rangle_{\{n,n_0\}} = \sum_{n=0}^{N}\sum_{n_0=0}^{N-n} q_N(n,n_0)nn_0. \tag{39}$$

Since the particle has three equally probable choices at each step (i.e., moving in the $\hat{x}$-direction, the $\hat{y}$-direction or not moving), the probability $q_N(n,n_0)$ is simply

$$q_N(n,n_0) = \frac{N\,!}{n\,!n_0\,!(N-n-n_0)\,!}\left(\frac{1}{3}\right)^N. \tag{40}$$

Using this function, we obtain

$$\langle n.n_0\rangle_{\{n,n_0\}} = \tfrac{1}{9}N(N-1). \tag{41}$$

The cross-correlation term is thus given by

$$\begin{aligned}\langle x^2(N)y^2(N)\rangle &= \tfrac{1}{3}N^2a^4 - \tfrac{1}{9}N(N-1)a^4 - \tfrac{1}{9}N(N+2)a^4 \\ &= \tfrac{1}{9}N\,(N-1)\,a^4. \end{aligned} \tag{42}$$

Substituting eqs. (35) and (42) in (18) we get

$$\langle r^4(N)\rangle = \tfrac{2}{9}\left(4N^2-N\right)a^4. \tag{43}$$

Since $N = t/\tau$ and $\tau = a^2/(6D_o)$, we can write

$$\langle r^4(t)\rangle = 32D_o^2t^2 - \tfrac{4}{3}a^2D_ot. \tag{44}$$

Comparing with eq. (11) we obtain

$$\frac{\langle r^4(t)\rangle}{\langle r^4(t)\rangle_{\rm G}} = 1 - \frac{a^2}{24D_ot}. \tag{45}$$

Just like in eq. (27), we have the correct leading term for the fourth moment, but the $\sim 1/t$ correction term is now three times smaller. This alternative algorithm, which allows the particle to stay put during a LMC step, is thus better at capturing short time dynamics. Although it is possible to eliminate the $\sim 1/t$ correction term by allowing diagonal jumps [3], this would lead to unclear difficulties when treating collisions with obstacles.

### C. Long time Exact solution for LMC algorithms

To compute the long time particle diffusivity, we use the numerical method introduced in [6, 7] since it produces exact results when using PBCs. The idea is that while the diffusion coefficient $D_x$ along $\hat{x}$ is not readily accessible for most obstacle configurations, it is relatively easy to calculate the particle's reduced velocity $v_x/v_{xo}$ in the presence of an external force oriented along $\hat{x}$ ($v_{xo}$ is the velocity in absence of obstacles). The diffusivity is then obtained via the Nernst-Einstein relation $D_x/D_{xo} = v_x/v_{0x}$ in the zero-force limit.

Velocity calculations can be reduced to solving a set of $N$ coupled linear equations, where $N$ is the number of available lattice sites. These equations can be written as a transition matrix $T$ containing the jumping probabilities between the different lattice sites. We have previously shown that it is possible to algebraically simplify the matrix problem and the passage to the zero-force limit such that the only remaining step is the numerical inversion of a matrix. Note that in the presence of disorder, the final diffusivity must also be averaged over an ensemble of different obstacle configurations. The numerical procedures are fully described in [6, 7].

### D. Markov process

A Markov process is characterized by the fact that predicting the next state of the system only requires information about the present state, *i.e.*, there are no memory effect. Symbolically, it is thus possible to write

$$|p(t+1)\rangle = T\,|p(t)\rangle = ... = T^t\,|p(t=0)\rangle\,, \tag{46}$$

where $|p(t)\rangle$ is the state of the system at step $t \in \mathbb{N}$ and $T$ is the transition matrix defining the evolution of $|p\rangle$. For our diffusion problem, $|p(t)\rangle$ is a vector that includes the probability for the particle to be on each of the accessible lattice sites at time $t$, $|p(0)\rangle$ is the initial location of the particle, and $T$ is a matrix that contains the jumping probabilities for the chosen LMC process.

The $1\times 1$ particle has access to $L_o^2(1-\phi)$ sites, where $L_o$ is the size of the lattice. In practice, we use a large value $L_o = 500$. Since we start the particle in the centre,

the value of $t$ is limited to about 249 since we cannot use PBC here. For systems with large correlation lengths $\lambda$, larger lattices may be needed to study the initial stages of diffusion via this approach. From the state vector $|p(t)\rangle$, one can easily obtain the exact distribution of displacement at time $t$ and all of its moments.

## III. METHODS: DATA ANALYSIS

We now introduce our methodology and test it using a system of $2 \times 2$ obstacles placed periodically in $5 \times 5$ primitive cells, giving $\phi = \frac{4}{25}$ (Fig. 1a). From now on, numerical data will be given using the mesh size $a$ as the unit of length, times will be in units of $a^2/D_o$ and diffusion coefficients will be in units of $D_o$.

### A. Plotting MSD data

Although the particle can start from 21 different initial positions in the primitive cell, only 5 of these are unique. Figure 3 shows two different log-log representations of the time evolution of the MSD, both for each of these 5 sites individually and for the MSD averaged over all 21 initial sites. The $\langle r^2(t)\rangle$ *vs.* $t$ plot, Fig. 3a, is clearly not useful. Instead, it is better to plot the diffusion ratio $\langle r^2(t)\rangle/4t$ *vs.* $t$, Fig. 3b, as we then see clear features. Since $\lim_{t\to\infty}\langle r^2(t)\rangle/4t = D$, this plot also provides us with an estimate of the long-time diffusion coefficient.

Let us examine Fig. 3b in detail. The MSD curves start from two different values after the first step (solid lines); this is because some starting sites are adjacent to an obstacle, while most are not. In the latter case, we find $D = 1$ because the particle behaves initially as a free particle until it hits an obstacle. The other value is lower since the particle then starts next to an obstacle and can thus hit it immediately. Such MSD curves correspond to experimental situations where all the particles of a sample start from the same location. When we average over all possible starting positions, which is equivalent to having a sample in equilibrium with the medium (the most common assumption), we obtain the dashed curve. All curves converge to the value of the exact long-time diffusion coefficient, as expected. However, it is clear that the intermediate regime greatly depends on the initial state of the system: none of the solid curves behave like the dashed curve, and two of them are even non-monotonic. It is simply not possible to define an anomalous exponent $\alpha$ for the solid curves.

As mentioned above, a uniform initial distribution (the dashed curve) is the standard choice. We will thus analyze this data to identify the intermediate and steady-state regimes. In order to estimate the anomalous exponent $\alpha$, we rewrite eq. (1) as:

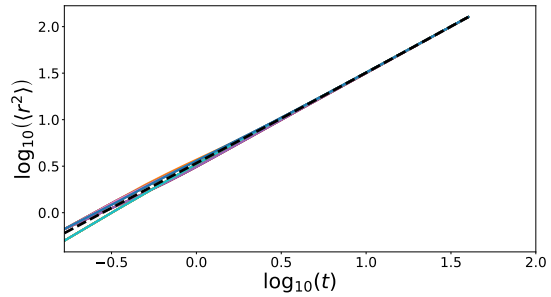


(a)

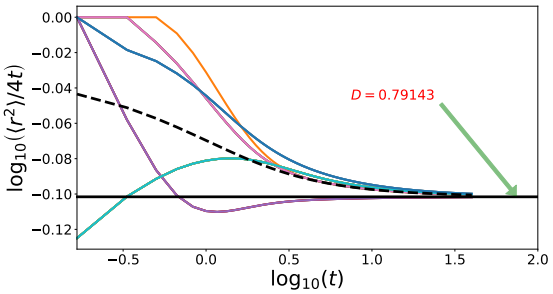


(b)

FIG. 3. Two different ways to plot the time evolution of the MSD on a log-log diagram. The y-axis shows (a) $\langle r^2(t)\rangle$, or (b) $\langle r^2(t)\rangle/4t$. The solid lines give the data for the different starting sites, while the dashed line gives the mean value. The horizontal line in (b) shows the long-time plateau corresponding to the exact value of $D = 0.79143$.

$$\log\left(\langle r^2(t)\rangle/4t\right) = (\alpha-1)\log(t) + \log(D_\alpha). \qquad (47)$$

If there is indeed a regime where eq. (1) applies, then it should show up as a straight line with a (negative) slope of $\alpha-1$ [2]; however, it is not obvious where it is located in Fig. 3b, or even if it exists at all.

### B. Estimating the anomalous exponent $\alpha$

Figure 4 shows the same data together with the construct that we propose to estimate $\alpha$ and locate the transition to the steady-state. The only non-arbitrary point that can be identified here is the inflection point separating short times (positive second derivative) and long times (negative second derivative). In our opinion, this should define the centre of the intermediate regime. Accordingly, the tangent at the inflection point can be used to estimate the values of $\alpha$ and $D_\alpha$.

The intersection between this tangent and the long-time plateau can be used to define the crossover time $t^*$ at which the intermediate regime transitions into the

steady-state (the corresponding length scale is $r^* = \sqrt{4Dt^*}$). This approach is not arbitrary and allows us to uniquely characterize the transient phase in absence of a clear linear regime in Fig. 4.

It is easy to find the location of the crossover in terms of the parameters describing the transient and steady-state regimes. Indeed, by construction, the crossover time $t^*$ is the solution of eq. (47) where we replace the *lhs* by $log(D)$. The solution is simply

$$t^* = \left(\frac{D_\alpha}{D}\right)^{\frac{1}{1-\alpha}}, \tag{48}$$

which directly leads to

$$r^{*2} = 4\left(\frac{D_\alpha}{D^\alpha}\right)^{\frac{1}{1-\alpha}}. \tag{49}$$

Another interpretation of the crossover time will be in Section III D.

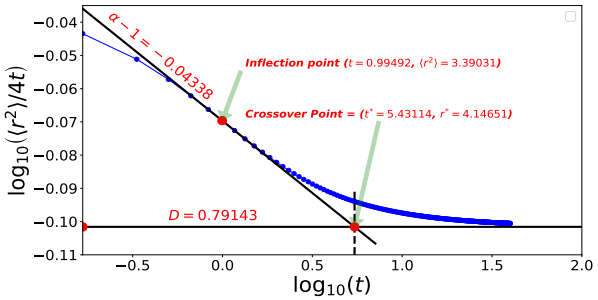


FIG. 4. Diffusion ratio $\langle r^2(t)\rangle/4t$ as a function of time. We also show the inflection point, the tangent used to estimate the anomalous exponent $\alpha = 0.95662$ and the value of the fitting parameter $D_\alpha = 0.85172$, the long-time diffusion plateau $D = 0.79143$, and the crossover point.

### C. Excess short-time diffusion

Diffusion is normal at long times: we then have $\alpha = 1$ in eq. (1). However, a particle initially diffuses faster because it takes several collisions with the obstacles to go from $D_o = 1$ to a steady state value $D < 1$. Indeed, all the data points are above the plateau value in Fig. 4. Therefore, in order to properly fit long time data and obtain a good value for $D$, we must use the expression

$$\langle r^2(t)\rangle = 4Dt + \beta^2, \tag{50}$$

where $\beta$ is the excess diffusion length due to the transient regime. Figure 5 presents a plot of $\beta$ *vs.* $1/\sqrt{t}$ for our example. The plateau value $\beta = 0.55215$ is reached at $t \approx t^*$. The length scale $\beta$ measures the importance of the transient, anomalous diffusion regime: $\beta < 1$ means that this regime has minimal importance, while values larger than the mean distance between obstacles would indicate large length scale effects.

One can also rewrite eq. 50 as

$$\langle r^2(t)\rangle = 4D(t + \tau_\beta), \tag{51}$$

where

$$\tau_\beta = \beta^2/4D \tag{52}$$

is the apparent excess time due to anomalous diffusion.

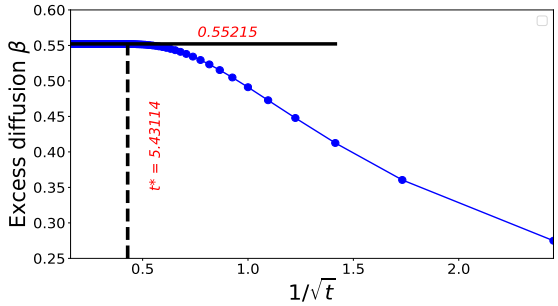


FIG. 5. Time evolution of the excess diffusion length $\beta$. The vertical dash line indicates the crossover time $t^*$. The asymptotic value is $\beta = 0.55215$, which corresponds to an excess time of $\tau_\beta = 0.17442$.

### D. Giving a physical meaning to $D_\alpha$

Clearly $D_\alpha$ is not a diffusion coefficient since its units depend on $\alpha$. Therefore, we cannot plot $D_\alpha$ vs. system parameters like $\phi$ (each data point would have its own unit of measurement). However, we may get useful information from the fitting parameters if we use a fitting function with proper units to replace eq. (1), such as

$$\langle r^2(t)\rangle = 4Dt\left(\frac{t}{t_\alpha}\right)^{\alpha-1}, \tag{53}$$

where the new fitting parameter $t_\alpha$ (replacing $D_\alpha$) is the time needed to *anomalously diffuse* over a distance $r_\alpha = \sqrt{4Dt_\alpha}$, i.e., the displacement that would have been achieved via normal diffusion (in other words, $r_\alpha^2 = 4Dt_\alpha = 4D_\alpha t_\alpha^\alpha$). But this is in fact the very definition of the crossover time in Fig. 4. Indeed, it is

easy to prove mathematically that $t_\alpha = t^*$ and $r_\alpha = r^*$. Alternatively, it is also possible to replace eq. (1) by

$$\langle r^2(t)\rangle = r_\alpha^2 \left(\frac{4Dt}{r_\alpha^2}\right)^\alpha, \tag{54}$$

where $r_\alpha = r^*$ would then replace $D_\alpha$ as the fitting parameter. However, eq. (53) is more intuitive.

In conclusion, the two physically meaningful fitting parameters are the anomalous exponent $\alpha$ and either the crossover time $t^*$ or the crossover distance $r^*$ (but not the oddly dimensioned parameter $D_\alpha$). We will be looking at both options in the Results section.

### E. Comparing the two Monte Carlo Algorithms

Figure (6) presents the MSD data obtained from both LMC algorithms; as expected they differ only at short times. Because the value of the correction factor for $\langle r^4(t)\rangle$ is three times higher with the standard LMC compare to the one obtained with the new LMC algorithm, the first collisions are delayed and the diffusion ratio $\langle r^2\rangle/4t$ is larger even slightly beyond the inflection point. The value of $\alpha$ is thus smaller with the standard LMC algorithm and the crossover distances $r^*$ and times $t^*$ are slightly underestimated.

It is interesting to note that this effect is sometimes inverted at high concentration when we have randomly distributed obstacles (see Chapter 3). In such cases, we believe that the fact that larger displacements are slightly less probable with the standard algorithm leads to longer trapping times in dense areas and hence smaller diffusion ratios $\langle r^2\rangle/4t$ (this is currently under investigation).

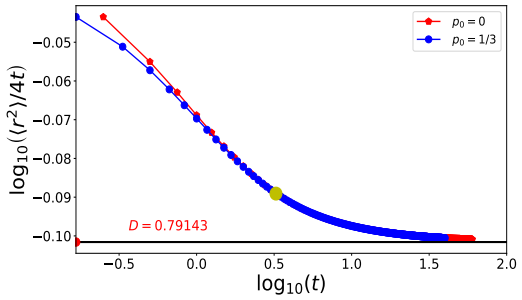


FIG. 6. Comparing the two LMC algorithms. The data sets differ by less than $10^{-5}$ starting at time $t = 3.2500$ and position $\langle r^2\rangle = 10.5892$ (the yellow circle). Key values for new algorithm: $\alpha = 0.95502$, $D_\alpha = 0.85172$, $r^* = 4.14651$ and $t^* = 5.43114$. For the standard algorithm, we obtain $\alpha = 0.95221$, $D_\alpha = 0.85329$, $r^* = 3.91002$ and $t^* = 4.82929$.

## IV. RESULTS

The data presented in this section were obtained using a square lattice of size $500 \times 500$ (for both short and long time calculations). We investigate various obstacle concentrations for three different obstacle sizes, namely $1 \times 1$, $2 \times 2$ and $3 \times 3$. We also compare periodic and random distributions of obstacles. For periodic systems of obstacles, the data is averaged over all possible starting positions in the periodic cell. For random systems, we average over 600 different realizations of the system of obstacles, and the starting position of the particle for the Markov chain is chosen randomly in a $10 \times 10$ box located in the centre of the lattice. We generally keep the obstacle concentration in the range $\phi \in [0.0, 0.4]$ to avoid problems with percolation thresholds [7].

### A. The asymptotic diffusion coefficient $D$

Figures 7 shows how the diffusivity $D$ varies with $\phi$. These results are in agreement with previous studies (see, *e.g.*, [7, 8]). For a given concentration $\phi$, large obstacles have less impact than small ones because aggregating obstacles increases the percolation threshold and leaves wider passages for the particle to migrate through. Our results also agree with the known value of the percolation threshold $\phi^* \approx 40.7254\%$ for unit size obstacles [7]. Note that the curvature of the $D(\phi)$ plots changes from positive for periodic obstacles to negative for random ones, a qualitative difference that we will see again later. As we showed in [8], we can get zero curvature (so that $D$ is a linear function of $\phi$) by creating *fuzzy* obstacle distributions.

### B. The excess diffusion length $\beta$

As mentioned before, the length scale $\beta$ can be used to measure the importance of the transient regime. Looking at Fig. 4, we can see that the area between the data points and the $D$ plateau, which is related to $\beta$, can increase either because $D$ decreases or because the crossover time $t^*$ decreases.

The random system is simpler, Fig. 8b: $\beta$ increases with concentration because $D$ decreases as $\phi$ increases, while both $t^*$ and $r^*$ increase because the correlation length of the obstacle distribution increases with $\phi$ (see section IV D). We note that the curves cross each other; this is due to the fact that the percolation threshold is larger for larger obstacles, which leads to a crossover time that diverges at lower concentrations for smaller obstacles (see Fig. 10b). Not surprisingly, we observe a very sharp increase of the excess diffusion time $\tau_\beta =$

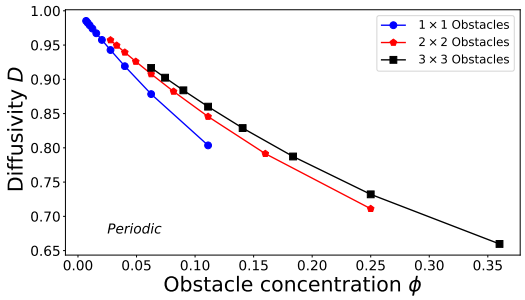


(a)

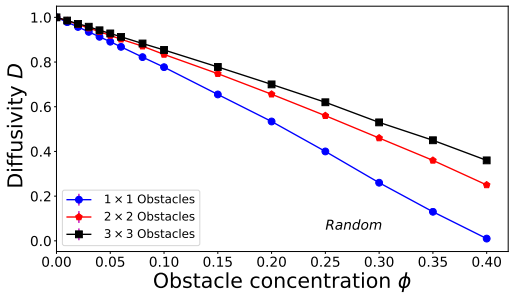


(b)

FIG. 7. Diffusivity $D$ *vs.* obstacle concentration $\phi$ for three different obstacle sizes. a) Periodically, and b) randomly distributed obstacles.

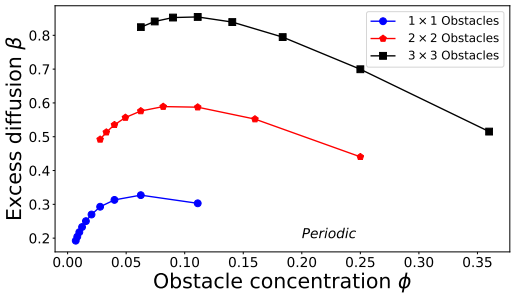


(a)

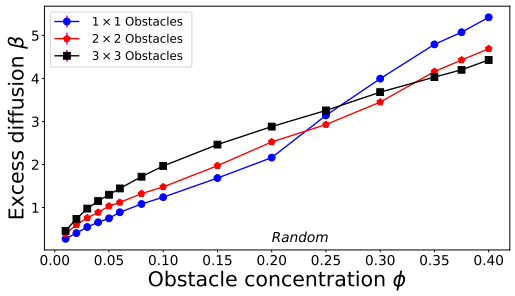


(b)

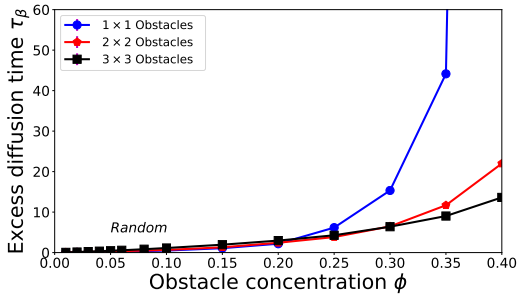


(c)

FIG. 8. Excess diffusion length $\beta$ vs. obstacle concentration $\phi$ for three different obstacle sizes. (a) Periodically, and (b) randomly distributed obstacles. (c) Excess diffusion time $\tau_\beta$ vs. $\phi$ for randomly distributed obstacles.

$\beta^2/4D$ when we approach the percolation concentration in Fig. 8c since $\beta$ increases while $D$ decreases.

Figure 8a shows that systems with periodic obstacles are very different: indeed, $\beta(\phi)$ is now a non-monotonic function. Here, as the concentration increases, both the diffusivity and the crossover time $t^*$ decrease. The competition between these two factors give a maximum at a critical value $\phi^*$ which depends on obstacle size. When $\phi < \phi^*$, $t^*$ is large but the exponent $\alpha$ is close to unity and anomalous diffusion becomes unimportant. When $\phi > \phi^*$, on the other hand, although $\alpha$ decreases, the corresponding anomalous diffusion takes place over very short time periods $t^*$ and the effect also decreases.

The difference between the periodic and random cases is striking and clearly demonstrates that obstacle placement can have a profound qualitative effect on diffusion. The excess diffusion length $\beta$ and time $\tau_\beta$ provide useful information about the nature of the diffusion process in these systems as they behave in completely different ways when the obstacle concentration increases.

### C. The anomalous exponent $\alpha$

The exponent $\alpha$ is often the main (or even the sole) parameter used to describe the transient or anomalous diffusion regime. Figure 9 shows how $\alpha$ varies with the obstacle concentration $\phi$. Similar to the diffusivity $D(\phi)$ in Fig. 7, the $\alpha(\phi)$ curves have a positive curvature for periodic systems but a negative one for random systems. We note that $\alpha$ has a very weak dependence on obstacle size for periodic systems. However, for random systems, the value of $\alpha$ drops and becomes dependent upon obstacle size at higher concentrations because we then get close to the percolation threshold. The exponent is smaller for random systems, confirming that diffusion is more anomalous in the presence of disorder. Overall, the data shown in Fig. 9b is similar to that of Fig. 3 in [8]; however, our results demonstrate that the

curves do not cross at low concentrations.

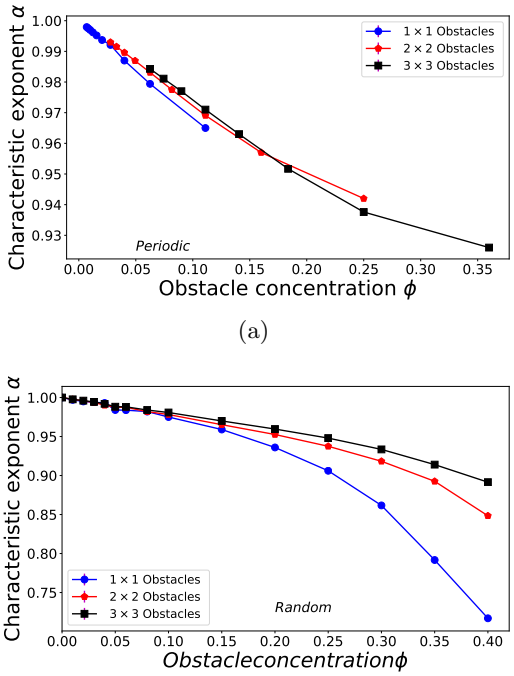


FIG. 9. Anomalous exponent $\alpha$ vs. obstacle concentration $\phi$ for three different obstacle sizes. (a) Periodically, and (b) randomly distributed obstacles.

### D. The crossover: time $t^*$ and length $r^*$

As mentioned previously, the transition between the anomalous and normal diffusion regimes can be characterized by a crossover time $t^*$ and a crossover length $r^*$ (these parameters are easily found using the approach described in Fig. 4). Moreover, these two variables can advantageously be used to replace the fitting parameter $D_\alpha$ since they have proper dimensions. In this section, we will examine them with this dual role in mind.

For periodic systems, $r^*$ trivially decreases as $\phi$ increases, Fig. 10a, since the distance between the obstacles plays the role of the correlation length and is essentially the distance the particle needs to travel before reaching the steady-state. Not surprisingly, the related crossover time, Fig. 11a, follows the same pattern.

Random systems of obstacles are quantitatively and qualitatively different. As Fig. 10b shows, $r^*$ increases with $\phi$ here and reaches values that greatly exceed the mean distance between obstacles ($\propto 1/\sqrt{\phi}$) because the correlation length of the obstacle distribution increases near the percolation threshold [7]. In the case of the smaller $1 \times 1$ obstacles, the crossover length $r^*$ actually diverges because we used concentrations very close to the percolation threshold $\phi^* = 0.407254$. The combined effect of an increased crossover distance $r^*$ and a reduced diffusivity $D$ at higher concentrations leads to a rapidly increasing crossover times $t^*(\phi)$, as shown in Fig. 11b. The curves cross because the percolation thresholds are lower for smaller obstacles (the divergence occurs for smaller values of $\phi$ when the obstacles are smaller). These results are in agreement with those of previous authors [1].

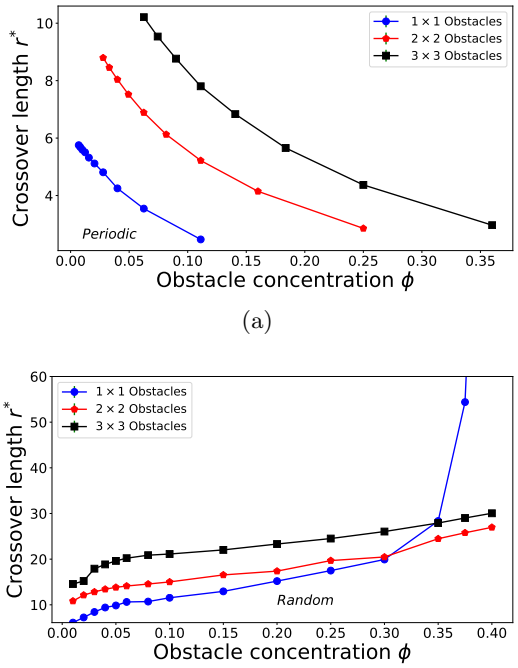


FIG. 10. Crossover length scales $r^*$ vs. obstacle concentration $\phi$ for three different obstacle sizes. (a) Periodically and (b) randomly distributed obstacles.

### E. The relation between the length scales $\beta$ and $r^*$

In diffusion problems of the kind studied here, the physics is controlled by a single length scale, the correlation length (or crossover length). Therefore, there must be a relation between the excess diffusion length $\beta$ and the crossover length $r^*$. As mentioned before, $\beta$, the constant term in the linear fit of the asymptotic (normal diffusion) behavior of the MSD, essentially measures the additional displacement due to the fact that diffusion is faster in the transient regime. We can define the instantaneous rate of diffusion as $\rho(t) = \partial\langle r^2(t)\rangle/\partial t$; we note that $\rho = 4D$ when we have normal diffusion, and

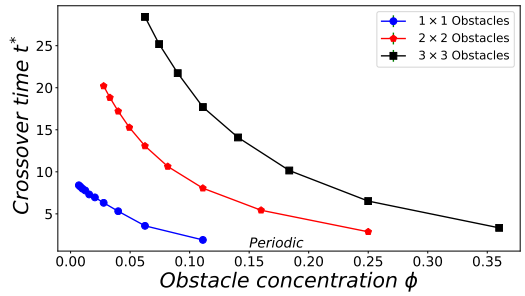


(a)

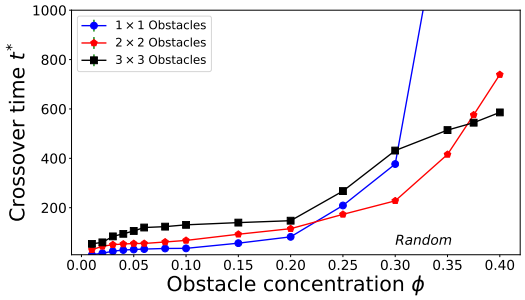


(b)

FIG. 11. Crossover time scales $t^*$ vs. obstacle concentration $\phi$ for three different obstacle sizes. (a) Periodically, and (b) randomly distributed obstacles.

$\rho = 4\alpha D_\alpha t^{\alpha-1}$ in the presence of anomalous diffusion. The two rates are equal at time

$$t_c = \alpha^{1/(1-\alpha)} t^*. \tag{55}$$

For $t < t_c$, anomalous diffusion is faster than normal diffusion but slows down up to time $t_c$. It is during this period of time that the excess diffusion $\beta$ builds up. We can thus estimate $\beta$ as

$$\beta^2 \approx 4D_\alpha t_c^\alpha - 4Dt_c = A(\alpha)\ r^{*2}, \tag{56}$$

where

$$A(\alpha) = (1-\alpha)\alpha^{\alpha/(1-\alpha)}\ . \tag{57}$$

Interestingly, this approximate relation between $\beta$ and $r^*$ is a function of the anomalous exponent $\alpha$ and nothing else. We also note that $A(\alpha = 1) = 0$, as expected since diffusion is then normal $\forall t \geq 0$.

In Fig. 12 we plot our data to show $\beta$ vs $r^* \times \sqrt{A(\alpha)}$, for both random and periodic distributions of obstacles, in order to check the accuracy of this estimate. For periodic obstacle systems, Fig. 12a, all data points collapse on a line of slope 1.056, in excellent agreement with our estimate. This is quite remarkable given the fact that $\beta(\phi)$ is a non-monotonic function of $\phi$, but not $r^*(\phi)$.

We have reproduced this best fit on Fig. 12b, where we show the data for randomly distributed obstacle systems. Again, the data for the three different obstacle sizes collapse to form a single curve, and the dashed line is in excellent agreement with the data to $\beta \approx 2.5$. Beyond that point, $\beta$ grows more slowly than what this simple theory predicts, suggesting that additional factors play a role as we approach percolation.

We thus showed that indeed there is a single characteristic length scale in the problem, and that the function $A(\alpha)$ given by eq. 57 allows us to collapse all the data, for periodic and random systems and for obstacles with different sizes, onto a single universal curve. The excess diffusion length $\beta$, which is almost always neglected, thus contains useful (and universal) information about a crowded system.

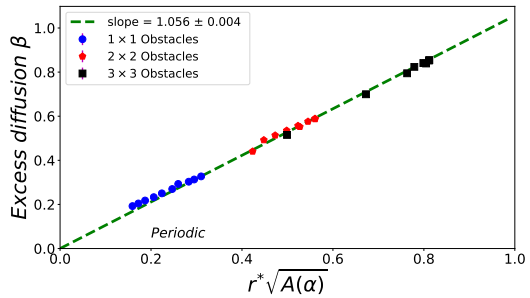


(a)

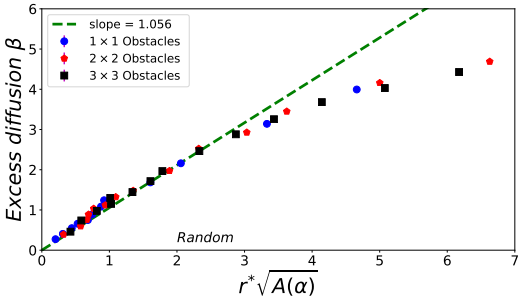


(b)

FIG. 12. Excess diffusion length $\beta$ vs. $r^* \times \sqrt{A(\alpha)}$ for three different obstacle sizes. a) Periodically, and b) randomly distributed obstacles. The dashed line in a) is a fit; it is reproduced in part b) of the figure.

## V. DISCUSSION

In this paper, we have revisited the classical problem of the nature and properties of the transient regime for a particle diffusing on a lattice populated by immobile obstacles. We first showed that the standard Monte Carlo

algorithm suffers from a narrower than expected displacement distribution function for short times. Since the properties of the transient regime depend on the precise timing of the first few collisions with obstacles, we proposed an improved LMC algorithm; however, more work has to be done since our algorithm also suffers from the same problem, albeit to a lesser extent. Introducing the diagonal jumps remains necessary.

Generally speaking, one can expect a transient regime with two sub-regimes. In some low-density cases, diffusing particles may take a non-negligible amount of time to collide with a first obstacle: during that period, one has essentially free diffusion. After the particles have started colliding with obstacles, their instantaneous diffusion coefficient decreases; the steady-state regime is reached when the particle has diffused over a length scale that characterizes the environment, e.g. the mean distance between nearest-neighbour obstacles when the latter are periodically distributed, or the correlation length of a random distribution.

Several authors have characterized the second part of the transient regime using the concept of anomalous diffusion, i.e. by fitting the MSD data using eq. 1. However, this raises the question of identifying the limits of the regime where this might apply since the value of the anomalous exponent $\alpha$ depends on the time interval chosen (not to mention the nature of the LMC algorithm). We used two numerical approaches in order to obtain extremely precise data and test our understanding of this often neglected issue. Our short-time MSD data came from a Markov chain methodology, which is equivalent to doing Monte Carlo simulations with an infinite ensemble size, while our exact matrix method provided the steady-state diffusion coefficients.

Our data showed that here is no time interval where eq. 1 applies perfectly, in the sense that a log-log plot of the MSD, $\langle r^2(t)\rangle$, vs time $t$ does not show a regime where the data falls on a straight line with a slope $\alpha$. Nevertheless, the concept of anomalous diffusion remains a useful tool to characterize the transient regime. We thus proposed to define the centre of this regime as the inflection point in the log-log plot of $\langle r^2(t)\rangle/4t$, vs $t$; this has the key advantage of being a well-defined and objective location. The anomalous exponent $\alpha$ is then simply related to the slope at the inflection point and this leads to straightforward and natural definitions for the crossover time $t^*$ and crossover length $r^*$. We also argued that these two parameters should be used to replace the traditional fitting parameter $D_\alpha$ since the latter has no physical meaning (*e.g.*, the units of measurement of $D_\alpha \sim cm^2/sec^\alpha$ depend on $\alpha$).

Using our improved LMC algorithm, the two numerical methods mentioned above and our definition for the transient regime and its parameters, we examined the physics of periodic and random distributions of obstacles of different sizes. We focused our work on these two factors as previous studies have shown their importance. For example, Ellery et al [2] recently stressed the fact that the size of the obstacles plays a major role for a given surface coverage $\phi$. We previously showed that the degree of randomness of the distribution of obstacles also has a major impact for a given $\phi$.

The asymptotic diffusion coefficient $D$ and the anomalous exponent $\alpha$ show similar dependence upon the surface concentration $\phi$: while $D(\phi)$ and $\alpha(\phi)$ are concave functions for periodic arrays of obstacles, they are convex functions for random ones. This shows the importance of the precise distribution of obstacles in such systems (in a previous paper [8], we showed that it is possible to design fuzzy obstacle systems for which the function $D(\alpha)$ is linear). We also noticed that small obstacles have a much larger impact than large ones for random distributions (but not for periodic ones), in agreement with the recent results by Ellery and coworkers; this difference between periodic and random distributions is due to the presence of a percolation threshold $\phi^*$ in the latter case, with $\phi^*$ increasing with obstacle size.

For periodic distributions of obstacles, the crossover distance $r^*$ trivially decreases when $\phi$ increases or the obstacles get smaller because the latter then get closer to each other while the geometric features remain unchanged. Not surprisingly, we observe the very same behavior for the crossover time $t^*$. For random distributions of obstacles, however, both $r^*$ and $t^*$ increase with concentration as we get closer to percolation. In this case, it is not the mean distance between obstacles that matter, but the size of the obstacle aggregates (which is measured by the correlation length) that form as $\phi$ increases.

In order to extract the diffusion coefficient $D$ from laboratory or via simulation data, it is customary to fit long-time data points on a $\langle r^2(t)\rangle$ vs. time $t$ plot using eq. 50. The constant $\beta$, which is a length scale, is almost always ignored. Our study of $\beta$ showed that it increases with $\phi$ for random systems, but that it is a non-monotonic function of $\phi$ for periodic arrays of obstacles. In the former case, $\beta$ simply follows the correlation length, while in the latter case the result can be explained by the competition between two competing factors (namely, the reduced impact of obstacles as their separation increases). We suggests that the excess diffusion $\beta$ is a measure of the importance of anomalous diffusion in a system.

It is well-known, however, that the physics of diffusion in systems of immobile obstacles should be related to a single length scale, e.g. the crossover length $r^*$. This raises the question of the relation between the length scales $\beta$ and $r^*$ for a given system. We have proposed a simple approximate relation between the two, eqs. 56

and 57, a relation that includes only the anomalous exponent $\alpha$. Remarkably, this relation is excellent for periodic distributions of obstacles (whatever the size of the obstacles is) in spite of the fact that $r^*(\phi)$ is a monotonic function of $\phi$ while $\beta(\phi)$ is not, a very interesting and surprising result. The same relation allows us to collapse the data for all three obstacle sizes on a universal curve when the obstacles are randomly distributed; however, it underestimates the value of $\beta$ when the concentration $\phi^*$ increases above $\approx 15\%$. Our study thus supports the idea that there is a direct relation between the two length scales (obviously, it is also possible to establish a similar connection between the time scales $\tau_\beta$ and $t^*$). Moreover, the function $A(\alpha)$, eq. 56, may be used in some cases to estimate $\alpha$ when both $r^*$ and $\beta$ are obtained through fits, as is often the case.

In conclusion, we have described a new methodology to better analyze the transient regime using the concept of anomalous diffusion, and we have designed an improved LMC algorithm for diffusion on a square lattice. While there is no time regime where $\langle r^2 \rangle \sim t^\alpha$, it is possible to obtain excellent results by using an inflection point as the basis of the analysis. We have also introduced the excess diffusion length scale $\beta$ in order to quantify the importance of the transient regime, and we have shown that there is a direct and universal relation between $\beta$ and the crossover length scale $r^*$. The fact that the ratio $\beta/r^*$ depends only on the anomalous exponent $\alpha$ may be used to conclude that the concept of anomalous diffusion provides a useful way to analyze the transient regime. Our analysis of the transient regime showed that periodic and random distributions of obstacles give qualitatively different results for all parameters used to describe the physics. However, in a real system like a biomembrane the obstacles are neither perfectly random nor perfectly periodic. It will be interesting to examine how these parameters evolve in systems with a tunable amount of disorder (in progress).

## ACKNOWLEDGMENTS

The authors would like to thank Dr. Mehran Bagheri for useful suggestions. This work was supported by the Canadian Queen Elizabeth II Diamond Jubilee Scholarship Program (QES II), the Natural Sciences and Engineering Research Council (NSERC; RGPIN/046434-2013) of Canada and the University of Ottawa.

[1] Saxton MJ. Anomalous diffusion due to obstacles: A Monte Carlo study. *Biophys. J*, **66**:394–401, 1994.

[2] Ellery A, Simpson M, McCue S, and Baker R. Characterizing transport through a crowded environment with different obstacle sizes. *J. Chem. Phys*, **140**:1–6, 2014.

[3] Chubynsky MV and Slater GW. Optimizing the accuracy of lattice Monte Carlo algorithms for simulating diffusion. *Phys. Rev. E*, **85**:016709:1–30, 2012.

[4] Ellery A, Baker R, and M Simpson. Distinguishing between short-time non-fickian diffusion and long-time fickian diffusion for a random walk on a crowded lattice. *J. Chem. Phys*, **144**:1–4, 2016.

[5] Ellery A, Baker R, McCue S, and Simpson M. Modeling transport through an environment crowded by a mixture of obstacles of different shapes and sizes. *Physica A*, **449**:74–84, 2016.

[6] Mercier JF and Slater GW. Numerical exact diffusion coefficients for lattice systems with periodic boundary conditions. I. Theory. *J. Chem. Phys*, **110**:6050–6056, 1999.

[7] Mercier JF and Slater GW. Numerical exact diffusion coefficients for lattice systems with periodic boundary conditions. II. Numerical approach and applications. *J. Chem. Phys*, **110**:6057–6065, 1999.

[8] Slater GW and Guo HL. An exactly solvable Ogston model of gel electrophoresis: I. The role of the symetry and randomness of the gel structure. *Electrophoresis*, **17**:977–988, 1996.

# 3

# Additional data and results

In this Chapter, we provide supplementary data and results that complement what we presented in Chapter 2.

## 3.1 Periodic obstacle distributions

### 3.1.1 Comparing the two LMC algorithms

Figure 6 presents a comparison between the two LMC algorithms for periodic obstacle distributions. One can see that at short time, because the value of the correction factor for $\langle r^4(t) \rangle$ of the standard LMC algorithm is three times higher than the one of the new LMC algorithm (see eq. (27) and eq. (45) in Chapter 2), the first collisions are delayed and the diffusion ratio $\langle r^2 \rangle / 4t$ is larger during the entire transient regime for periodic systems.

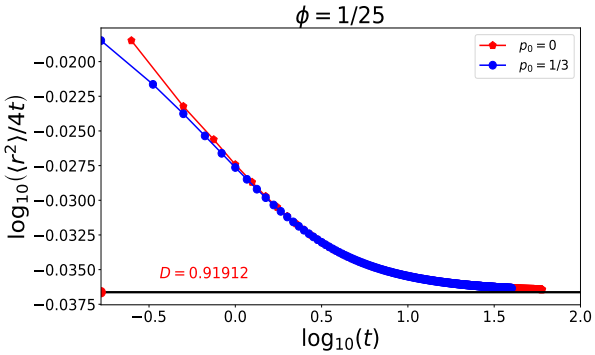


(a)

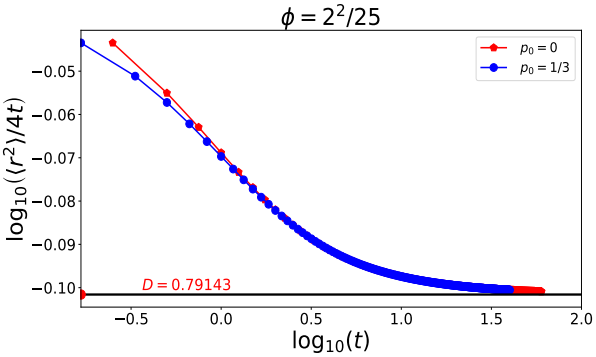


(b)

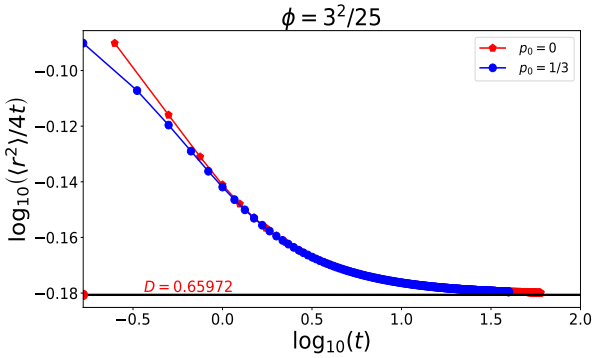


(c)

Figure 6: Comparing the two LMC algorithms. The red marker and line represent the data for the standard algorithm and the blue ones the data for the new algorithm. The legend $p_0$ is the probability to stay put for each algorithm. Plot $(a)$ gives the results for obstacles of size $1 \times 1$ separated by 5 sites, so that the concentration is $\phi = 1/25$. Plots $(b)$ and $(c)$ show respectively the results obtained for obstacles of size $2 \times 2$ ($\phi = 2^2/25$) and $3 \times 3$ ($\phi = 3^2/25$). The long time diffusion plateau $D$ is also showed.

### 3.1.2 Propagation of the probability distribution function over the lattice

Here using a density plot we show the propagation of the probability distribution function of the particle over the lattice. For Fig. 7, the logarithm of the probability density has been used. One can see that the probability density propagates from the centre of the lattice (inner dark red) to the outer area (dark blue). The centre of the density plot appears to be dark red because the particle has visited those sites many times. The white spots on the density plot represent the obstacles and thus, they cannot be visited by the particle. The white outer surface represents all the sites where the probability of presence is extremely small or zero. The boundary of the density plot is not a circle (it looks more or less like a square) because we are using a square lattice and diagonal jumps have not been included in the LMC algorithm. This result has been obtained using our new LMC algorithm and the plot represents the final state after 70 iterations.

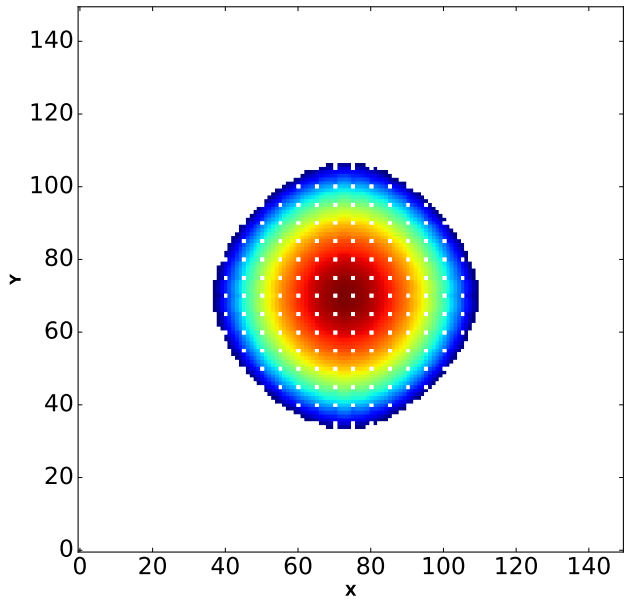


Figure 7: We present an example of the propagation of the probability distribution function of the particle over a lattice that contains periodic obstacles of size $1\times1$ separated by 5 sites (concentration $\phi = 1/25$). The propagation starts from the centre of the ring (inner dark red) and proceeds towards the outer of the ring (outer dark blue). The white spots represent the obstacles and the white outer surface on the lattice, the sites for which the probability of presence is extremely small or zero. This result is for the final state after 70 iterations.

### 3.1.3 Complete data sets for periodic obstacle distributions

We present from Fig. 8 to Fig. 13 all of the MSD data for a particle moving over a lattice periodically populated with obstacles of different sizes. The figures also show all of the characteristic points used in Chapter 2.

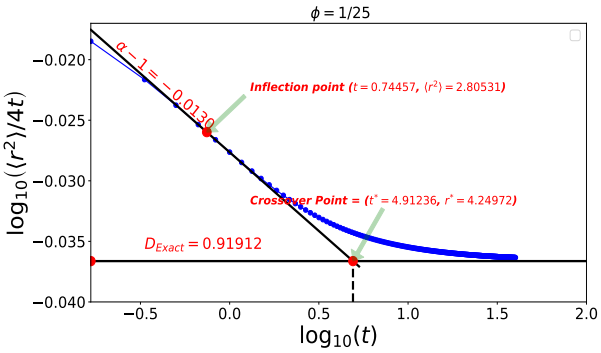


(a)

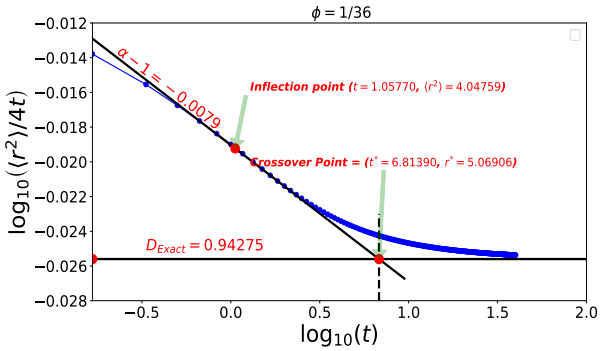


(b)

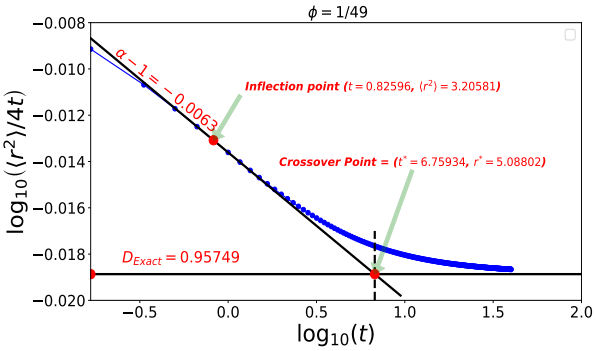


(c)

Figure 8: Diffusion ratio $\langle r^2(t) \rangle / 4t$ as a function of time for obstacles of size $1 \times 1$. We also show the inflection point, the tangent used to estimate the anomalous exponent $\alpha$ and the value of the fitting parameter $D_\alpha$, the long-time diffusion plateau $D$, and the crossover point.

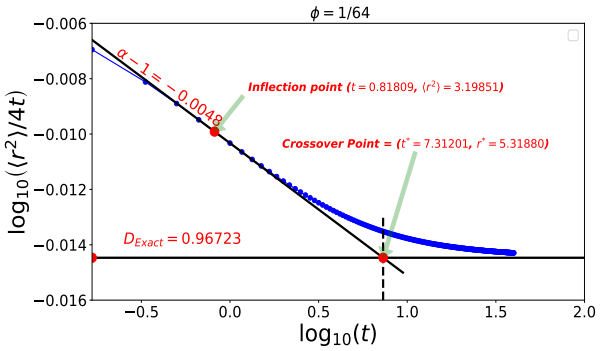


(a)

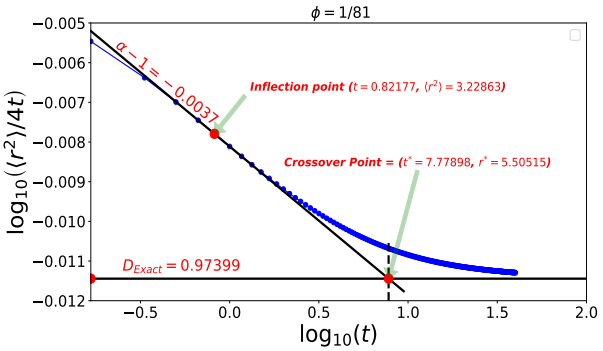


(b)

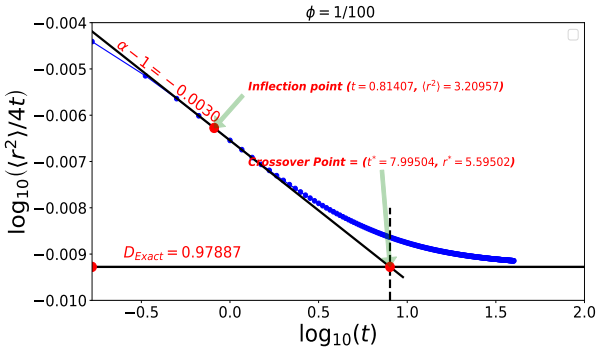


(c)

Figure 9: Diffusion ratio $\langle r^2(t) \rangle / 4t$ as a function of time for obstacles of size $1 \times 1$. We also show the inflection point, the tangent used to estimate the anomalous exponent $\alpha$ and the value of the fitting parameter $D_\alpha$, the long-time diffusion plateau $D$, and the crossover point.

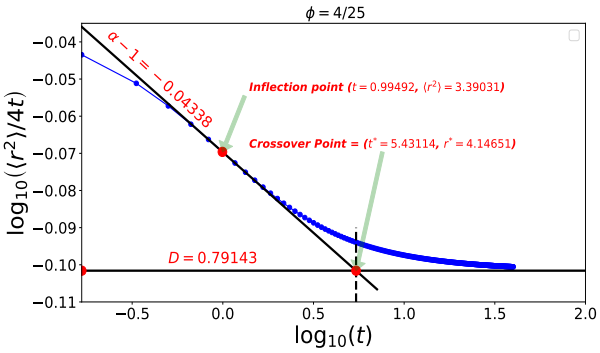


(a)

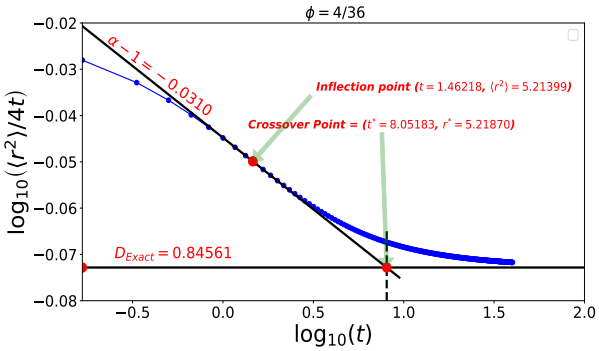


(b)

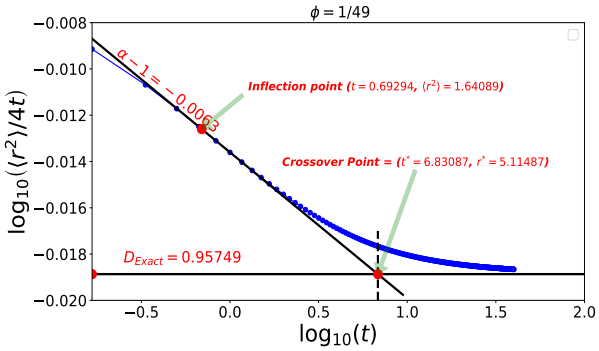


(c)

Figure 10: Diffusion ratio $\langle r^2(t) \rangle / 4t$ as a function of time for obstacles of size $2 \times 2$. We also show the inflection point, the tangent used to estimate the anomalous exponent $\alpha$ and the value of the fitting parameter $D_\alpha$, the long-time diffusion plateau $D$, and the crossover point.

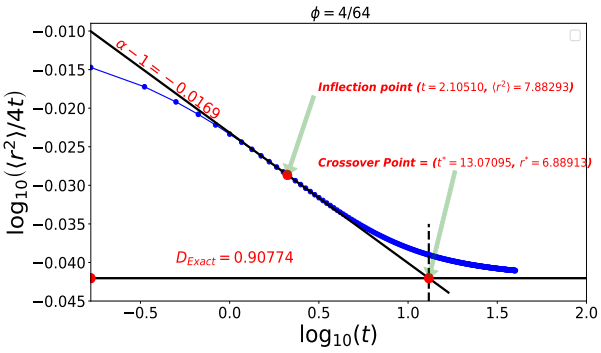


(a)

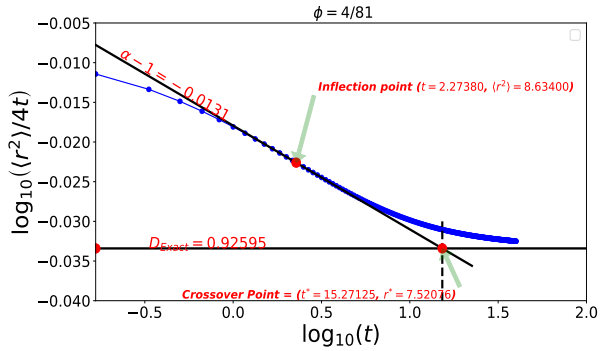


(b)

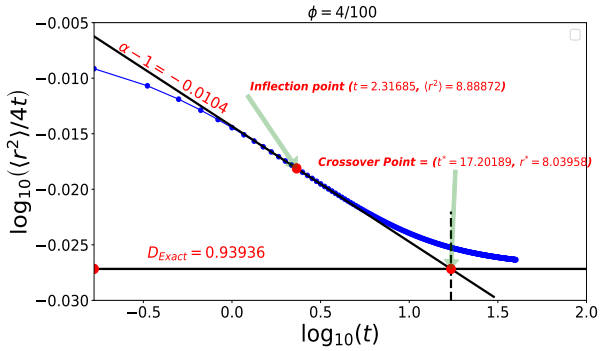


(c)

Figure 11: Diffusion ratio $\langle r^2(t) \rangle / 4t$ as a function of time for obstacles of size $2 \times 2$. We also show the inflection point, the tangent used to estimate the anomalous exponent $\alpha$ and the value of the fitting parameter $D_\alpha$, the long-time diffusion plateau $D$, and the crossover point.

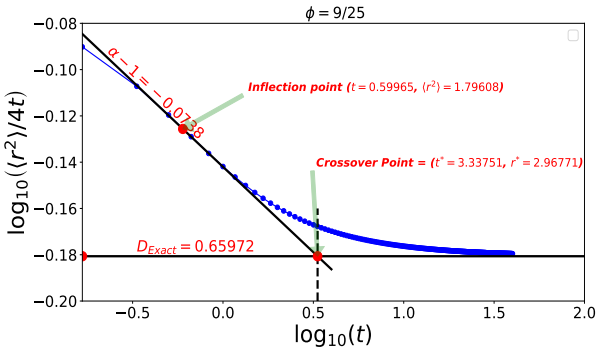


(a)

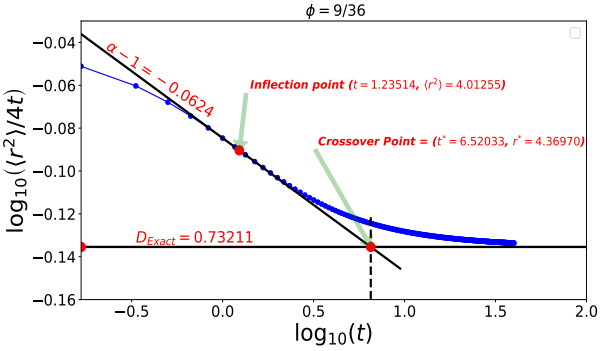


(b)

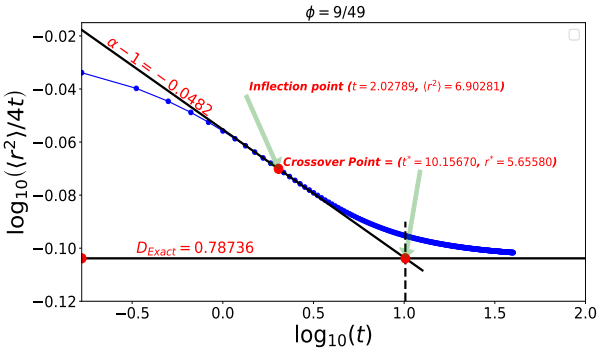


(c)

Figure 12: Diffusion ratio $\langle r^2(t) \rangle / 4t$ as a function of time for obstacles of size $3 \times 3$. We also show the inflection point, the tangent used to estimate the anomalous exponent $\alpha$ and the value of the fitting parameter $D_\alpha$, the long-time diffusion plateau $D$, and the crossover point.

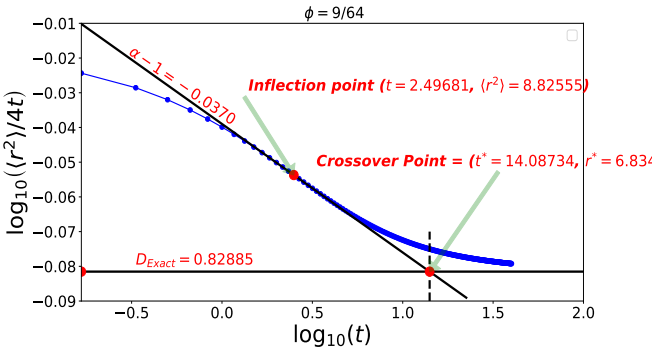


(a)

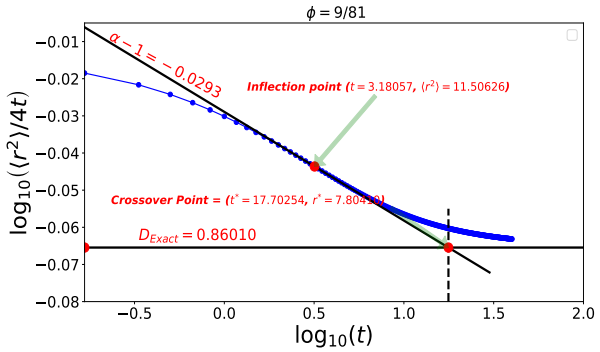


(b)

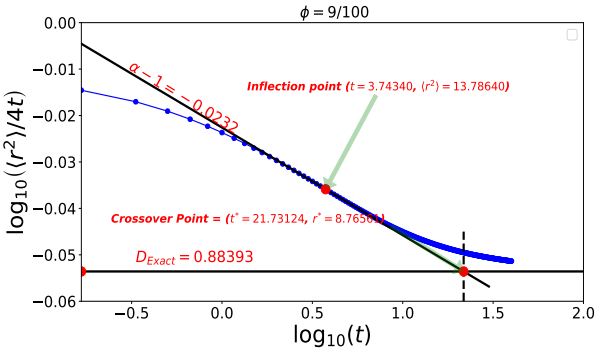


(c)

Figure 13: Diffusion ratio $\langle r^2(t) \rangle / 4t$ as a function of time for obstacles of size $3 \times 3$. We also show the inflection point, the tangent used to estimate the anomalous exponent $\alpha$ and the value of the fitting parameter $D_\alpha$, the long-time diffusion plateau $D$, and the crossover point.

### 3.1.4 Concentration effect

Figure 14 shows the effect of the concentration of obstacles on the MSD of the particle. At low concentration, the particle takes more time before it collides with a first obstacle, i.e. the particle freely diffuses for a longer period of time compared to high concentrations. As the concentration of obstacles in the medium decreases, the first phase of the particle's movement become more visible, and the position of the inflection point (red point on each curve) moves upwards to the right: both the diffusion coefficient $D$ and the crossover time $t^*$ increase.

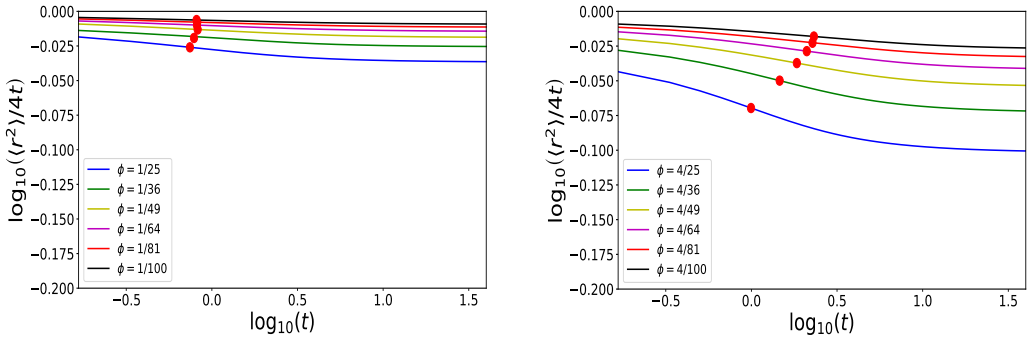


(a) (b)

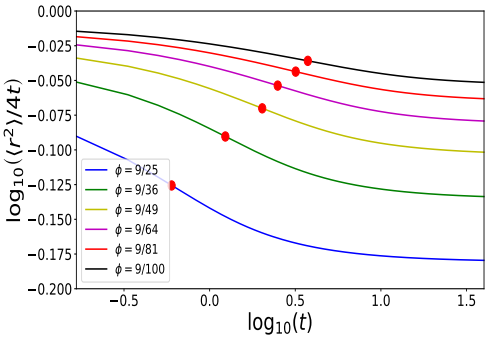


(c)

Figure 14: Effect of obstacle concentrations on the MSD of the particle. Plot $(a)$ corresponds to media with obstacles of size $1 \times 1$, $(b)$ and $(c)$ to media with obstacles of size $2 \times 2$ and $3 \times 3$, respectively. The inflection points (red points) are shown.

### 3.1.5 The effect of concentration and time on the excess diffusion length $\beta$

Figure 15 shows how the excess diffusion length $\beta$ varies with time (and reaches a plateau value at long time) for different concentrations of obstacles. We can see that the curves cross each other, in agreement with Fig. 8a in Chapter 2.

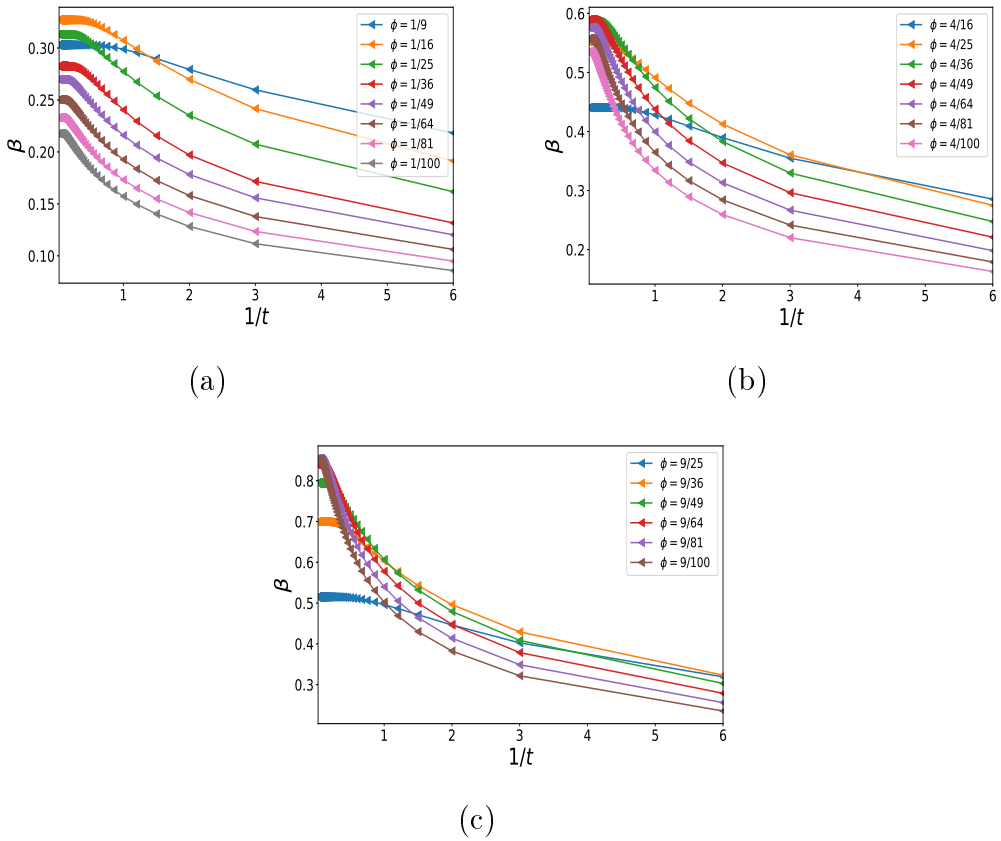


Figure 15: Effect of concentration and time on the excess diffusion length $\beta$. Plot (a) corresponds to obstacles of size $1 \times 1$, (b) and (c) to obstacles of size $2 \times 2$ and $3 \times 3$, respectively.

### 3.1.6 Excess diffusion time $\tau_\beta$

We present in Fig. 16 the apparent excess time $\tau_\beta$ (defined by eq. (52) in Chapter 2) due to the transient regime. It exhibits the same behaviour as the excess diffusion length $\beta$. This means that it is also affected by the competition between the concentration dependence of the diffusion coefficient $D$ and of the crossover time $t^*$.

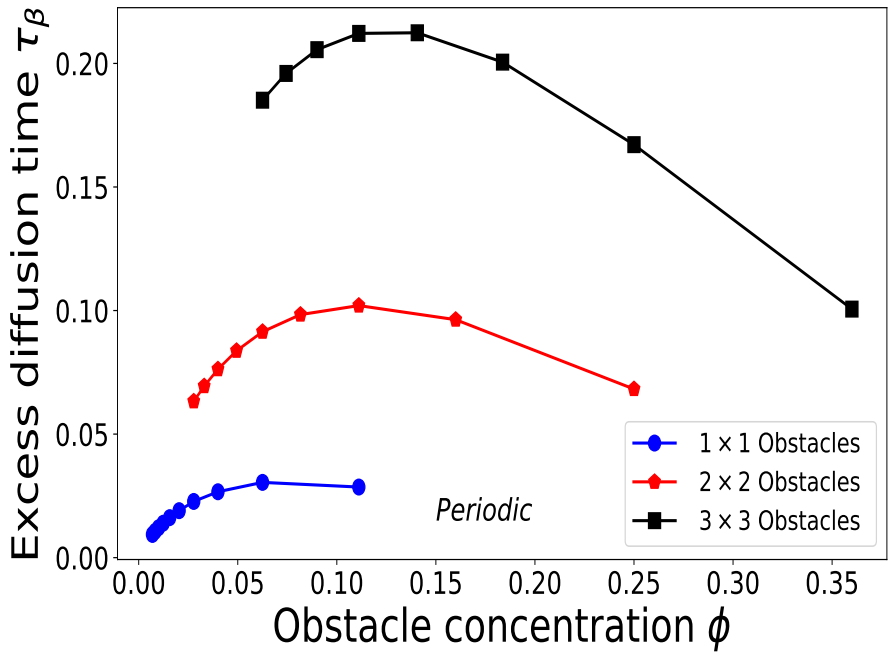


Figure 16: Excess diffusion time $\tau_\beta$ versus obstacle concentration $\phi$.

### 3.1.7 Diffusion deficit length $\gamma$

Figure 17 presents the diffusion deficit length $\gamma$ defined as the difference at the first time step between the tangent passing through the inflection point and the average MSD of the particle at the first time step without the $\log - \log$. In fact it measures the loss of free diffusion due to collisions that occur immediately at the first jump. We see that it exhibits the same behaviour as the excess diffusion $\beta$. This means that $\gamma$ is also affected by the competition between the concentration dependence of the diffusion coefficient $D$ and of the crossover time $t^*$. Figure 18 shows how the value of $\gamma$ has been estimated for a particle moving over a lattice that contains obstacles of size $2 \times 2$ separated by 5 sites (concentration $\phi = 4/25$).

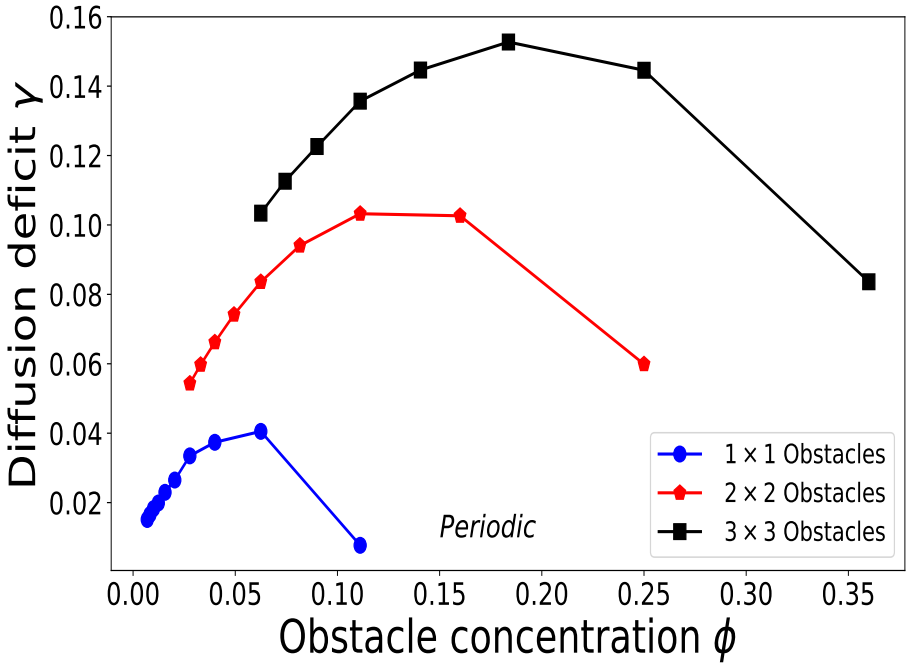


Figure 17: Diffusion deficit length $\gamma$ as a function of the obstacle concentration $\phi$.

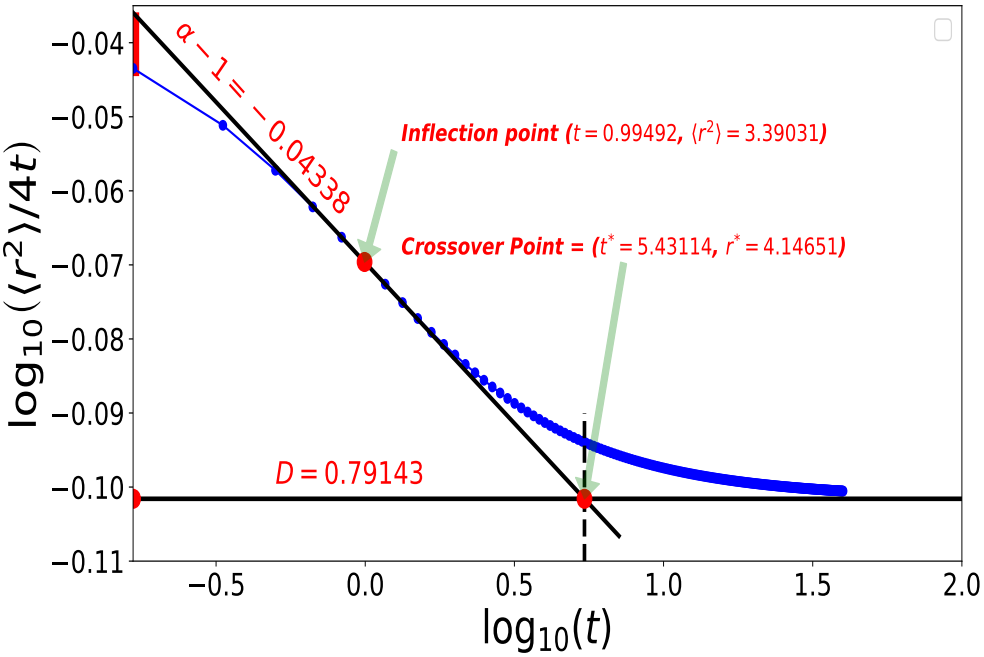


Figure 18: Diffusion ratio $\langle r^2(t)\rangle / 4t$ as a function of time for obstacles of size $2 \times 2$ (this is Fig. 4 in Chapter 2). The red vertical line at the very beginning shows where the variable $\gamma$ comes from. The diffusion deficit length $\gamma$ is estimated by taking the value of the $y$-intercept of the tangent passing through the inflection point and the value of $\log_{10}(\langle r^2(t)\rangle / 4t)$ at the first time step, removing the $\log - \log$, multiplying by $4t$, taking the square root and calculating the difference.

### 3.1.8 The width $\Sigma_\alpha$ of the time interval where we observe anomalous diffusion

We have estimated the width $\Sigma_\alpha$ of the anomalous interval on the $\log - \log$ plot by defining it as the ratio between the slope of the tangent passing through the inflection point and the value of the third derivative of the fitting function $f(x)$ at that point

$$\Sigma_\alpha^2 = \left. \frac{\partial f(x)/\partial x}{\partial^3 f(x)/\partial x^3} \right|_{x=log_{10}(t_I)}, \tag{63}$$

where $\log_{10}(t_I)$ is the inflection point abscissa. At the inflection point, this ratio gives the square of the width of the interval over which it is possible to consider that the function $f$ is approximately a straight line centred at the inflection point. That interval on a Cartesian plot is located between $\log_{10}(t_I) - \frac{1}{2}\Sigma_\alpha$ and $\log_{10}(t_I) + \frac{1}{2}\Sigma_\alpha$.

Figure 19 shows that the width of the anomalous interval decreases as one increases the obstacle concentration, just like in the case of the crossover length $r^*$ and time $t^*$. The plot shows some fluctuations that come from the choice of the fitting polynomial, and that are amplified by the third derivative.

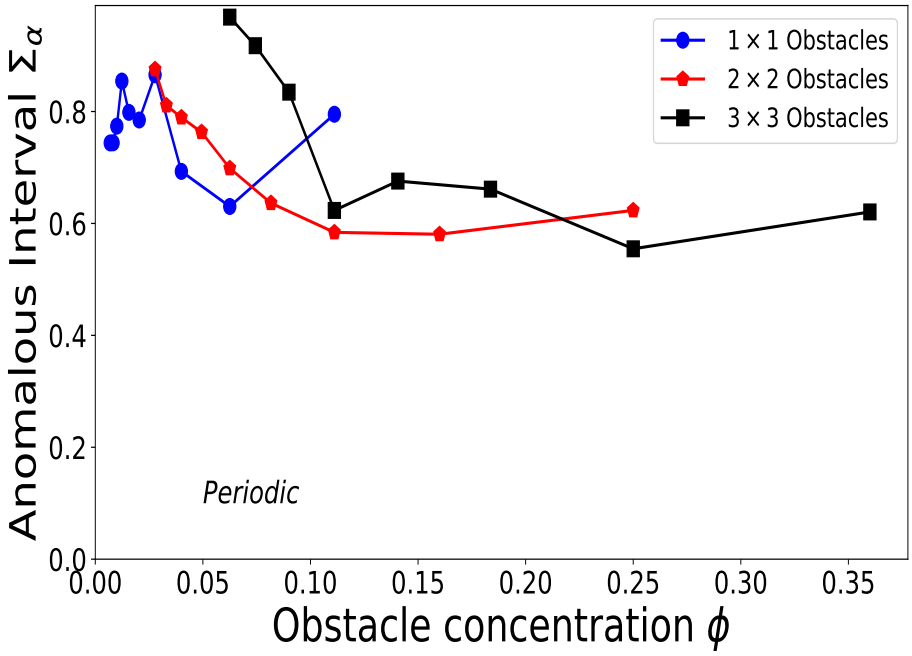


Figure 19: Estimated width $\Sigma_\alpha$, of the anomalous interval on the plot of $\log_{10}(\langle r^2(t)\rangle / 4t)$ vs $\log_{10}(t)$, as a function of the obstacle concentration $\phi$.

## 3.2 Random obstacle distributions

### 3.2.1 Choice of the starting site of the random walk

For random distributions, after populating our medium with the appropriated concentration of obstacles, we localize a square box of size 10 at the centre of the $500 \times 500$ lattice and we let the particle start its random walk on one site chosen randomly in that box. We repeat the procedure for 600 different obstacle environments. Figure 20 shows an example of a random system of size $25 \times 25$ populated at concentration $\phi = 0.1$ with obstacles of size $1 \times 1$. The $10 \times 10$ square box located at the centre of the lattice contains the particle (in pink).

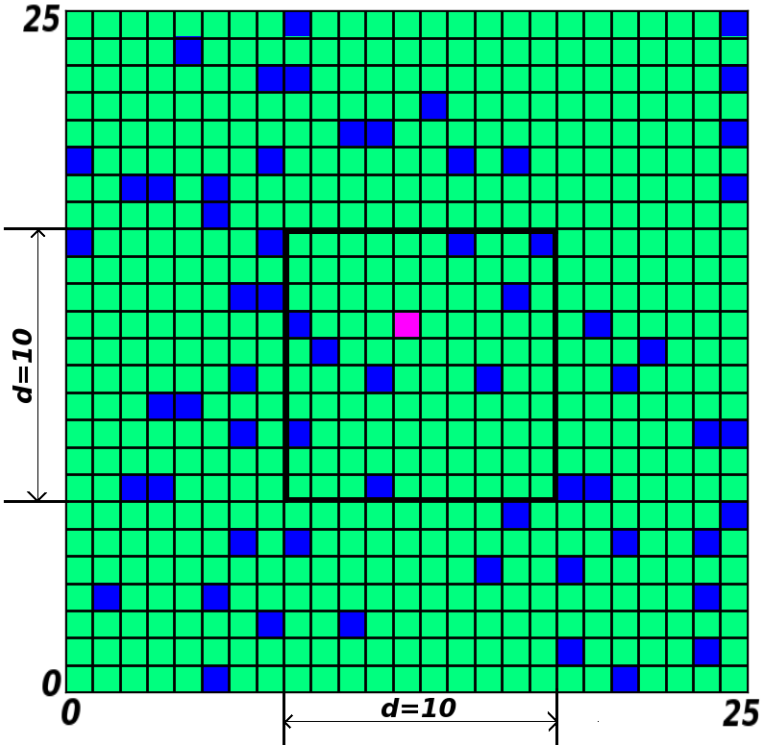


Figure 20: A of square lattice randomly crowded at a concentration $\phi = 0.1$ with obstacles of sizes $1 \times 1$. The particle is in pink, and its starting position is chosen randomly inside the central box of size $10 \times 10$

### 3.2.2 The effect of the starting site on the MSD of the particle

In addition to the fact that the particle starts its movement on a randomly chosen site in a $10 \times 10$ square box located at the centre of the lattice configuration, the number of obstacles adjacent to that starting site is also important because it has an impact on the MSDs at short time. Figure 21 presents four different points at the first time step $t = 1/6$ (which corresponds to $\log_{10}(t = 1/6) \approx -0.778$ on the graph) depending on the number of obstacles adjacent to the starting site. If the starting site does not have any adjacent obstacles, we have $\langle r^2 \rangle = 4/6$ and then dividing by $4t = 4/6$ and applying the logarithm, one obtains $\log_{10}(\langle r^2 \rangle / 4t) = 0$. Similarly, if we have one adjacent obstacle $\log_{10}(\langle r^2 \rangle / 4t) \approx -0.125$, for two adjacent obstacles we have $\log_{10}(\langle r^2 \rangle / 4t) \approx -0.301$, and for three adjacent obstacles we have $\log_{10}(\langle r^2 \rangle / 4t) \approx -0.602$. We can also see that no matter how many obstacles are adjacent to the starting site, all MSDs converge to the same plateau at long time.

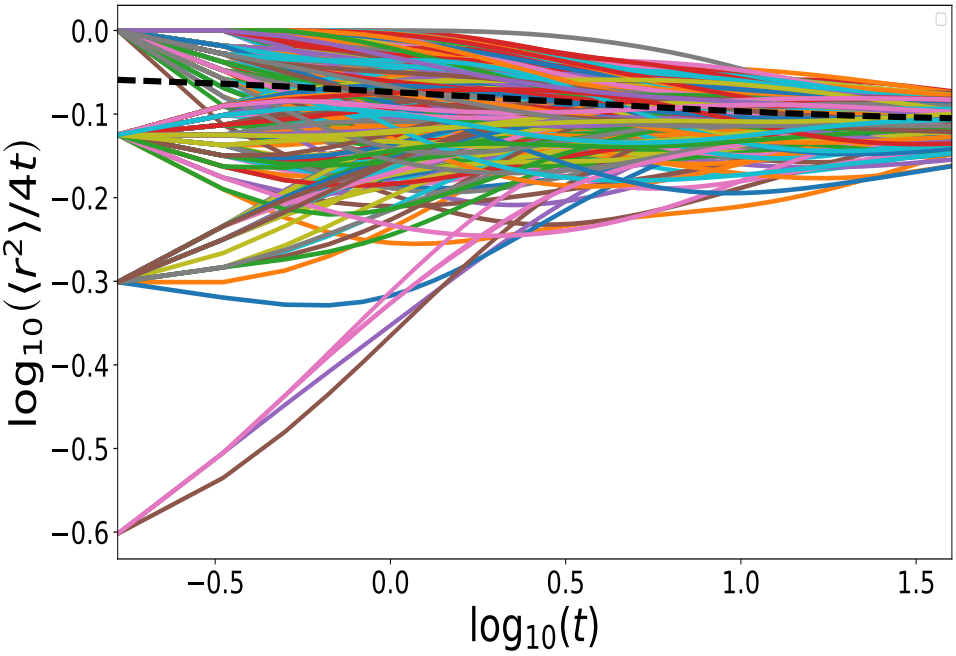


Figure 21: Plot of the time evolution of the MSD on a log-log diagram. The solid lines give the data for four different starting sites, while the dashed line gives the mean value. This result has been obtained for obstacles of size $1 \times 1$ with a concentration $\phi = 0.1$.

### 3.2.3 Propagation of the probability distribution function over the lattice

The observations in this section are similar to the ones of Section 3.1.2 except that here we have a random distribution of obstacles.

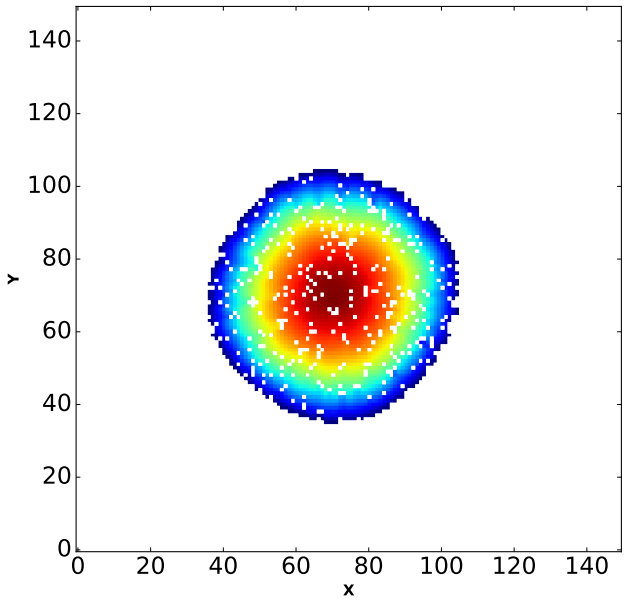


Figure 22: We present an example of the propagation of the probability distribution function of the particle over a lattice that contains obstacles of size $1 \times 1$ randomly distributed at concentration $\phi = 0.1$. The propagation starts from the centre of the ring (inner dark red) and proceeds towards the outer of the ring (outer dark blue). The white spots represent the obstacles and the white outer surface on the lattice, the sites for which the probability of presence is extremely small or zero. This result is for the final state after 70 iterations.

### 3.2.4 Complete data sets for random obstacle distributions

We present from Fig. 23 to Fig. 34 all of the MSD data for a particle moving over a lattice randomly populated with obstacles of different sizes. The figures also show all of the characteristic points as done previously for periodic distribution.

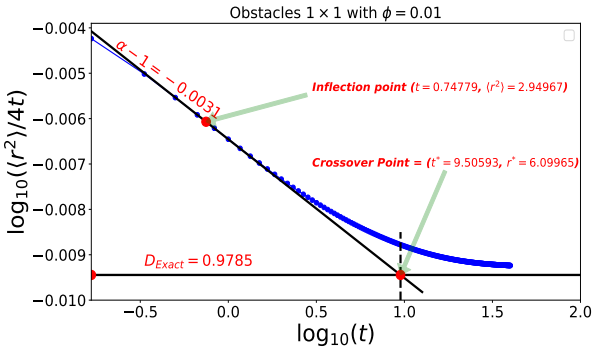


(a)

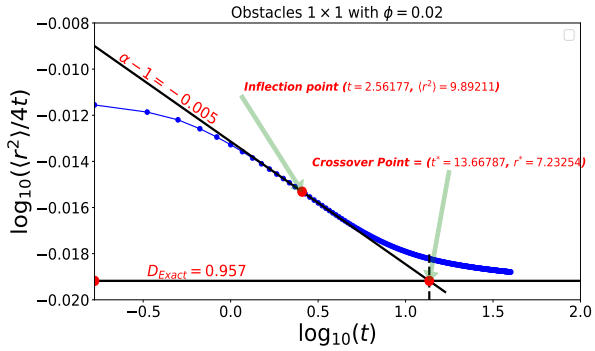


(b)

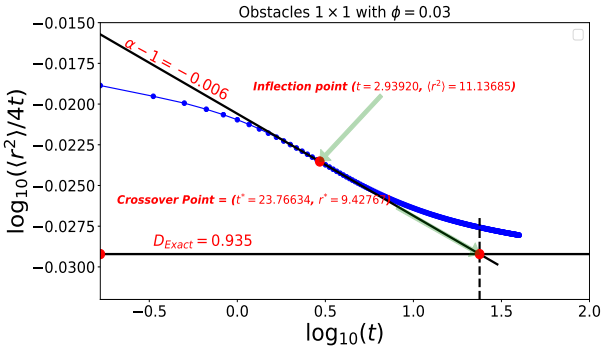


(c)

Figure 23: Diffusion ratio $\langle r^2(t)\rangle /4t$ as a function of time for obstacles of size $1 \times 1$. We also show the inflection point, the tangent used to estimate the anomalous exponent $\alpha$ and the value of the fitting parameter $D_\alpha$, the long-time diffusion plateau $D$, and the crossover point.

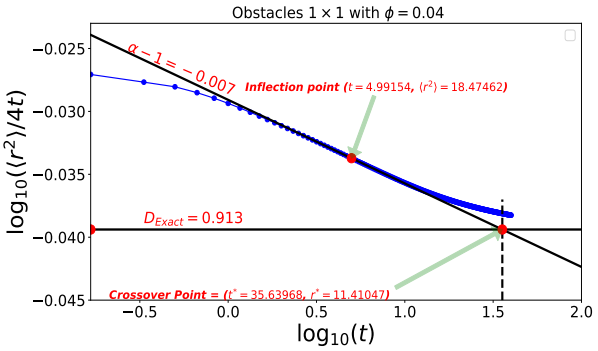


(a)

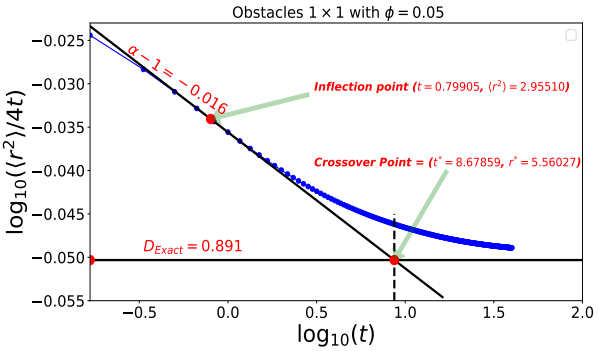


(b)

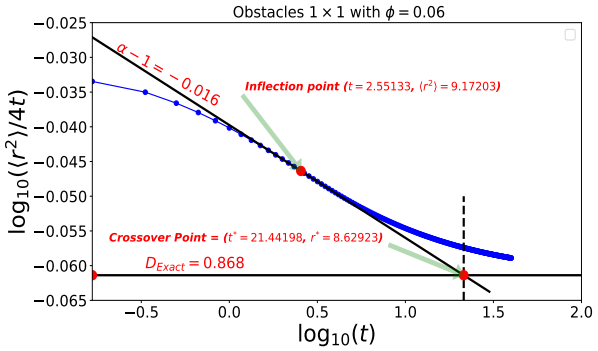


(c)

Figure 24: Diffusion ratio $\langle r^2(t) \rangle / 4t$ as a function of time for obstacles of size $1 \times 1$. We also show the inflection point, the tangent used to estimate the anomalous exponent $\alpha$ and the value of the fitting parameter $D_\alpha$, the long-time diffusion plateau $D$, and the crossover point.

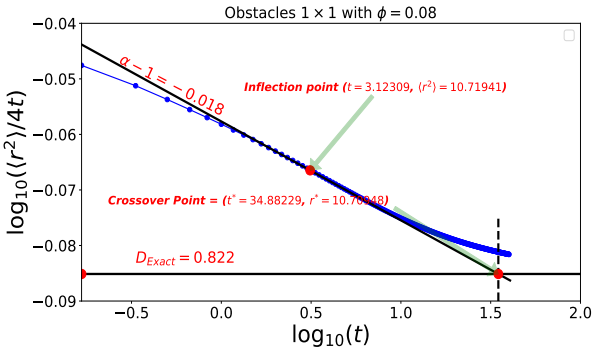


(a)

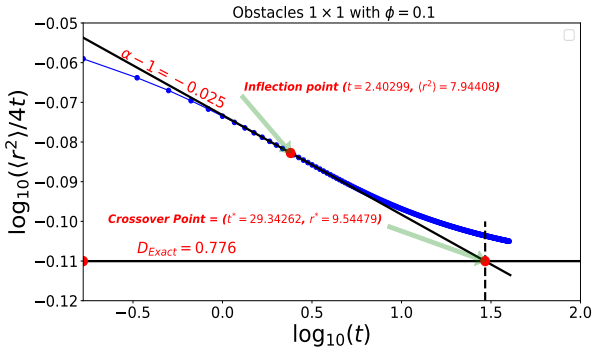


(b)

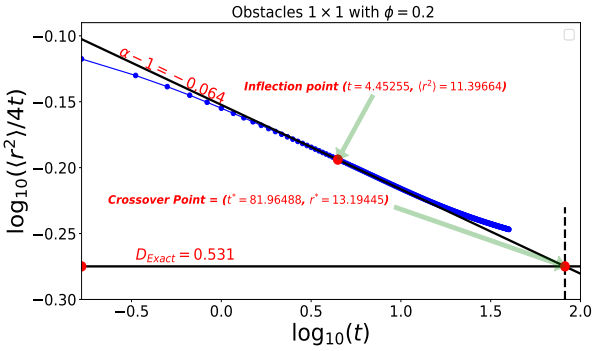


(c)

Figure 25: Diffusion ratio $\langle r^2(t)\rangle / 4t$ as a function of time for obstacles of size $1 \times 1$. We also show the inflection point, the tangent used to estimate the anomalous exponent $\alpha$ and the value of the fitting parameter $D_\alpha$, the long-time diffusion plateau $D$, and the crossover point.

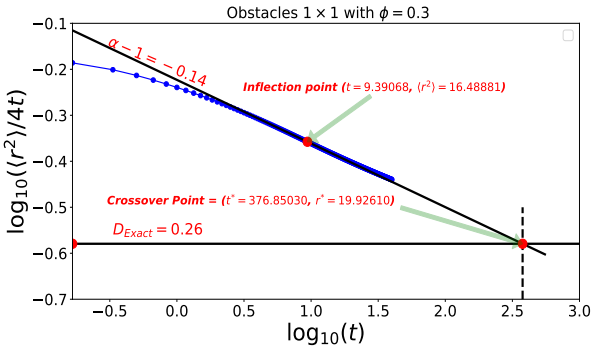


Figure 26: Diffusion ratio $\langle r^2(t)\rangle / 4t$ as a function of time for obstacles of size $1 \times 1$. We also show the inflection point, the tangent used to estimate the anomalous exponent $\alpha$ and the value of the fitting parameter $D_\alpha$, the long-time diffusion plateau $D$, and the crossover point.

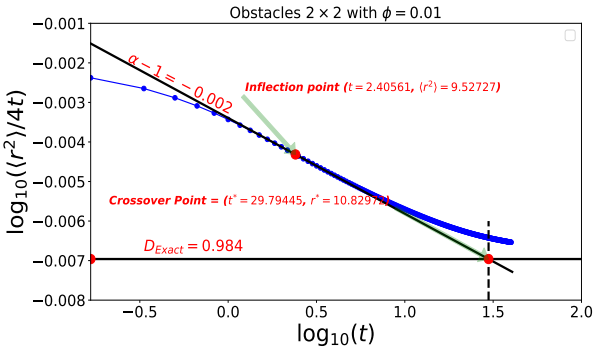


(a)

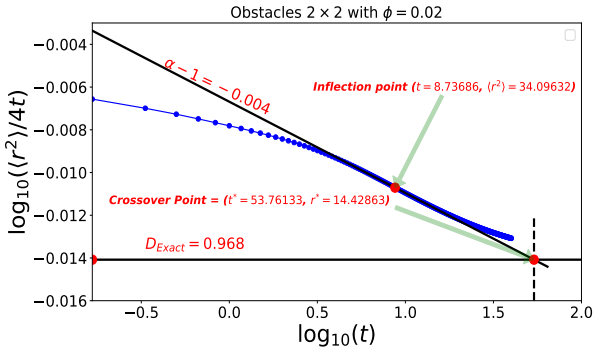


(b)

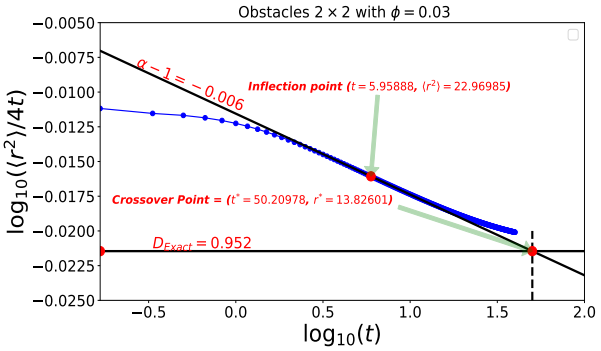


(c)

Figure 27: Diffusion ratio $\langle r^2(t) \rangle / 4t$ as a function of time for obstacles of size $2 \times 2$. We also show the inflection point, the tangent used to estimate the anomalous exponent $\alpha$ and the value of the fitting parameter $D_\alpha$, the long-time diffusion plateau $D$, and the crossover point.

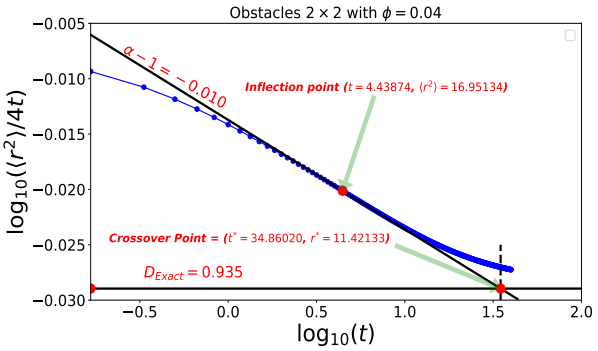


(a)

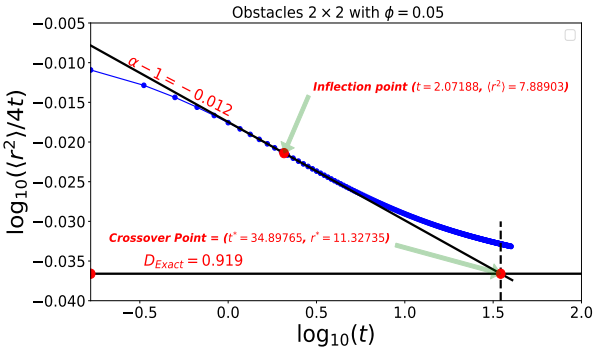


(b)

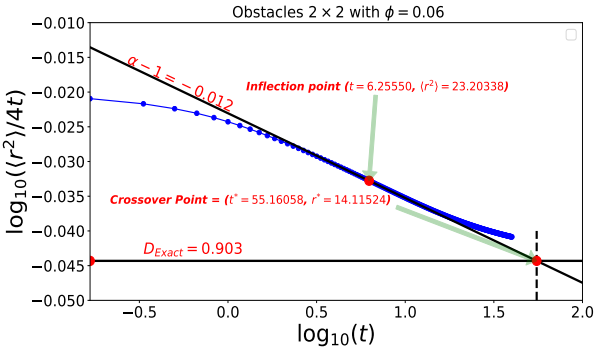


(c)

Figure 28: Diffusion ratio $\langle r^2(t)\rangle/4t$ as a function of time for obstacles of size $2 \times 2$. We also show the inflection point, the tangent used to estimate the anomalous exponent $\alpha$ and the value of the fitting parameter $D_\alpha$, the long-time diffusion plateau $D$, and the crossover point.

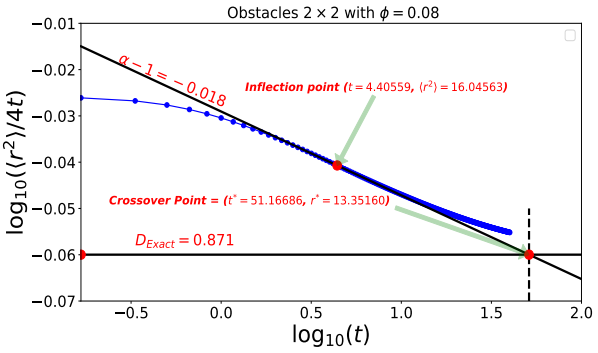


(a)

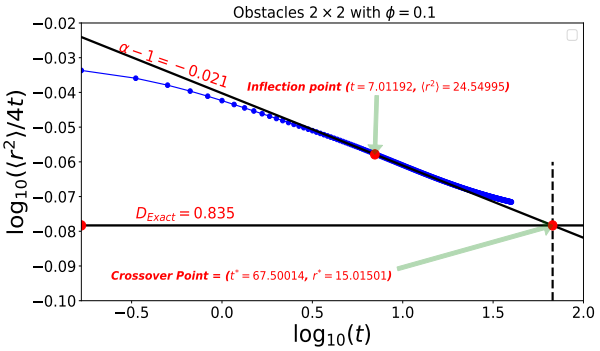


(b)

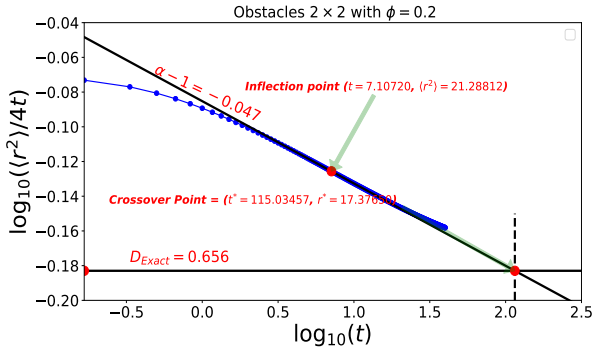


(c)

Figure 29: Diffusion ratio $\langle r^2(t) \rangle / 4t$ as a function of time for obstacles of size $2 \times 2$. We also show the inflection point, the tangent used to estimate the anomalous exponent $\alpha$ and the value of the fitting parameter $D_\alpha$, the long-time diffusion plateau $D$, and the crossover point.

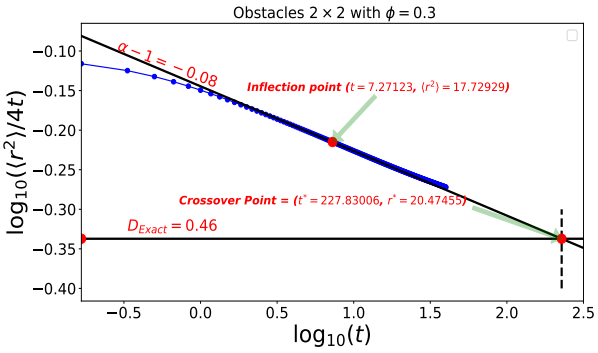


(a)

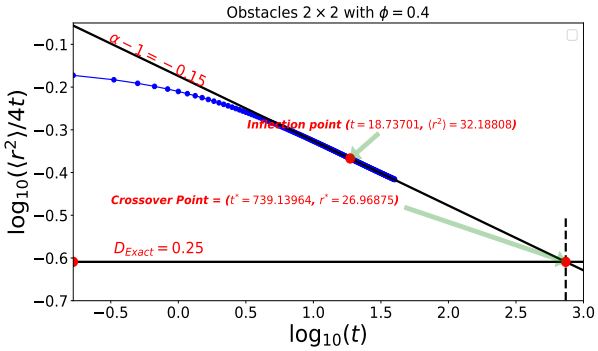


(b)

Figure 30: Diffusion ratio $\langle r^2(t) \rangle / 4t$ as a function of time for obstacles of size $2 \times 2$. We also show the inflection point, the tangent used to estimate the anomalous exponent $\alpha$ and the value of the fitting parameter $D_\alpha$, the long-time diffusion plateau $D$, and the crossover point.

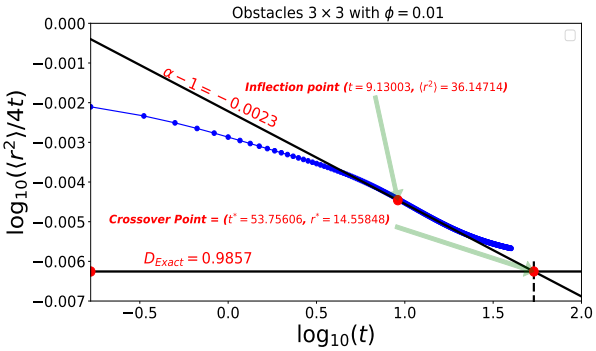


(a)

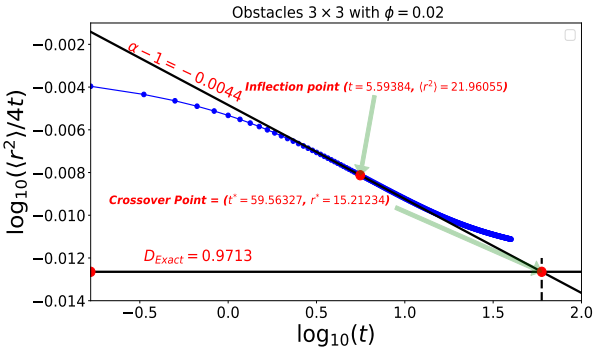


(b)

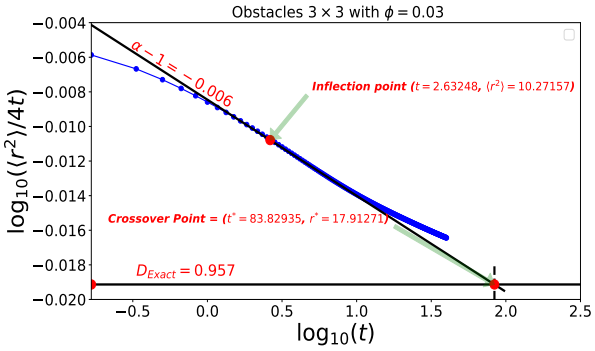


(c)

Figure 31: Diffusion ratio $\langle r^2(t) \rangle / 4t$ as a function of time for obstacles of size $3 \times 3$. We also show the inflection point, the tangent used to estimate the anomalous exponent $\alpha$ and the value of the fitting parameter $D_\alpha$, the long-time diffusion plateau $D$, and the crossover point.

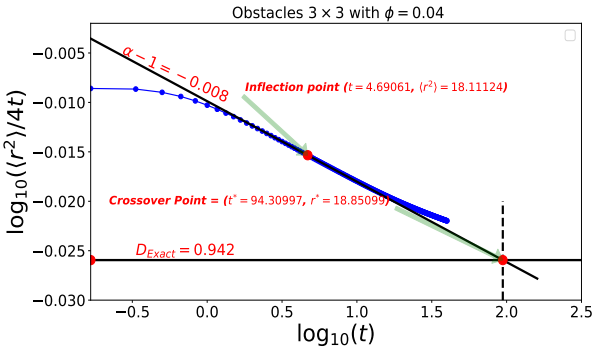


(a)

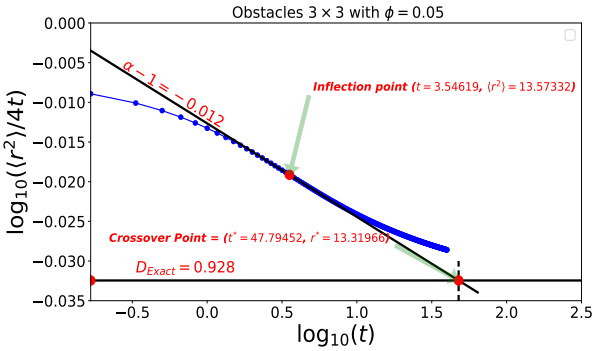


(b)

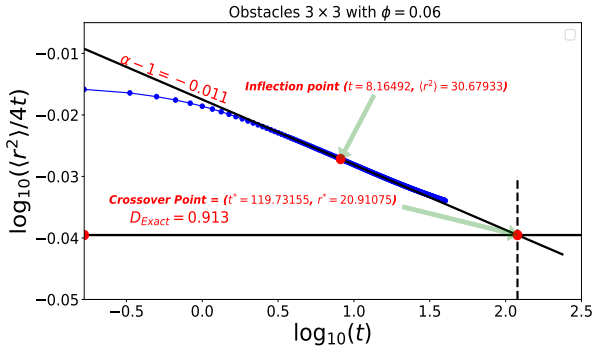


(c)

Figure 32: Diffusion ratio $\langle r^2(t) \rangle / 4t$ as a function of time for obstacles of size $3 \times 3$. We also show the inflection point, the tangent used to estimate the anomalous exponent $\alpha$ and the value of the fitting parameter $D_\alpha$, the long-time diffusion plateau $D$, and the crossover point.

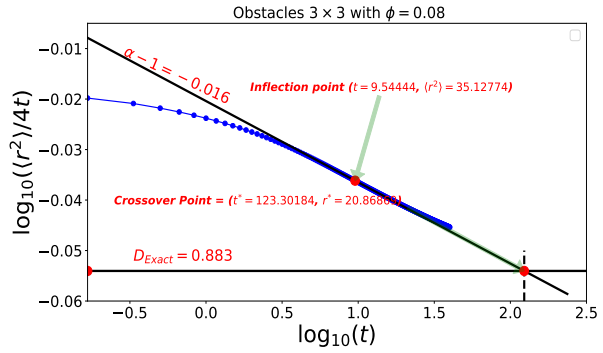


(a)

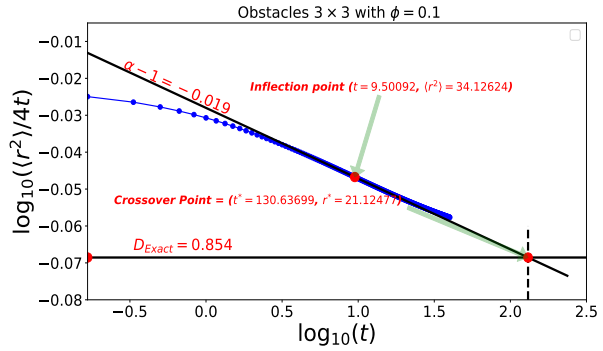


(b)

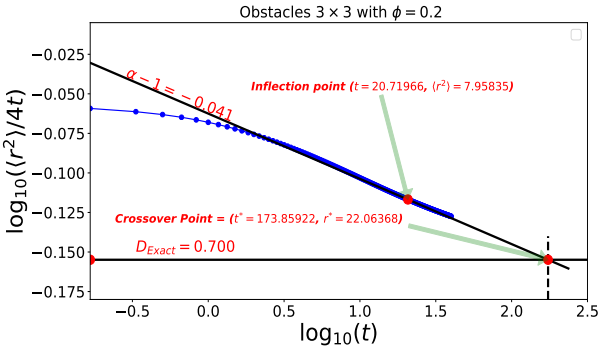


(c)

Figure 33: Diffusion ratio $\langle r^2(t) \rangle / 4t$ as a function of time for obstacles of size $3 \times 3$. We also show the inflection point, the tangent used to estimate the anomalous exponent $\alpha$ and the value of the fitting parameter $D_\alpha$, the long-time diffusion plateau $D$, and the crossover point.

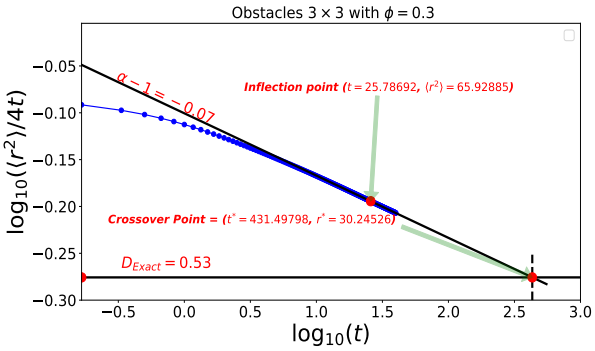


(a)

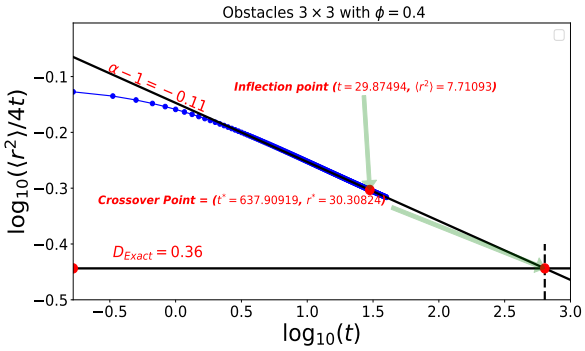


(b)

Figure 34: Diffusion ratio $\langle r^2(t) \rangle / 4t$ as a function of time for obstacles of size $3 \times 3$. We also show the inflection point, the tangent used to estimate the anomalous exponent $\alpha$ and the value of the fitting parameter $D_\alpha$, the long-time diffusion plateau $D$, and the crossover point.

### 3.2.5 Comparing the two LMC algorithms

Figure 35 presents a comparison between the two LMC algorithms for random obstacle distributions. We see that at short time, because the value of the correction factor for $\langle r^4(t)\rangle$ of the standard LMC algorithm is three times higher than the one of the new LMC algorithm (see eq. (27) and eq. (45) in Chapter 2), the first collisions are delayed and the diffusion ratio $\langle r^2\rangle/4t$ is larger (Fig. 35a and b). However, we believe that with the standard algorithm, the particle then takes longer to move around big obstacles and get out of a cavity. So its escape time is high, and this reduces the diffusion ratio $\langle r^2\rangle/4t$ in Fig. 35c. This effect exists only for random systems.

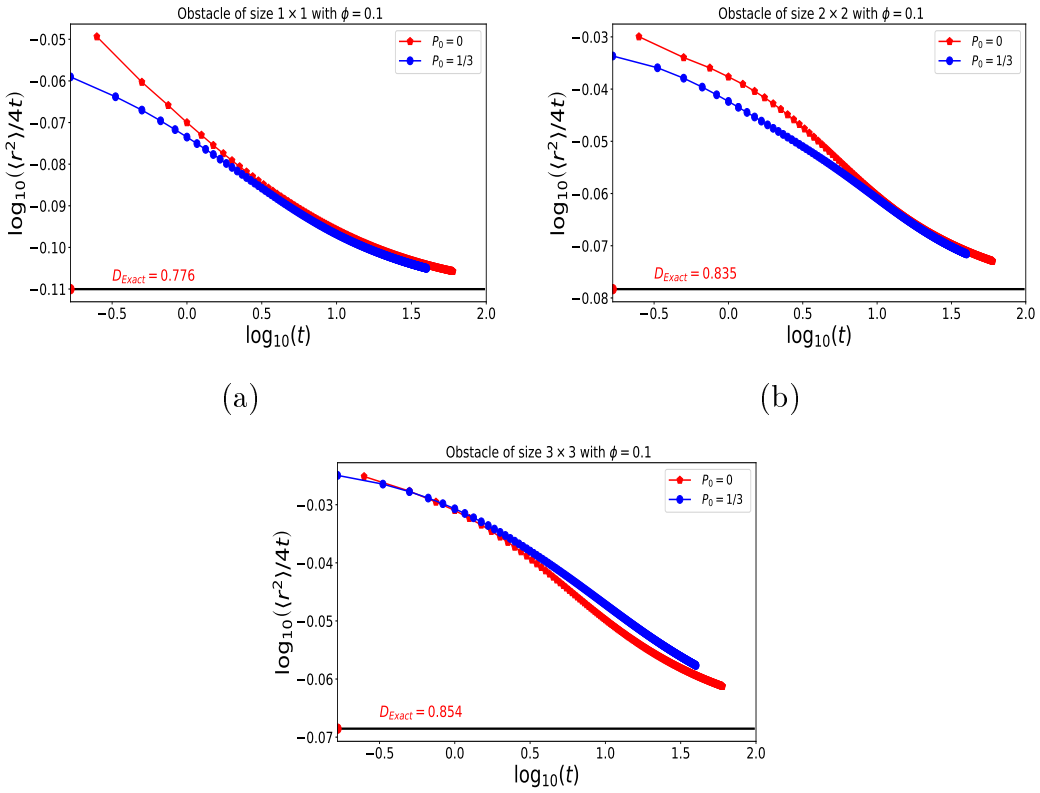


Figure 35: Comparing the two LMC algorithms. The red marker and line represent the data for the standard algorithm and the blue ones the data for the new algorithm. The legend $p_0$ is the probability to stay put for each algorithm. The results were obtained for different obstacle sizes distributed at concentration $\phi = 0.1$. Plot $(a)$ gives the results for obstacles of size $1 \times 1$, $(b)$ and $(c)$ show respectively the results obtained for obstacles of size $2 \times 2$ and $3 \times 3$. The long time diffusion plateau $D$ is also shown.

### 3.2.6 Concentration effect

Figure 36 gives the effect of the concentration of obstacles on the MSD of the particle. As the concentration of obstacles in the medium increases, the particle spends more time in the transient phase because the crossover time $t^*$ diverges. At low concentration, the fact that the curves cross each other may be due to the fact that the chosen ensemble of obstacle configurations was not large enough.

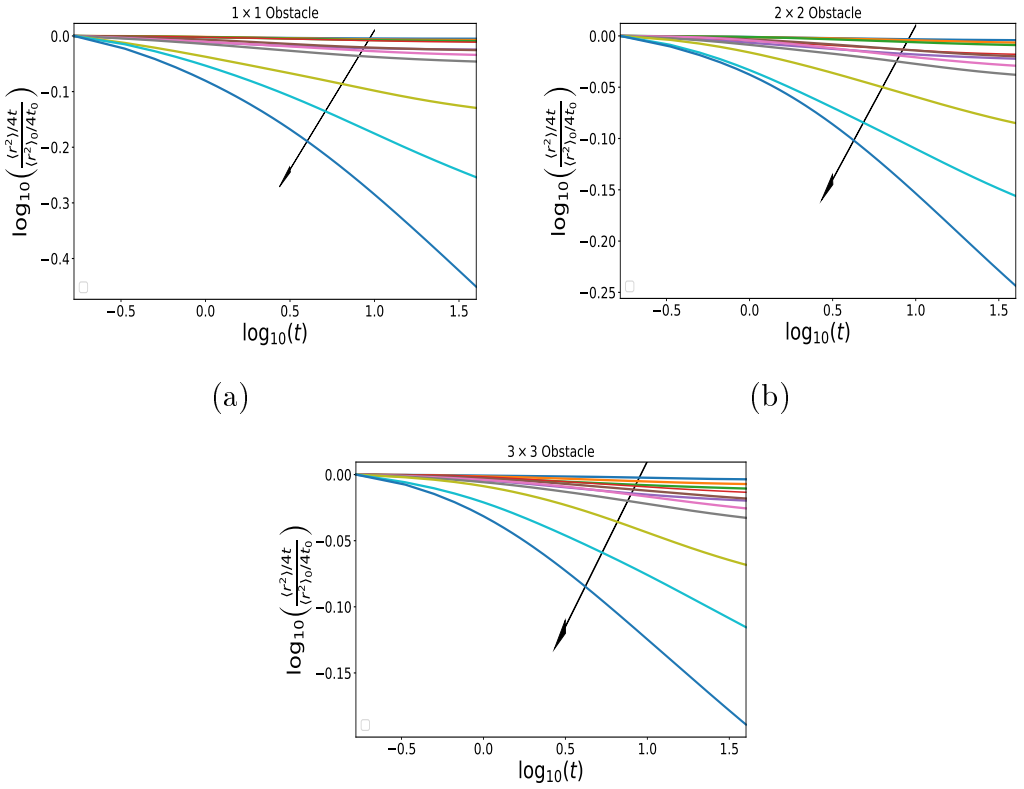


(a) (b)

(c)

Figure 36: Effect of the concentration of obstacles on the MSD of the particle. Plot $(a)$ corresponds to obstacles of size $1 \times 1$, $(b)$ and $(c)$ to obstacles of size $2 \times 2$ and $3 \times 3$, respectively. $\langle r^2(t)\rangle_0$ is the MSD at the first time step $t_0$. The arrows indicate the direction of increasing concentrations.

### 3.2.7 Diffusion deficit length $\gamma$

We present in Fig. 37 the diffusion deficit length $\gamma$ defined in Section 3.1.7. We see that it exhibits the same behaviour as the excess diffusion length $\beta$: $\gamma$ increases monotonically as the concentration increases and appears to increase as one approaches the percolation threshold. The fluctuations that appear at low concentration are due to the fact that we have to average over an ensemble of obstacle configurations.

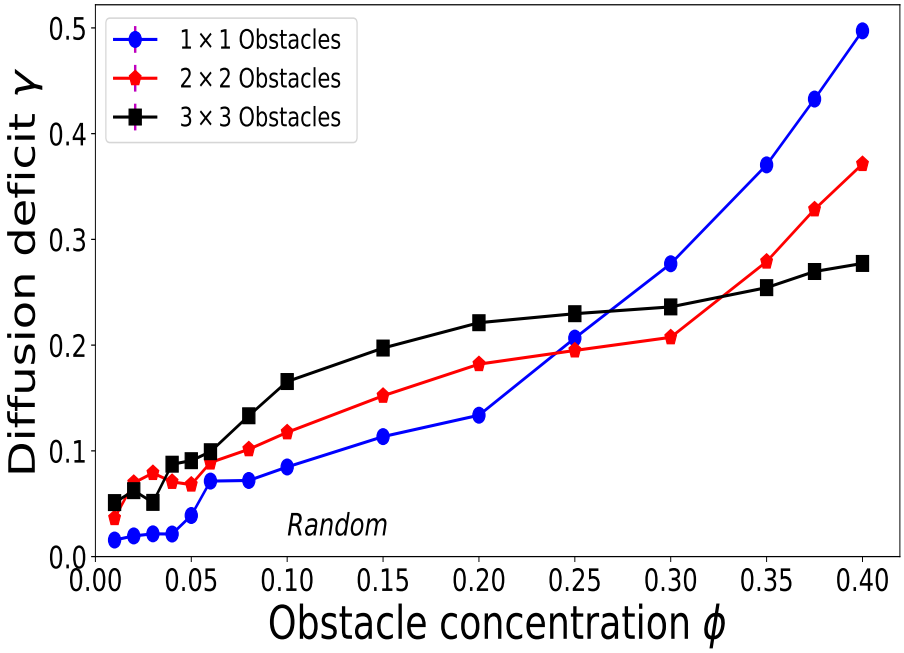


Figure 37: Diffusion deficit length $\gamma$ as a function of concentration $\phi$.

### 3.2.8 The width of the interval where we observe anomalous diffusion

We now present the estimate of the width $\Sigma_\alpha$ of the anomalous interval defined in Section 3.1.8. In Fig. 38 the anomalous interval increases as the concentration of obstacles increases, like in the case of the crossover length $r^*$ and time $t^*$. The plot also shows fluctuations that come from the choice of the fitting polynomial, and also from the fact that we have to average over an ensemble of obstacle configurations. The fluctuations are further amplified by the third derivative of the fitting function.

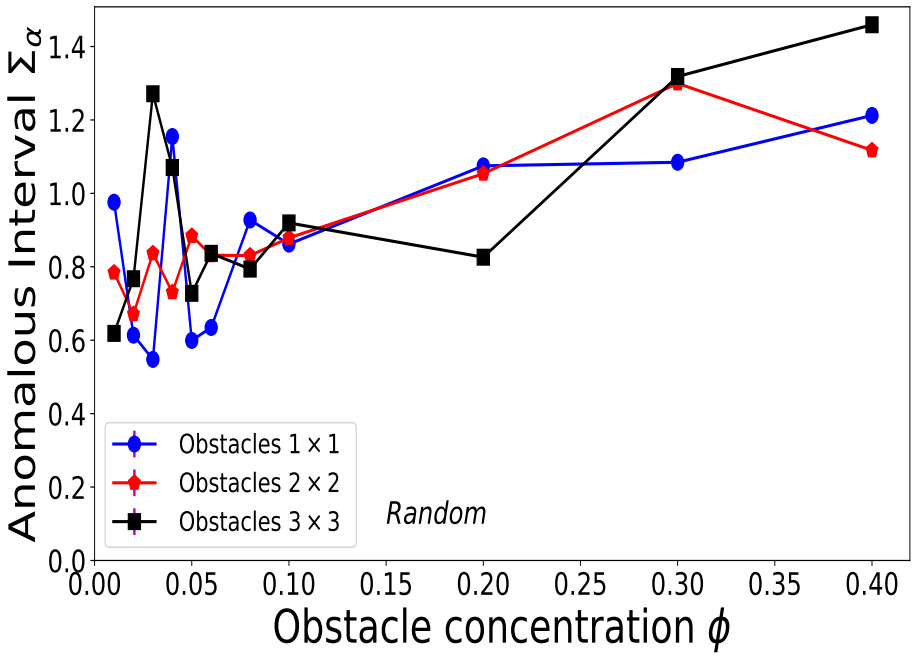


Figure 38: Estimated width $\Sigma_\alpha$, of the anomalous interval on the plot of $\log_{10}(\langle r^2(t)\rangle / 4t)$ vs $\log_{10}(t)$, as a function of the obstacle concentration $\phi$.

# 4

# Conclusion

This thesis revisits the well known problem of diffusion in media crowded with immobile obstacles, using a novel LMC algorithm as well as a new approach to defining the temporal location of the transient regime.

Instead of using the standard LMC algorithm where, when executing a random walk over a 2D lattice, the particle can make a jump in one of the four Cartesian directions with an equal probability 1/4, we have proposed that in addition, the particle can stay at the same position during its random walk. Thus, the particle can make a move in one of the four directions with a probability 1/6 and stay at the same position with a probability 1/3. The characterization of the particle's motion in this thesis has been done using this new LMC algorithm. We have used this new LMC algorithm to obtain the transition matrix and at long time to compute the diffusivity of the particle. The propagation of the particle in the medium at short time has been investigated using Markov chains. Even though our new algorithm does not completely reflects the reality of the continuum, one can see that the correction term that appears in the fourth moment vanishes three times faster compared to the standard LMC algorithm. It is clear that for our algorithm to be perfectly correct, one would need to consider diagonal jumps. However, it is not obvious how one could implement diagonal jumps because of the unclear difficulties when

treating collisions with obstacles. As mentioned, our medium was a lattice discretized so that the particle size was equal to the size of a lattice site.

During the movement, the dynamics of the particle describe two regimes: the short time transient regime and the steady state regime. Note that when the particle starts its movement in the medium, it diffuses freely until it collides with the first obstacle. After many collisions with obstacles the particle has a view of the whole system. Once this is done, it enters in the steady state regime.

Many researchers have worked on this topic, but often their methods were arbitrary. For example, the most recent is Adam Ellery, who, to characterize the movement of the particle in the transient regime, has considered a given interval of the transient regime and fitted the MSD data in that interval in order to obtain an estimate of the characteristic exponent $\alpha$. That interval was the same for all obstacle concentrations in the medium ([15], page 3).

Due to the change of curvature in the diffusion ratio $\langle r^2 \rangle / 4t$ of the particle, we have proposed to use the inflection point as the centre of the transient regime. That inflection point is the key of the method that we proposed in order to better determine the value of the characteristic exponent $\alpha$ of the particle motion. This exponent is related to the slope of the tangent at that point. Using this tangent and the plateau of the long time diffusivity, we have defined the crossover length $r^*$ and the crossover time $t^*$. Furthermore, we have shown that these variables can replace the fitting parameter $D_\alpha$ that appears in eq. (1) in Chapter 2, given that its units do not have significant meaning. We have seen that for periodic system, $r^*$ and $t^*$ decrease as the concentration of obstacles increase because the distance between the obstacles then decreases. For the random distribution, both $r^*$ and $t^*$ increase with the concentration and diverge as one approaches the percolation threshold. Once the crossover point is reached, the particle enters progressively in the steady state regime and its equation of motion characterized by $\langle r^2 \rangle = 4Dt$. This is normal diffusion.

The study presented in this document shows that the characteristic exponent $\alpha$ of the particle is not much dependent on the obstacle size in the case of periodic distributions. In the case of random distributions, this exponent becomes dependent upon the obstacle size at high concentrations. We have discovered that the excess diffusion $\beta$ contains information potentially useful. Indeed, usually when people fit the MSD data, they simply consider the long time dynamics of the particle. However, at short time there exists an excess diffusion because anomalous diffusion is faster than normal diffusion.

We have seen that for random distributions of obstacles, $\beta$ increases monotonically with the concentration of obstacles because the correlation length increases. For periodic distributions, $\beta$ is a non-monotonic function of the concentration and has a maximum that depends on the size of the obstacles: this is due to the competition between the diffusion coefficient and the cross over time. We have also shown that the variables $\beta$ and $r^*$ are related to each other by a function of $\alpha$ defined by $A(\alpha)$ in Chapter 2. For periodic distributions of obstacles, the fit of the data for the plot of $\beta$ vs. $r^*\sqrt{A(\alpha)}$ gives a straight line. Whatever the size of the obstacles, all the data collapse on the same line. For random distributions of obstacles, the same relation between $\beta$ and $r^*$ allows the data to collapse on the same curve. However, it underestimates the value of $\beta$ when the concentration $\phi$ increases above $\approx 15\%$. Thereby, our study strongly supports the idea that there is a direct relation between the two length scales (obviously, it is also possible to establish a similar connection between the time scales $\tau_\beta$ and $t^*$).

Our work can be extended to the study of particle diffusion in other systems. For example the first to which all our procedures can be applied is a fuzzy system since in a real system like a biomembrane, the obstacles are neither perfectly periodic nor perfectly random. Such systems would allow us to understand the behaviour of the particle when the degree of randomness of obstacles in the medium can be controlled progressively from periodic distributions to random distributions. Indeed, looking at the different curvatures presented by the characteristic exponent $\alpha$ and the diffusion coefficient $D$ in Figs. 7 and 9 of Chapter 2, it would be exciting to see the evolution of these curves as we move from periodic to random distributions.

It could also be interesting to study the movement of particles in closed systems. For instance, the results would depend on how the experiments are done and particularly on the initial conditions. Indeed, the results would be quite different if the particles were to start from a given position far from (or close to) the boundaries of the closed system. There are three characteristic lengths in the system, namely $r_I$, $\beta$ and $r^*$. With these lengths, we have four different situations. If the size of the system is smaller than $r_I$ it is impossible to estimate the parameters $\alpha$ and $D_\alpha$ of the MSD of the particle, the particle cannot experience anomalous diffusion. The second case is when the size of the system is between $r_I$ and $\beta$: anomalous diffusion would then dominate normal diffusion. When the size of the system is between $\beta$ and $r^*$, we are right in the transition between anomalous and normal diffusion, and as such, both process should coexist. Finally, we have the fourth one when the size of the system is greater than $r^*$: one can then characterize

the dynamics using the approach described in this thesis. In all these situations, the challenge will be to find how to extract useful physical parameters (such that $D$, $D_\alpha$, $\alpha$, etc.) from the raw data because $\langle r^2 \rangle$ plateaus when the particles reach the boundaries of the system.

To work with closed media, one would have to use reflective boundary conditions instead of periodic boundary conditions.

There are lots of other systems that one can study. For example, since biological environments are generally made of different obstacle sizes, it would be interesting to study systems that contain different obstacle sizes mixed together. This would just follow what has been started by A. Ellery et al [17]. The major limit of our model is that we have just considered the immobile obstacles of unique size and shape in the medium. In fact, in the biological environments the constituents are of different sizes and shapes, the obstacles are not completely immobile i.e can move, the particle can stick on the obstacle, many particles can move in the system. There is a lot of work to do in the future using the methodologies presented in this thesis (especially our new LMC algorithm, the idea of using the inflection point as the centre of the anomalous regime, and comparing the excess diffusion $\beta$ and the correlation length in a given system).

Since the methodology to study particle diffusion a lattice is well established, all the work presented here can be done again using lattices larger than those that we have considered and for larger ensemble sizes. This would allow us to increase the precision of the results and clarify the points that remain unclear. As mentioned previously, our new algorithm is only an improvement of the standard algorithm since the fourth moment is still not perfectly correct. The fourth moment will be totally correct only if we implement diagonal jumps. Even if it is true that the use of diagonal jumps was shown to be needed for the treatment of diffusion problems in 2D [20] and 3D or more [29, 21], their numerical implementation remains non trivial.

# 5

# Data obtained from our simulations

## 5.1 Definition of the variables

- $\phi$: the surface concentration of obstacles.
- $D$: the steady state diffusivity of the particle.
- $\alpha$: the characteristic exponent.
- $\beta$: the excess diffusion length.
- $r^*$: the crossover length.
- $t^*$: the crossover time.
- $r_I$: the root mean square displacement at the inflection point.
- $t_I$: the time at the inflection point.

## 5.2 Periodic Obstacle distributions

| $1 \times 1$ Obstacles | | | | | | | |
|---|---|---|---|---|---|---|---|
| $\phi$ | $D$ | $\alpha$ | $\beta$ | $r^*$ | $t^*$ | $r_I$ | $t_I$ |
| 1/9 | 0.8035 | 0.9652 | 0.3030 | 2.471 | 1.906 | 0.9171 | 0.2435 |
| 1/16 | 0.8784 | 0.9794 | 0.3272 | 3.544 | 3.576 | 1.472 | 0.5949 |
| 1/25 | 0.9191 | 0.9870 | 0.3131 | 4.249 | 4.912 | 1.674 | 0.7445 |
| 1/36 | 0.9427 | 0.9921 | 0.2929 | 5.069 | 6.813 | 2.011 | 1.057 |
| 1/49 | 0.9574 | 0.9937 | 0.2698 | 5.114 | 6.830 | 1.640 | 0.6929 |
| 1/64 | 0.9672 | 0.9952 | 0.2503 | 5.318 | 7.312 | 1.788 | 0.8180 |
| 1/81 | 0.9739 | 0.9962 | 0.2329 | 5.505 | 7.778 | 1.796 | 0.8217 |
| 1/100 | 0.9788 | 0.9969 | 0.2177 | 5.595 | 7.995 | 1.791 | 0.8140 |
| 1/121 | 0.9824 | 0.9975 | 0.2043 | 5.684 | 8.223 | 1.805 | 0.8247 |
| 1/144 | 0.9852 | 0.9979 | 0.1924 | 5.733 | 8.398 | 1.806 | 0.8237 |

| $2 \times 2$ Obstacles | | | | | | | |
|---|---|---|---|---|---|---|---|
| $\phi$ | $D$ | $\alpha$ | $\beta$ | $r^*$ | $t^*$ | $r_I$ | $t_I$ |
| 4/16 | 0.7111 | 0.9421 | 0.4405 | 2.8563 | 2.868 | 0.5041 | 1.259 |
| 4/25 | 0.7914 | 0.9566 | 0.5521 | 4.146 | 5.431 | 1.841 | 0.9949 |
| 4/36 | 0.8456 | 0.9690 | 0.5873 | 5.218 | 8.051 | 2.283 | 1.462 |
| 4/49 | 0.8822 | 0.9775 | 0.5891 | 6.126 | 10.63 | 2.600 | 1.842 |
| 4/64 | 0.9077 | 0.9831 | 0.5761 | 6.889 | 13.07 | 2.807 | 2.105 |
| 4/81 | 0.9259 | 0.9869 | 0.5568 | 7.520 | 15.27 | 2.938 | 2.273 |
| 4/100 | 0.9393 | 0.9896 | 0.5352 | 8.039 | 17.20 | 2.981 | 2.316 |
| 4/121 | 0.9494 | 0.9915 | 0.5133 | 8.454 | 18.82 | 3.005 | 2.336 |
| 4/144 | 0.9572 | 0.9929 | 0.4921 | 8.795 | 20.20 | 3.031 | 2.364 |

| $3 \times 3$ Obstacles | | | | | | | |
|---|---|---|---|---|---|---|---|
| $\phi$ | $D$ | $\alpha$ | $\beta$ | $r^*$ | $t^*$ | $r_I$ | $t_I$ |
| 9/25 | 0.6597 | 0.9261 | 0.5152 | 2.9672 | 3.337 | 1.340 | 0.599 |
| 9/36 | 0.7321 | 0.9371 | 0.6995 | 4.367 | 6.520 | 2.003 | 1.235 |
| 9/49 | 0.7873 | 0.9527 | 0.7947 | 5.655 | 10.15 | 2.627 | 2.027 |
| 9/64 | 0.8288 | 0.9631 | 0.8391 | 6.834 | 14.08 | 2.970 | 2.496 |
| 9/81 | 0.8601 | 0.9712 | 0.8543 | 7.804 | 17.70 | 3.392 | 3.180 |
| 9/100 | 0.8839 | 0.9775 | 0.8525 | 8.765 | 21.73 | 3.713 | 3.743 |
| 9/121 | 0.9023 | 0.9811 | 0.8410 | 9.535 | 25.18 | 4.057 | 4.412 |
| 9/144 | 0.9168 | 0.9843 | 0.8239 | 10.20 | 28.42 | 4.282 | 4.863 |

## 5.3 Random Obstacle distributions

| $1 \times 1$ Obstacles | | | | | | | |
|---|---|---|---|---|---|---|---|
| $\phi$ | D | $\alpha$ | $\beta$ | $r^*$ | $t^*$ | $r_I$ | $t_I$ |
| 0.01 | 0.9785 | 0.9969 | 0.2736 | 6.099 | 9.505 | 1.717 | 0.7477 |
| 0.02 | 0.9571 | 0.9950 | 0.4065 | 7.232 | 13.66 | 3.145 | 2.561 |
| 0.03 | 0.9352 | 0.9943 | 0.5480 | 9.427 | 23.76 | 3.337 | 2.939 |
| 0.04 | 0.9132 | 0.9934 | 0.6577 | 11.41 | 35.63 | 4.298 | 4.991 |
| 0.05 | 0.8914 | 0.9842 | 0.7501 | 5.560 | 8.678 | 1.719 | 0.7990 |
| 0.06 | 0.8683 | 0.9837 | 0.8910 | 8.629 | 21.44 | 3.028 | 2.551 |
| 0.08 | 0.8224 | 0.9822 | 1.082 | 10.70 | 34.88 | 3.274 | 3.123 |
| 0.1 | 0.7766 | 0.9752 | 1.241 | 9.544 | 29.34 | 2.818 | 2.402 |
| 0.15 | 0.6554 | 0.9593 | 1.685 | 12.94 | 56.35 | 3.024 | 3.628 |
| 0.2 | 0.5311 | 0.9363 | 2.160 | 13.19 | 81.96 | 3.375 | 4.452 |
| 0.25 | 0.4022 | 0.9066 | 3.141 | 17.48 | 208.9 | 3.702 | 6.892 |
| 0.3 | 0.2603 | 0.8610 | 3.994 | 19.92 | 376.8 | 4.060 | 9.390 |
| 0.35 | 0.1381 | 0.7922 | 4.791 | 28.35 | 1546 | 4.625 | 13.89 |
| 0.375 | 0.06342 | 0.7913 | 5.073 | 54.39 | $0.1232 \times 10^4$ | 5.063 | 21.49 |
| 0.4 | 0.01031 | 0.7171 | 5.420 | 186.9 | $0.7044 \times 10^6$ | 5.323 | 34.73 |

| $2 \times 2$ Obstacles | | | | | | | |
|---|---|---|---|---|---|---|---|
| $\phi$ | D | $\alpha$ | $\beta$ | $r^*$ | $t^*$ | $r_I$ | $t_I$ |
| 0.01 | 0.9840 | 0.9980 | 0.3920 | 10.82 | 29.79 | 3.086 | 2.405 |
| 0.02 | 0.9681 | 0.9960 | 0.5977 | 14.42 | 53.76 | 5.839 | 8.736 |
| 0.03 | 0.9522 | 0.9942 | 0.7596 | 13.82 | 50.20 | 4.792 | 5.958 |
| 0.04 | 0.9353 | 0.9902 | 0.8883 | 11.42 | 34.86 | 4.117 | 4.438 |
| 0.05 | 0.9194 | 0.9876 | 1.034 | 11.32 | 34.89 | 2.808 | 2.071 |
| 0.06 | 0.9036 | 0.9876 | 1.119 | 14.11 | 55.16 | 4.816 | 6.255 |
| 0.08 | 0.8715 | 0.9829 | 1.322 | 13.35 | 51.16 | 4.005 | 4.405 |
| 0.1 | 0.8356 | 0.9797 | 1.479 | 15.01 | 67.50 | 4.954 | 7.011 |
| 0.15 | 0.7482 | 0.9656 | 1.972 | 16.54 | 92.48 | 4.738 | 7.042 |
| 0.2 | 0.6567 | 0.9534 | 2.524 | 17.37 | 115.0 | 4.613 | 7.107 |
| 0.25 | 0.5540 | 0.9375 | 2.927 | 19.68 | 173.0 | 4.351 | 6.952 |
| 0.3 | 0.4632 | 0.9183 | 3.450 | 20.47 | 227.8 | 4.210 | 7.271 |
| 0.35 | 0.3761 | 0.8926 | 4.159 | 24.36 | 415.7 | 4.517 | 8.045 |
| 0.375 | 0.2830 | 0.8732 | 4.427 | 25.77 | 575.5 | 4.824 | 11.43 |
| 0.4 | 0.2510 | 0.8484 | 4.689 | 26.96 | 739.1 | 5.673 | 18.73 |

| $3 \times 3$ Obstacles | | | | | | | |
|---|---|---|---|---|---|---|---|
| $\phi$ | D | $\alpha$ | $\beta$ | $r^*$ | $t^*$ | $r_I$ | $t_I$ |
| 0.01 | 0.9857 | 0.9977 | 0.4602 | 14.58 | 53.75 | 6.012 | 9.130 |
| 0.02 | 0.9713 | 0.9956 | 0.7392 | 15.21 | 59.56 | 4.686 | 5.593 |
| 0.03 | 0.9572 | 0.9940 | 0.9763 | 17.91 | 83.82 | 3.204 | 2.632 |
| 0.04 | 0.9423 | 0.9922 | 1.150 | 18.85 | 94.31 | 4.255 | 4.690 |
| 0.05 | 0.9284 | 0.9882 | 1.297 | 13.31 | 47.79 | 3.684 | 3.546 |
| 0.06 | 0.9135 | 0.9881 | 1.444 | 20.91 | 119.7 | 5.538 | 8.164 |
| 0.08 | 0.8837 | 0.9839 | 1.716 | 20.86 | 123.3 | 5.926 | 9.544 |
| 0.1 | 0.8547 | 0.9844 | 1.966 | 21.12 | 130.6 | 5.541 | 9.500 |
| 0.15 | 0.7781 | 0.9802 | 2.462 | 22.02 | 139.5 | 6.325 | 12.93 |
| 0.2 | 0.7002 | 0.9587 | 2.881 | 22.06 | 173.8 | 7.958 | 20.71 |
| 0.25 | 0.6202 | 0.9596 | 3.255 | 24.51 | 267.3 | 8.041 | 21.05 |
| 0.3 | 0.5341 | 0.9340 | 3.680 | 30.24 | 431.4 | 8.119 | 25.78 |
| 0.35 | 0.4503 | 0.9335 | 4.031 | 27.91 | 514.3 | 8.207 | 26.13 |
| 0.375 | 0.4063 | 0.9143 | 4.201 | 29.02 | 544.3 | 7.943 | 27.54 |
| 0.4 | 0.3600 | 0.8942 | 4.429 | 30.30 | 637.9 | 7.710 | 29.87 |

# References


[1] Ellery A. *Modelling transport through biological environments that contain obstacles.* PhD thesis, Queensland University of Technology, 2016.

[2] Nelson P. *Biological Physics, Energy, Information, Life.* W. H. Freeman and Company, 2004.

[3] Weiss M, Elsner M, Kartberg F, and Nilsson T. Anomalous subdiffusion is a measure for cytoplasmic crowdingin living cells. *Biophys. J.*, **87**:3518–3524, 2004.

[4] Barkai E, Garini Y, and Metzler R. The irreproducibility of time-averaged observables in living cells poses fundamental questions for statistical mechanics and reshapes our views on cell biology. *Phys. Today*, **137**:29–35, 2012.

[5] Skaug MJ, Faller R, and Longo ML. Correlating anomalous diffusion with lipid bilayer membrane structure using single molecule tracking and atomic force microscopy. *J. Chem. Phys*, **134**:215101, 2011.

[6] Dix JA and Verkman AS. Crowding effects on diffusion in solutions and cells. *Annu. Rev. Biophys*, **27**:247–263, 2008.

[7] Cakaj S. *Modeling, Simulation and Optimization Tolerance and Optimal Control.* In-Teh, Olajnica 19/2, 32000 Vukovar, Croatia, 2010.

[8] Saxton MJ. Anomalous diffusion due to obstacles: A Monte Carlo study. *Biophys. J*, **66**:394–401, 1994.

[9] Whitaker S. *The Method of Volume Averaging.* Springer, 1999.

[10] Kim SJ, Naruse M, Aono M, Hori H, and Akimoto T. Random walk with chaotically driven bias. *Scientific Reports*, **6**:38634, 2016.

[11] Smith S, Cianci C, and Grima R. Macromolecular crowding directs the motion of small molecules inside cells. *J. R. Soc. Interface*, **14**:20170047, 2017.

[12] Bewerunge J, Ladadwa I, Platten F, Zunke C, Heuer A, and Egelhaaf S. Time and ensemble averages in evolving systems: the case of Brownian particles in random potentials. *J. Chem. Phys.*, **18**:18887–18895, 2016.

[13] Fyta M. Threading DNA through nanopores for biosensing applications. *J. Phys: Condens. Matter*, **27**:273101, 2015.

[14] Lee YK and Sinno T. Analysis of the lattice kinetic Monte Carlo method in systems with external fields. *J. Chem. Phys*, **145**:234104, 2016.

[15] Ellery A, Simpson M, McCue S, and Baker R. Characterizing transport through a crowded environment with different obstacle sizes. *J. Chem. Phys*, **140**:054108, 2014.

[16] Ellery A, Baker R, and Simpson M. Distinguishing between short-time non-Fickian diffusion and long-time Fickian diffusion for a random walk on a crowded lattice. *J. Chem. Phys*, **144**:171104, 2016.

[17] Ellery A, Baker R, McCue S, and Simpson M. Modeling transport through an environment crowded by a mixture of obstacles of different shapes and sizes. *Physica A*, **449**:74–84, 2016.

[18] Mercier JF and Slater GW. Numerical exact diffusion coefficients for lattice systems with periodic boundary conditions. I. Theory. *J. Chem. Phys*, **110**:6050–6056, 1999.

[19] Mercier JF and Slater GW. Numerical exact diffusion coefficients for lattice systems with periodic boundary conditions. II. Numerical approach and applications. *J. Chem. Phys*, **110**:6057–6065, 1999.

[20] Chubynsky MV and Slater GW. Optimizing the accuracy of lattice Monte Carlo algorithms for simulating diffusion. *Phys. Rev. E*, **85**:016709, 2012.

[21] Gauthier M and Slater GW. Building reliable lattice Monte Carlo models for real drift and diffusion problems. *Phys. Rev. E*, **70**:015103, 2004.

[22] Cantoni G. On some physical conditions of chemical affinity and on Brownian motion. *Il Nuevo Cimento*, **27**:156–167, 1867.

[23] Einstein A. *Investigations on the theory of the Brownian movement.* Dover Publication, 1956.

[24] Pathria RK and Beale P. *Statistical Mechanics Third Edition*. Elsevier, 2011.

[25] Slater GW, J Rousseau, and J Noolandi. On the stretching of dna in the reptation theories of gel electrophoresis. *Biopolymers*, **26**:863–872, 1987.

[26] Slater GW. Theory of band broadening for dna gel electrophoresis and sequencing. *Electrophoresis*, **14**:1–7, 1993.

[27] Tolver A. *An Introduction to Markov Chains*. Department of Mathematical Sciences, University of Copenhagen, 2016.

[28] Stauffer D and Aharony A. *Introduction to percolation theory 2nd ed.* Taylor and Francis, London, 1992.

[29] Gauthier M and Slater GW. A new set of Monte Carlo moves for lattice random-walk models of biased diffusion. *Physica A*, **355**:283–296, 2005.